NUNO HÉLDER
DA CRUZ SIMÕES
SILVA

PRODUÇÃO DE NANOFIBRAS PROTEICAS E A SUA APLICAÇÃO NO DESENVOLVIMENTO DE NOVOS MATERIAIS

PRODUCTION OF PROTEIN NANOFIBERS AND THEIR APPLICATION IN THE DEVELOPMENT OF INNOVATIVE MATERIALS

NUNO HÉLDER DA CRUZ SIMÕES SILVA

PRODUÇÃO DE NANOFIBRAS PROTEICAS E A SUA APLICAÇÃO NO DESENVOLVIMENTO DE NOVOS MATERIAIS

PRODUCTION OF PROTEIN NANOFIBERS AND THEIR APPLICATION IN THE DEVELOPMENT OF INNOVATIVE MATERIALS

Tese apresentada à Universidade de Aveiro para cumprimento dos requisitos necessários à obtenção do grau de Doutor em Engenharia Química, ramo Bioengenharia, realizada sob a orientação científica da Doutora Carmen Sofia da Rocha Freire Barros, Investigadora Principal do Departamento de Química da Universidade de Aveiro, e da Doutora Isabel Maria Marrucho, Professora Associada com Agregação do Departamento de Engenharia Química do Instituto Superior Técnico.

Dedico este trabalho, de coração cheio, à minha mãe. Por tudo.

o júri

presidente   Prof. Doutor Domingos Moreira Cardoso
Professor Catedrático do Departamento de Matemática da Universidade do Aveiro

Prof. Doutor Jorge Fernando Jordão Coelho
Professor Auxiliar com Agregação do Departamento de Engenharia Química da Universidade de Coimbra

Prof. Doutor Ana Rita Cruz Duarte
Professora Associada do Departamento de Química da Faculdade de Ciências e Tecnologia da Universidade Nova de Lisboa

Doutora Maria Isabel Rodrigues Correia
Investigadora Principal do Centro de Química Estrutural do Instituto Superior Técnico

Prof. Doutor Armando Jorge Domingues Silvestre
Professor Associado com Agregação do Departamento de Química da Universidade de Aveiro

Doutora Carmen Sofia da Rocha Freire Barros
Investigadora Principal do Departamento de Química da Universidade de Aveiro

agradecimentos

Para esta maratona académica, muito foi o apoio recebido de forma extra-académica. Ao BEST e ao Toastmasters por me terem dado múltiplas oportunidades de complementar a minha formação académica com inúmeras competências. À amizade de muitos que me motivam diariamente a tentar fazer sempre melhor. Entre eles, ao Nuno, Ana, Silvia, Milena, Luís, João, Ivo, Manuela. Ao Quim e à São por fazerem sentir-me sempre parte da família. Ao Dr. Joaquim Claro, mentor e amigo, por todos os conselhos e grandes jornadas.

Ao longo da vida somos surpreendidos por pessoas com um coração tão genuíno, que entram na nossa vida para ficar. Obrigado Tixinha por toda a paixão e apoio incansável, por todos os momentos especiais que tornam esta vida encantadora.

A toda a minha família. Tios e primos. Vô Celeste e Vô Nau. Mami e Papi. Somos grande parte de quem nos educa, e não há maior pilar na vida que a família.

À minha mana que se dá ao luxo de ter um irmão babado a muitos níveis! És um orgulho e não há maior riqueza que ter uma irmã como tu Cláudinha.

Ao papa. Por iluminar-me ao longo de todo este percurso. Muito do meu sucesso é o resultado da educação de um pai sempre presente. Um pai que deu tudo, e dou graças todos os dias por isso. Até um dia…

À mama. De coração cheio! Esta Tese também é tua! Viveste como se tua tratasse. Pela tua preocupação, interesse, energia e motivação transmitidas. Tens em ti uma força inabalável que me faz acreditar. Acreditar que no trabalho, na resiliência e na paixão por aquilo que fazemos, conseguimos chegar sempre mais além. Que esta Tese te orgulhe tanto quanto me inspiras.

A Nossa Senhora, Maria Santíssima, que continue a iluminar os nossos caminhos.

resumo

As nanofibras proteicas, também conhecidas como fibrilas amilóide, estão a ganhar muito interesse devido às suas propriedades únicas, nomeadamente elevada resistência mecânica e propriedades funcionais. Estas nanofibras caracterizam-se por depósitos proteicos que resultam de um processo onde a molécula proteica adquire uma conformação estrutural em folhas-β. Dadas as suas propriedades, estas nanofibras têm sido estudadas como elementos estruturais e funcionais no desenvolvimento de materiais inovadores para aplicação em diferentes áreas como, por exemplo, em biosensores, membranas bioactivas e estruturas tridimensionais ($\mathrm{scaffolds}$) para engenharia de tecidos.

No entanto, uma das principais limitações na exploração de nanofibras proteicas está relacionada com o tempo necessário para a sua produção, uma vez que a fibrilação é um processo moroso que pode levar horas, dias ou até mesmo semanas. A utilização de solventes alternativos como agentes promotores de fibrilação, nomeadamente líquidos iónicos (ILs), foi recentemente demonstrada como uma via para reduzir o tempo de fibrilação. Estes resultados serviram de inspiração para estudarmos o processo de fibrilação de uma proteína modelo, a lisozima, em soluções aquosas de líquidos iónicos baseados nos catiões imidazólio ou colina com diferentes aniões derivados de ácidos orgânicos. A presença de qualquer um dos ILs testados no meio de fibrilação demonstrou ser muito eficiente obtendo-se taxas de conversão superiores a 80% de fibrilas. Seguindo uma abordagem semelhante, estudou-se também um solvente eutéctico profundo (DES) baseado em cloreto de colina e ácido acético (1:1) como possível promotor da fibrilação da lisozima, diminuindo-se o tempo de fibrilação de 8-15 h para apenas 2-3 h. Foi também demonstrado que a temperatura tem um papel fundamental na aceleração da fibrilação e tanto a temperatura como o pH influenciam significativamente as dimensões das nanofibras, nomeadamente em termos de comprimento e largura. Com o objectivo de ajustar a razão de aspecto das nanofibras (razão comprimento/largura), foram ainda estudados vários DES baseados em cloreto de colina e com ácidos mono-, di- e tri-carboxílicos, tendo-se observado que o ácido carboxílico do DES desempenha um papel fundamental no comprimento das nanofibras produzidas, sendo as razões de aspecto sempre superiores às obtidas por fibrilação apenas com cloreto de colina.

O potencial das nanofibras proteicas como elementos de reforço em materiais compósitos foi avaliado pela preparação de filmes nanocompósitos à base de pululano com nanofibras de lisozima em diferentes proporções. Foram obtidos filmes transparentes com maior resistência mecânica à tracção, particularmente para as nanofibras com razões de aspecto mais elevadas. Além disso, a incorporação de nanofibras de lisozima nos filmes de pululano conferiu propriedades bioativas aos filmes, nomeadamente capacidade antioxidante e atividade antibacteriana contra a Staphylococcus aureus. O aumento do conteúdo de nanofibras nos filmes promoveu um aumento das propriedades antioxidante e antibacteriano dos filmes, sugerindo-se como possível aplicação a utilização destes nanocompósitos como filmes comestíveis e ecológicos para embalagens alimentares bioactivas.

As nanofibras de lisozima foram também misturadas com fibras de nanocelulose com o objectivo de produzir um filme sustentável para a remoção de mercúrio (II) de águas naturais. Os filmes foram obtidos por filtração sob vácuo e mostraram-se homogéneos e translúcidos. A incorporação das nanofibras de lisozima nos filmes de nanocelulose promoveu um reforço mecânico significativo. Em termos da capacidade de remoção de mercúrio (II) a partir de água natural, a presença das nanofibras de lisozima proporcionou um aumento muito expressivo com eficiências de 82% (pH 7) < 89% (pH 9) < 93% (pH 11), utilizando concentrações de mercúrio (II) de acordo com o limite estabelecido nos regulamentos da União Europeia (50 µg L^{-1}).

Em suma, foi demonstrado nesta tese que o uso de líquidos iónicos e de solventes eutécticos profundos assume um papel fundamental na formação de nanofibras de lisozima morfologicamente alongadas e finas, que podem ser exploradas no desenvolvimento de bionanocompósitos para diversas aplicações desde embalagens bioactivas a sistemas de purificação de água.

keywords

Protein Nanofibers, Lysozyme, Ionic liquids, Deep Eutectic Solvents, Bionanocomposites, Films, Pullulan, Nanofibrillated Cellulose, Mechanical Reinforcement, Functional Properties.

abstract

Protein nanofibers, also known as amyloid fibrils, are gaining much attention due to their peculiar morphology, mechanical strength and functionalities. These nanofibers are characterized as fibrillar assemblies of monomeric proteins or peptides that underwent unfolding-refolding transition into stable β-sheet structures and are emerging as building nanoblocks for the development of innovative functional materials for application in distinct fields, for instance, in biosensors, bioactive membranes and tissue engineering scaffolds.

However, one of the main limitations pointed out for the exploitation of protein nanofibers is their high production time since fibrillation is a time-consuming process that can take hours, days, and even weeks. The use of alternative solvents, such as ionic liquids (ILs), as fibrillation agents has been recently reported with considerable reduction in the fibrillation time. This fact encouraged us to study the fibrillation of a model protein, hen egg white lysozyme (HEWL), in the presence of several ILs based on imidazolium and cholinium cations combined with different anions derived from organic acids. All ILs used were shown to fibrillate HEWL within a few hours with conversion ratios over than 80% and typically worm-like nanofibers were obtained. In another study, a deep eutectic solvent (DES) based on cholinium chloride and acetic acid (1:1) was studied as a possible promoter of HEWL fibrillation, and a considerably reduction of the fibrillation time from 8-15 h to just 2-3 h was also observed. Temperature has a key role in the acceleration of the fibrillation and both temperature and pH significantly influence the nanofibers dimensions, in terms of length and width. In what concerns the nanofibers aspect-ratio, several DES combining cholinium chloride and mono-, di- and tri-carboxylic acids were studied. It was observed that carboxylic acid plays an important role on the length of the nanofibers produced with aspect-ratios always higher than those obtained by fibrillation with cholinium chloride alone.

The potential of the obtained protein nanofibers as reinforcing elements was evaluated by preparing pullulan-based nanocomposite films containing lysozyme nanofibers with different aspect-ratios, resulting in highly homogenous and transparent films with improved mechanical performance, particularly for the nanofibers with higher aspect-ratios. Furthermore, the incorporation of lysozyme nanofibers in the pullulan films imparted them also with bioactive functionalities, namely antioxidant capacity and antibacterial activity against $Staphylococcus\ aureus$. The results showed that the antioxidant and antibacterial effectiveness increased with the content of nanofibers, supporting the use these films as, for example, eco-friendly edible films for active packaging.

Lysozyme nanofibers were also blended with nanocellulose fibers to produce a sustainable sorbent film to be used in the removal of mercury (II) from natural waters. Homogenous and translucent films were obtained by vacuum filtration and the incorporation of these nanofibers in a nanocellulose film promoted a considerable mechanical reinforcement. In terms of the capacity to remove mercury (II) from natural water, the presence of lysozyme nanofibers demonstrated to increase expressively the mercury (II) removal with efficiencies of 82% (pH 7) < 89% (pH 9) < 93% (pH 11), using realistic concentrations of mercury (II) under the limit established in the European Union regulations (50 µg L^{-1}).

In sum, it was demonstrated in this thesis that the use of ionic liquids and deep eutectic solvents can accelerate the formation of long and thin lysozyme nanofibers that can be explored as nanosized reinforcing elements for the development of bionanocomposites with applications ranging from food packaging to water purification systems and nanotechnology.

Table of Contents

Thesis guideline

This thesis focuses on the production of protein nanofibers, using ionic liquids and deep eutectic solvents as promoters of fast fibrillation processes, and their use in the development of novel functional bio-based nanocomposites. Specifically, pullulan and nanofibrillated cellulose were combined with protein nanofibers through different methodologies to generate novel functional materials. The resulting materials were characterized in detail, in terms of structural, thermal, mechanical and functional properties, in order to assess their potential in diverse fields.

This thesis is organized in 4 chapters, as described below.

Chapter 1: Introduction

The aim of this chapter is to provide a brief overview of the state of the art methodologies used to obtain protein nanofibers and their potential applications in the material science field, highlighting the novelty of the present thesis: the fast production of protein nanofibers with tuned properties to be used in the development of protein-based materials.

Chapter 2: Production of Protein Nanofibers

This chapter describes in detail the use of ionic liquids and deep eutectic solvents to promote and accelerate protein fibrillation, using hen egg white lysozyme as a model protein. The chapter includes the results of 3 papers, in which the investigation of the role of various cholinium and imidazolium based ionic liquids and a set of different deep eutectic solvents based on cholinium chloride is thoroughly explored and described.

Chapter 3: Development of Innovative Materials based on Protein Nanofibers

This chapter is devoted to the development of new functional materials based on protein nanofibers and considers the results of 2 papers. The first paper focuses on the development of pullulan films with protein nanofibers for packaging applications, while the second is dedicated to the preparation of nanofibrillated cellulose membranes with protein nanofibers and their use for mercury (II) removal from natural waters.

Chapter 4: Conclusion and Final Remarks

The final chapter summarizes the overall conclusions of the work carried out during this thesis and offers a perspective on the future work that can be developed based on the obtained results.

Publications and Communications

Published Papers

Silva, NHCS; Vilela, C; Almeida, A; Marrucho, IM; Freire, CSR (2018) *Pullulan-based nanocomposite films for functional food packaging: exploiting lysozyme nanofibers as antibacterial and antioxidant reinforcing additives*, FOOD HYDROCOLLOIDS, 77, 921-930. DOI : 10.1016/j.foodhyd.2017.11.039

Silva, NHCS; Pinto, RJB; Freire, CSR; Marrucho, IM (2016) *Production of lysozyme nanofibers using deep eutectic solvent aqueous solutions*. COLLOIDS AND SURFACES B-BIOINTERFACES, 147, 36-44. DOI: 10.1016/j.colsurfb.2016.07.005

Silva, NHCS; Vilela, C; Marrucho, IM; Freire, CSR; Neto, CP; Silvestre, AJD (2014) *Protein-based materials: from sources to innovative sustainable materials for biomedical applications*. JOURNAL OF MATERIALS CHEMISTRY B, 2, 24, 3715-3740. DOI: 10.1039/c4tb00168k

Submitted Papers

Silva, NHCS; Pinto, RJB; Ferreira, R; Correia, I; Freire, CSR; Marrucho, IM (2017) *Potential use of different ionic liquids to promote a faster lysozyme fibrillation*, submitted.

Silva, NHCS; Pinto, RJB; Freire, CSR; Marrucho, IM (2017) *Tuning lysozyme nanofibers dimensions using deep eutectic solvents for improved reinforcement ability*, submitted.

Papers in Preparation

Silva, NHCS; Figueira, P; Vilela, C; Pinto, RJB; Marrucho, IM; Pereira, ME ; Freire, CSR (2018) *Innovative membranes based on nanocellulose and protein nanofibers for the removal of mercury (II) from natural water,* in preparation.

Oral Communications

Silva, NHCS; Freire, CSR; Marrucho, IM (2017) *Production of lysozyme nanofibers using ionic liquids and deep eutectic solvents for the design of innovative biomedical applications,* 2nd Edition Path Spring Meeting 2017 – Deep Eutectic Solvents, Aveiro (Portugal), 8 June 2017

Silva, NHCS; Pinto, RJB; Freire, CSR; Marrucho, IM (2017) *Innovative bionanocomposites based on polysaccharides and protein nanofibers,* ACS Spring Meeting 2017, San Francisco (USA), 2-6 April 2017

Silva, NHCS; Carvalho, T; Silvestre, AJD; Freire, CSR; Marrucho, IM (2017) *Production of protein nanofibers using new timesaving methodologies for the design of innovative biomedical applications,* ACS Spring Meeting 2017, San Francisco (USA), 2-6 April 2017

Silva, NHCS; Freire, CSR; Marrucho, IM (2016) *Production of lysozyme nanofibers using ionic liquids and deep eutectic solvents for the design of innovative biomedical applications.* COST EXIL – Exchange on Ionic Liquids, Poznan (Poland), 19-20 April 2016

Poster Communications

Silva, NHCS; Pinto, RJB; Marrucho, IM; Freire, CSR (2017) *Development of innovative bionanocomposites based on polysaccharides and protein nanofibers,* II Jornadas de Caracterização de Materiais, University of Aveiro (Portugal), 24-26 January 2017

Silva, NHCS; Pinto, RJB; Marrucho, IM; Freire, CSR (2016) *Development of innovative bionanocomposites based on polysaccharides and protein nanofibers,* EPNOE Junior Scientist Meeting 2016, Antibes (France), 13-14 October 2016

Silva, NHCS; Pinto, RJB; Freire, CSR; Marrucho, IM (2016) *Fibrillation of proteins using ionic liquids and deep eutectic solvents as a strategy for the design of innovative biomaterials,* Green-it – Bioresources4Sustainability, ITQB-UNL, Oeiras (Portugal), 7-8 July 2016

Silva, NHCS; Pinto, RJB; Marrucho, IM; Freire, CSR (2016) *Fibrillation of proteins using ionic liquids and deep eutectic solvents as a strategy for the design of innovative biomaterials,* Encontro de Ciência 2016, Lisbon (Portugal), 4-6 July 2016

Silva, NHCS; Pinto, RJB; Marrucho, IM; Freire, CSR (2016) *Fibrillation of proteins using ionic liquids and deep eutectic solvents as a strategy for the design of innovative biomaterials,* Research Day 2016, University of Aveiro (Portugal), 15 June 2016

Silva, NHCS; Pinto, RJB; Freire, CSR; Marrucho, IM (2015) *Production of Lysozyme Nanofibers using a Deep Eutectic Solvent,* IMIL – Iberoamerican meeting on ionic liquids, Madrid (Spain), 2-3 July 2015

1.
Introduction

Nowadays, there is a growing interest on the use of natural polymers, such as polysaccharides (cellulose, starch, chitosan), as well as proteins for the development of new sustainable materials with distinct functionalities and applications.[1–5] These natural polymers are not only used individually but also in blends and composites, to improve the properties and functionalities of the final materials and extend their application fields, opening new perspectives for the development of innovative biomaterials. The growing interest of scientists in these materials has been triggered by their great potential for high added-value applications in different fields like pharmaceutical, biomedical and food industries, as a result of the enormous versatility of the synthetic processes and the almost endless choices of feasible combinations that can be employed to obtain biocomposites and blends.[6,7]

1.1. Protein-based materials

Proteins are attracting considerable interest in a large number of fields as eco-friendly/green source of new materials, including composites and, especially, functional biomaterials.[8] Proteins are one of the most versatile group of macromolecules in living systems and play a crucial role in all biological processes, including enzymatic catalysis, transport and storage, coordination, motion, mechanical support, immune protection, generation and transmission of nerve impulses, control and differentiation of cells and tissues.[9] Research and development of protein-based materials is essentially focused on films, sheets, adhesives , foams, blends, composites and gels,[8,10,11] mainly for biomedical applications, such as scaffolds for tissue regeneration, drug delivery systems, stimuli-responsive materials[12] and biosensors.[11,13–16]

Several reviews have recently been published on this field, showing that the interest in proteins for the development of new materials has increased considerably in the past years.[11,15,17] For instance, Silva *et al.*[17] conducted an overview on protein-based materials, from the sources, structure and properties through the materials derived from several different proteins, namely elastin, collagen, silk, keratin and soy protein, up to their applications. Throughout this review it is possible to evaluate how promising this research field is in terms of the use of proteins either as matrices, or fibers in composites with other compatible natural or synthetic polymers, to produce panoply of biomaterials with tunable properties. Due to their intrinsic biocompatibility, biodegradability, and specific properties together with their relatively high cost when compared with other natural polymers like cellulose and starch, protein-based materials are being mainly developed for biomedical purposes. Nevertheless, the knowledge gathered in the development of protein-based materials for biomedical applications certainly opens new perspectives for the development of new materials for application in other fields or even suggest other innovative and growing fields of research. One example is the ability of proteins to form protein nanofibers, also known as amyloid fibrils, and their use in the preparation of new biomaterials as presented in the following chapters.

1.2. Protein nanofibers (Amyloid fibrils)

The term amyloid was firstly introduced by Rudolph Virchow in 1854, to denote a macroscopic tissue abnormality that exhibited a positive iodine staining reaction.[18] At that time, Virchow suggested that the substance underlying the evident macroscopic abnormality was starch, so the name amyloid was given (from latin *amylum* and the greek *amylon*). In 1859, Friedreich and Kekule demonstrated the presence of proteins in the mass of amyloid deposits, based on its high nitrogen content. Since then, amyloid was always related to the presence of proteins and much attention was given to the study of the protein conformation changes that result in fibril formation.[18]

Amyloid fibrils are currently known as abnormal extracellular fibrous protein deposits, resistant to degradation, found in organs and tissues and formed by a process of

amyloidosis, *i.e.* the assembly of commonly soluble proteins.[19] This process normally leads to tissue damage and it is frequently associated with some diseases, including systemic amyloidosis, Alzheimer's and Parkinson's diseases, maturity onset diabetes, and the prion-related transmissible spongiform encephalopathies.[20]

In each of these pathological states, a specific protein or protein fragment changes from its natural soluble form into insoluble fibrils, which accumulate in a variety of organs and tissues. For instance, the Alzheimer's disease is characterized by this process of amyloidosis that leads to the deposition of insoluble amyloid fibrils in the neuropil. These amyloid fibrils are composed by the ordered aggregation of amyloid-β peptide (Aβ), a 39-42 amino acid residue peptide, which is deposited extracellularly as amyloid plaques.[21] Although there are several amyloid fibril diseases in which proteins vary considerably in their structure, function and size, the amyloid fibrils formed show very few structural differences. In fact, the ability to form amyloid fibrils is an intrinsic property of all native proteins (Fig. 1), and it happens rapidly when proteins are held near their denaturation temperatures or are acidified.
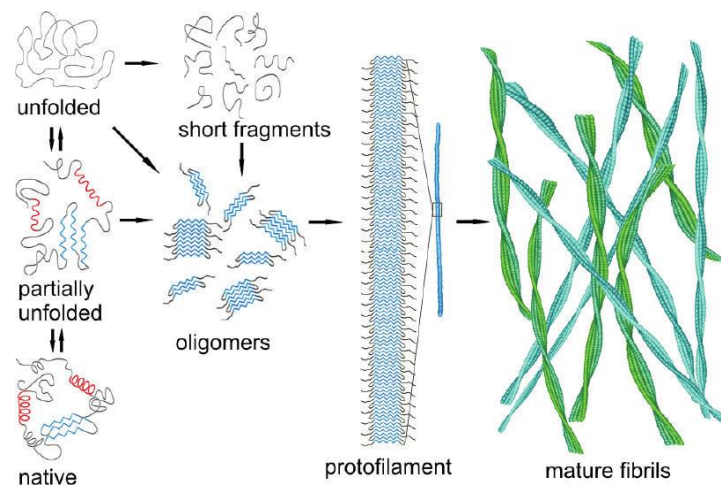
Fig. 1 - Schematic illustration of the mechanism of conversion of globular proteins into amyloid fibrils.[22]

Despite the fact that amyloid fibrils are much associated to disease related proteins, they are also at the basis of vital phenomena such as adhesion, hyphae and secretory granules.[23,24] For instance, bacteria such as *Escherichia coli* produce amyloid fibrils

expressed extracellularly, which are involved in their communication process with other bacteria.[24] Moreover, these bacterial amyloid fibrils, also called curli fibers, are the proteinaceous component of the extracellular matrix that facilitates the formation of biofilms in many enterobacteria (**Fig. 2**).[24]
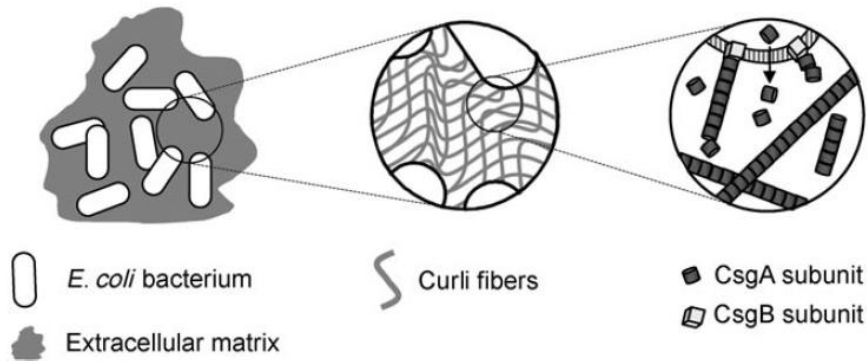
Fig. 2 - Schematic illustration of the formation of amyloid fibrils (Curli fibers) by bacteria.[24]

Amyloid proteins can also be obtained *in vitro*, as it is approached in the next section (*1.3. Mechanism and conditions for protein fibrillation*).

1.2.1. Structure of amyloid fibrils

Amyloid fibrils of both non-disease and disease related proteins show similar structures and morphologies including enriched antiparallel β-sheets, with a perpendicular orientation to the longitudinal fibrils axis.[22,25,26] These fibrillar states are highly ordered, with lengths in the order of microns and diameters of 100-200 Å.[27] Their mechanical properties are comparable to that of dragline silk and much greater than those of most biological filaments, such as actin and microtubules.[28] Amyloid fibrils can possess very high kinetics and thermodynamic stabilities, often exceeding those of the functional folded states of proteins,[29] as well as a greater resistance to degradation by chemical and biological means.[30]

The morphology and secondary structure of amyloid fibrils was first studied by Transmission Electron Microscopy (TEM), X-ray diffraction, and chemical staining. For

example, TEM images of negatively stained amyloid fibrils of the islet amyloid polypeptide (IAPP) showed long and unbranching fibrils of 70-120 Å in diameter (Fig. 3A).[31] The X-ray diffraction showed a cross-β diffraction with 2 characteristics signals: a sharp reflection at 4.7 Å along the same direction as the fibril, and a more diffuse reflection around 10 Å perpendicular to the fibril direction (Fig. 3B).[32,33]
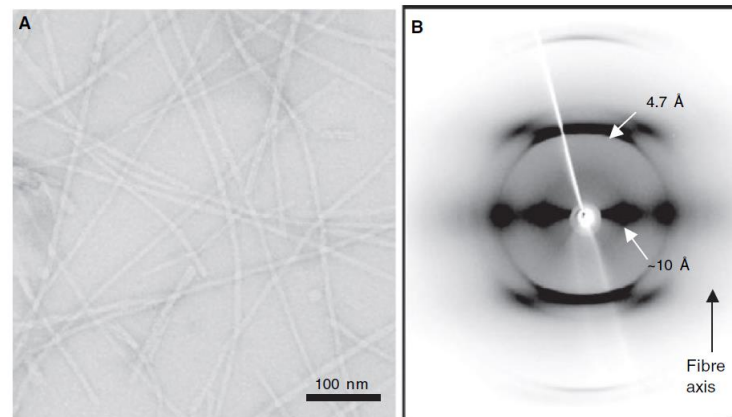
Fig. 3 - The morphology and structure of amyloid fibrils studied by TEM and X-ray diffraction.[25]

Chemical staining has been used for a long time to identify the presence of amyloid fibrils, since in the presence of certain dyes, amyloid-like fibrils display characteristic optical properties. Congo red dye has been used to identify amyloid fibrils in tissue sections, which under cross polarizers shows an apple-green birefringence. This dye has been commonly used in the cellulose industry due to its affinity to cellulose fibers, though it has undergone several chemical modifications to improve its sensitivity and specificity to amyloid fibrils.[34–36] For example, Puchtler *et al.*[37] described in 1962 a method that stains amyloid selectively by using Congo red in an 80% alcohol alkaline solution saturated with NaCl. Other chemical staining methods include Thioflavine T (ThT), a fluorescent stain. ThT associates with β-sheet aggregated fibrils, having an excitation maximum at 450 nm and an enhanced emission at 482 nm.[36,38]

For many years, the amyloid fibrils have been characterised by these techniques. Despite the structural insights given by imaging techniques as electron microscopy or atomic force microscopy (AFM), they could not give much information concerning the

ultra-structure and the fact of being not crystalline and not soluble to be studied by liquid nuclear magnetic resonance (NMR) spectroscopy. Major developments were achieved when solid-state NMR started being used, and consequently, explored for this purpose.[20] This technique was used to study an amyloid-β structure formed from the 40-residue peptide - Aβ(1-40), at pH 7.4 and 24 °C.[39–41] In this structure, each Aβ(1-40) residue has two β-strands, spanning approximately residues 12-24 and 30-40, to the core region of fibrils, and inter-connected by the look 25-29. Two molecules of Aβ(1-40) form a protofilament (**Fig. 4**), in which the β-sheets 30-40 face to each other. It has been suggested that a single protofilament is composed of four β-sheets separated by distances of ~10Å.[20]
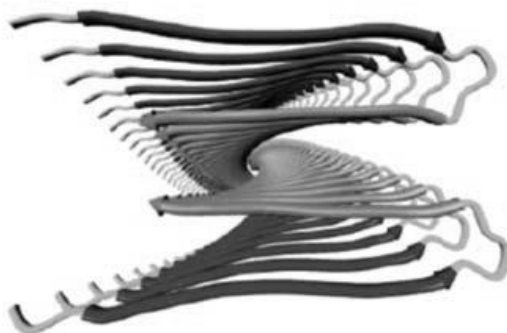
Fig. 4 - Representation of a structural amyloid fibril model for Aβ(1-40), viewed down the long axis of the protofilament. Each molecule contains two β-strands that form separate parallel β-sheets in a double-layered cross- motif.[42]

Solid-state NMR technique was also very important to study the orientation of the β-sheets in protein fibrils. Structural models for Aβ fibrils, published before 2000,[43–46] were consensual that the cross-β motifs in amyloid fibrils were comprised of antiparallel β-sheets. This belief was overturned by several studies published afterwards, showing that peptides Aβ(1-35) and Aβ(1-40) contain only parallel β-sheets.[39,41,47,48] However, certain amyloid fibrils have been shown to contain antiparallel β-sheets, particularly fibrils formed by relatively short peptides, suggesting that there is no truly universal supramolecular structure for amyloid fibrils.[49–51] Furthermore, according to Antzutkin *et al.*,[41] who conducted solid-state NMR measurements using a multiple quantum ^{13}C NMR technique, parallel β-sheets are preferentially favoured in amyloid fibrils because parallel alignment of

β-strand segments maximizes hydrophobic contacts and permits favourable interactions among polar side chains within a single β-sheet.

Interestingly, Magic Angle Spinning (MAS) NMR experiments also revealed a parallel β-sheet geometry within the sheets of the amyloid fibrils and indicates a full complement of backbone-backbone hydrogen bonds along the entire length of the structure.[52,53] In fact, the architecture of the fully assembled amyloid fibrils is not dependent on the sequence of the subunits since the constituent β-strands, within the core of the fibril, are linked by a vast array of interbackbone hydrogen bonds.[54] In more detail, the hydrogen bonds that connect juxtaposed β-strands into a pleated β-sheet structure are aligned parallel to the main fibril axis (**Fig. 5**A). In contrast, the amino acid side chains extend perpendicular to the fibril axis. Therefore, the side chains define the intra- or intermolecular interactions within the plane of the fibril cross-section (**Fig. 5**B).[55]
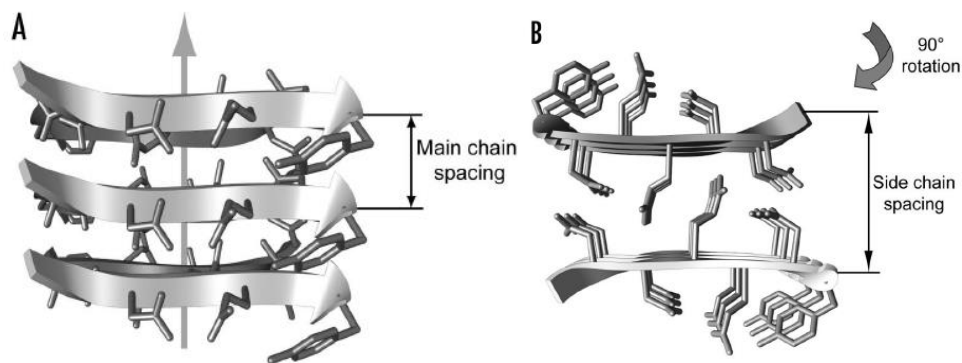
Fig. 5 - Amyloid fibrils cross-β core structure. Side (A) and top (B) view.[55]

Recently, Fitzpatrick *et al.*[52] combined five diverse and complementary techniques to determine the structure of each of the motifs that transform an 11-residue of the protein transthyretin (TTR) - TTR(105-115) - into amyloid fibrils. MAS NMR spectroscopy with high-resolution electron density maps from cryoelectron microscopy (Cryo-TEM), together with X-ray diffraction, TEM and AFM measurements enable to derive high precision structural restraints on the secondary, tertiary and quaternary structure of such amyloid fibrils (**Fig. 6**).
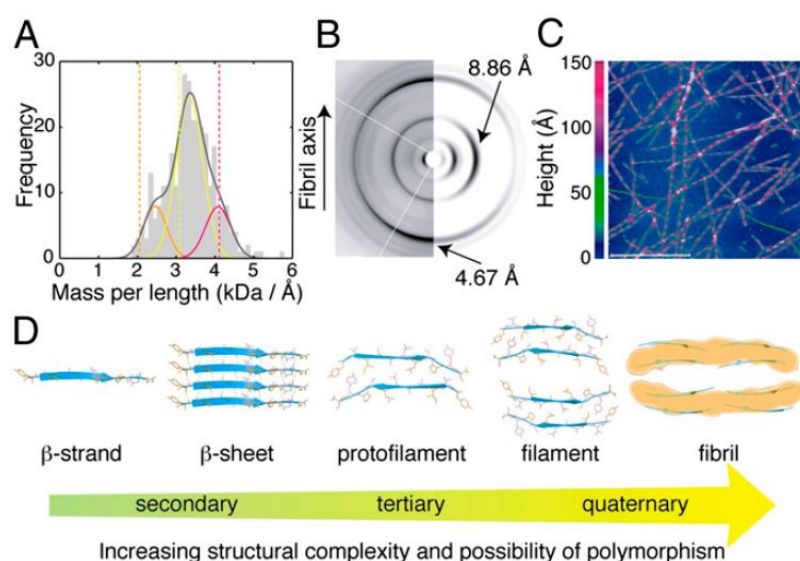
Fig. 6 - Results of five biophysical techniques combined to determine the structure of TTR(105-115) amyloid fibrils. (A) Histogram of STEM MPL (80-1000Å). (B) High-resolution X-ray diffraction (3-100Å). (C) AFM image – scale bar 1μm (30-1000Å). (D) Combination of MAS NMR (0,1-10Å) and Cryo-EM (8-1000Å).[52]

X-ray diffraction has shown again a vertical fibril axis, with a meridional reflection at 4.67Å and an equatorial reflection at 8.86Å, characteristic of cross-β structures (**Fig. 6**B). Through AFM imaging it was possible to measure an average height of the filament fibril of around 38.7Å (**Fig. 6**C). MAS NMR studies helped to determine the intermolecular interactions within the building blocks of the fibril, and to define a hierarchy of atomic-resolution motifs involved in the self-assembly of the amyloid fibrils. Unlike other authors[20], Fitzpatrick *et al.*[52] defined a protofilament as having just 2 peptides. Two protofilaments interlaced formed a filament (4 peptides) and a group of 2 filaments constitute a fibril (**Fig. 6**D). In order to obtain an independent estimative of the number of peptides contained in the fibril, cross-sections Scanning Transmission EM (STEM) mass-per-length (MPL) measurements were performed, revealing three populations of fibrils, formed according to the mass per length (2.5, 3.3 and 4.1 kDa/Å), corresponding to doublets (8 peptides), triplets (12 peptides) and quadruplets (16 peptides), respectively (**Fig. 6**A). These MPL measurements are in good agreement with the cryo-TEM fibril reconstructions, showing a two-fold symmetry with 4, 6 and 8 two-β-sheet protofilaments (**Fig. 7**). This represents one kind of polymorphism.

14
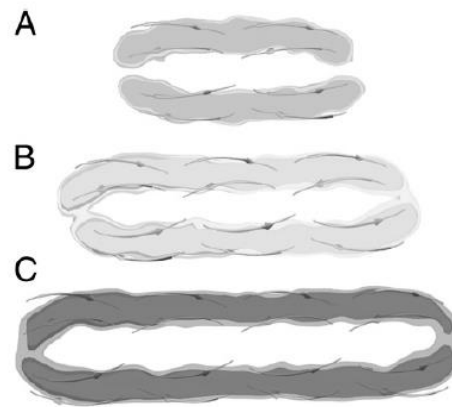
Fig. 7 - Atomic resolutions of the 3 types of TTR(105-115) amyloid fibrils, determined by MAS NMR and Cryo-EM maps. (A) Doublet. (B) Triplet. (C) Quadruplet.[52]

1.2.2. Polymorphism of amyloid fibrils

Amyloid fibrils formed from different polypeptides contain a common cross-β spine. Nevertheless, amyloid fibrils formed from the same polypeptide can occur in a range of structurally different morphologies. Thus, with respect to morphology, amyloid fibrils are usually polymorphic, meaning that fibrils formed by a given peptide or protein can have multiple distinct supramolecular structures depending on the precise conditions under which the fibrils grow.[56]

The heterogeneity of amyloid fibrils can reflect different types of polymorphism (**Fig. 8**) based on variations in the protofilament number, in the protofilament arrangement or in the polypeptide conformations.[55]
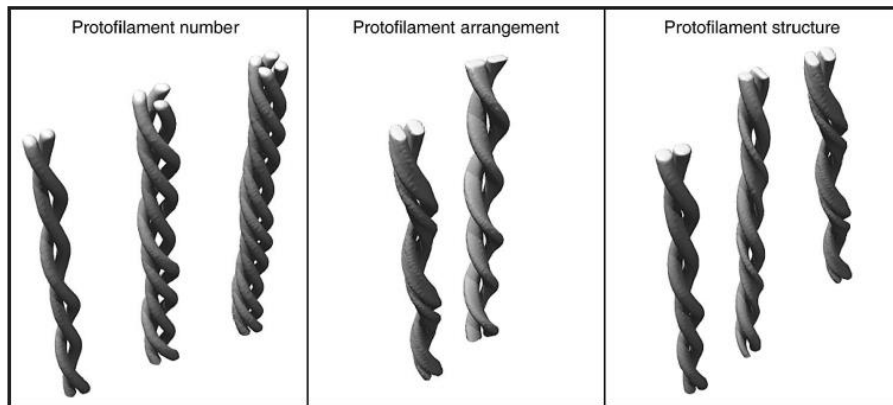
Fig. 8 - Structural types of amyloid polymorphism.[55]

One example of such polymorphism involves the peptide hormone glucagon, wherein fibrils formed at different temperatures (25 °C and 50 °C) are morphologically different. Circular Dichroism and FTIR spectroscopy reveal differences in the secondary structure adopted by the constituent peptide molecules.[57] Similarly, mammalian fibrils from different species vary in the secondary structure morphology (**Fig. 9**), and these differences seem to be controlled by one or two residues in a critical region of the polypeptide sequence.[58]
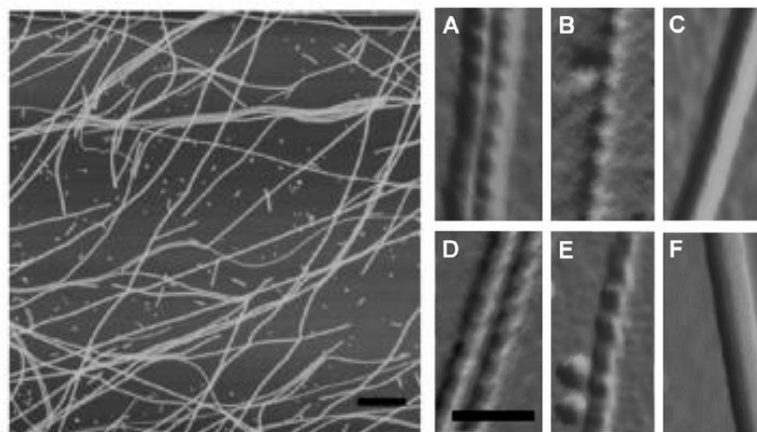
Fig. 9 - Mammalian fibrils visualized by AFM. Cross-seeding with preformed fibrils from other species result in different fibril morphologies.[58]

Furthermore, the C- and N-terminal domains of the protein appear to interact with each other, and these fibrils do not have the characteristic 4.7 Å reflection typical of a cross-β structure.[59,60] As proposed by Fitzpatrick *et al.*,[52] fibrils may consist of a different number of protofilaments. This possibility has also been demonstrated by cryo-TEM reconstruction

of different insulin fibrils containing 2, 4 and 6 protofilaments, in compact shape.[61] Using STEM analysis together with MPL, Goldsbury and coworkers[62,63] have shown multiple assembly pathways of Aβ(1-40) fibril polymorphism.[62,63] Although it is known that different conditions of incubation can lead to different fibril structures, polymorphism can even occur within the same sample.[62]

Cryo-TEM reconstruction of Aβ(1-40) fibrils suggests that fibrils may also differ in the relative orientation of their protofilaments, and so in the interaction between them.[64] In this case, different fibrils formed under the same conditions differ in the position of the protofilaments. In one, protofilaments are side-by-side, while in the other they are offset from one another.[64]

In addition, fibrils can differ in their protofilament structure, and therefore, in the conformation of the underlying peptides. Examples were provided by solid-state NMR spectra of different fibril morphologies from Aβ(1-40),[48] α-synuclein,[65] and amylin fragments.[66] These studies demonstrated that different amyloid fibril samples can give rise to a diversity of interactions within the structure, having as a consequence different fibril morphologies.[48]

These features of the protein fibrillation processes reveal that polypeptide chains can adopt multiple conformational states, which can interchange among them. A schematic representation of some of the many conformational states is shown in **Fig. 10**.[20] Taking the protein biosynthesis from a ribosome as starting point, the polypeptide chain is unfolded. Depending on the conditions for protein aggregation, the partial folding can occur until the protein achieves the native conformation, with its functional properties. This native conformation can lead to the arrangement of the polypeptide chain into functional oligomers, functional fibers and native-like aggregates. However, this is merely a pathway, since the unfolded or partially unfolded polypeptide chains can originate disordered aggregates of different natures. Furthermore, a vast majority of proteins may be degraded as part of normal biochemical processes.[20]

On the other hand, peptides and proteins that are partially unfolded, as well as fragments of proteins which are unable to fold due to the absence of proper folding conditions, can also aggregate under some circumstances, forming amorphous aggregates. Some of these aggregates simply dissociate again (interchanging conformations), but others

may re-organise to form β-structured aggregates (amyloid protofibrils), including several morphological states as previously discussed.
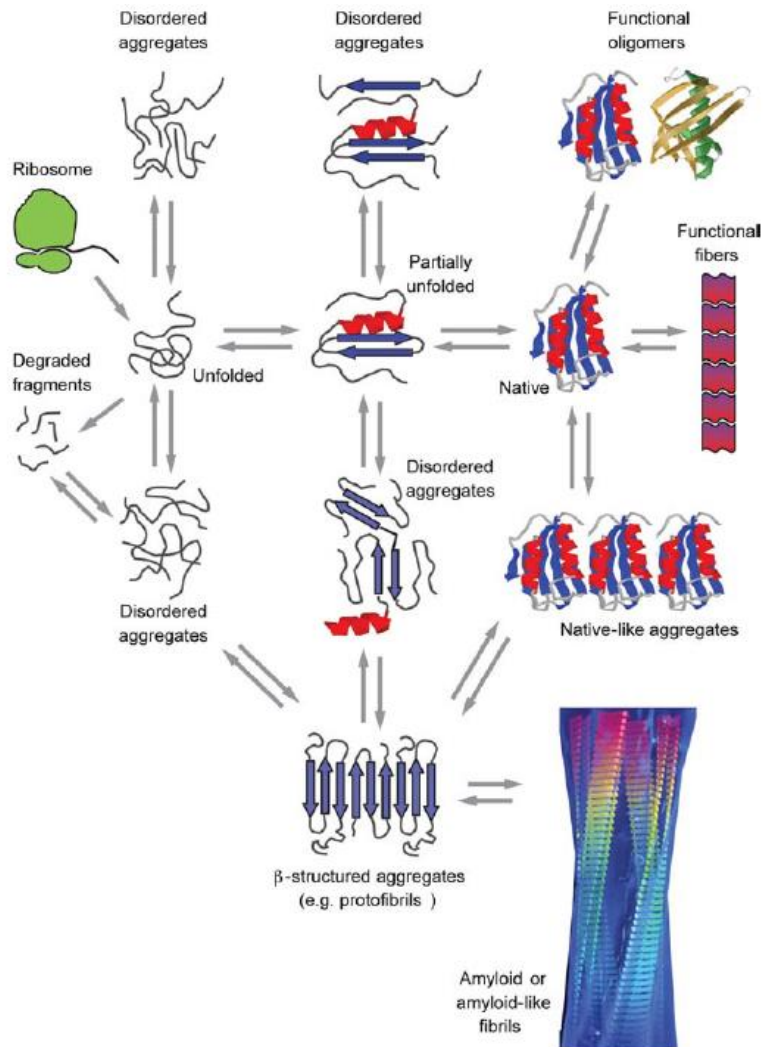
Fig. 10 - Schematic representation of some conformational states adopted by polypeptides during fibrillation.[20]

These structural differences in fibrils can probably be caused by the slightly different conditions used when fibrils are formed. These outcomes show that each protein sequence can form a spectrum of structurally distinct fibrillar aggregates and that kinetic factors can dictate which of these alternatives is dominant under given circumstances.

18

1.3. Mechanism and conditions for protein fibrillation

The understanding of the mechanism behind protein fibrillation is important in the adequate control of the protein fibrillation process *in vitro*, opening a way to the production of nanometric fibers that might provide valuable applications in material sciences. Much efforts have been dedicated to the study of the mechanism of protein fibrillation in the last decade and some reviews were recently published, providing an overview of historical contributions to the understanding of the kinetics and thermodynamic of protein fibrillation.[67–69]

Fibrillation is widely recognized as a nucleation-elongation process, also known as a "nucleated growth" mechanism.[20,70] A characteristic sigmoidal growth profile for the increase in mass-of-aggregate is observed for a wide range of *in vitro* protein fibrillation phenomena (**Fig. 11**). The time course of the conversion of a peptide or protein into its fibrillar form (measured by ThT fluorescence, light scattering, or other techniques) typically includes a lag phase that is followed by a rapid growth phase, and ending in a plateau phase.[71–73]
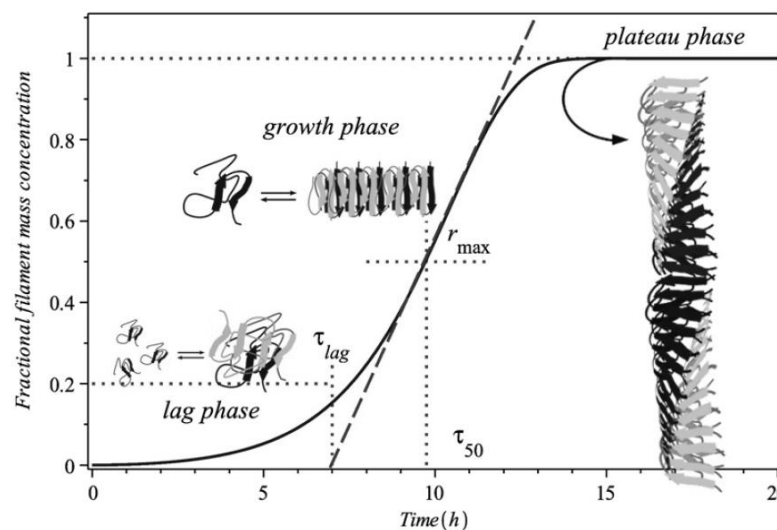
Fig. 11 - The sigmoidal growth profile of protein fibrils mass formation.[70]

The lag phase is assumed to be the time required for "nuclei" to form, during which no measurable aggregation occurs. Once a nucleus is formed, fibrils growth proceeds

rapidly by further association of either monomers or oligomers to the nucleus. The effective growth rate then increases as significant number of aggregates are produced, until a maximum growth rate $r_{máx}$ (s^{-1}) is reached at the inflection point (**Fig. 11**). Such a nucleated growth mechanism has been well studied both experimentally and theoretically in many other contexts, most notably for the process of crystallization of both large and small molecules.[74] In the end, the monomer population is mostly depleted, the reaction rate slows down and a plateau phase characterizes the end point of the process.

As with many other processes dependent on a nucleation step, addition of preformed fibrillar species to a sample of a protein under aggregation conditions ("seeding") causes the lag phase to be shortened and ultimately abolished when the rate of the aggregation process is no longer limited by the need for nucleation.[71] It has been also shown that changes in experimental conditions can also reduce the length of the lag phase.[72,73,75] The absence of a lag phase does not necessarily imply that a nucleated growth mechanism does not take place, but it may simply be that the time required for fibril growth is sufficiently slow relative to the nucleation process and that the latter is no longer the slowest step in the conversion of a soluble protein into the amyloid state. Although fibrils do not appear to a significant extent during the lag phase, it is increasingly clear that this stage in fibril formation is an important event in which a variety of oligomers forms, including β-sheet-rich species that provide nuclei for the formation of mature fibrils.

Amyloid fibrils can be obtained under specific conditions and several proteins have been used to unveil the mechanism of amyloid fibrils formation.[76]

Hen egg white lysozyme (HEWL) has been widely used as a model protein in *in vitro* fibrillation studies, and the influence of a variety of conditions,[77] including pH of the media (using acidic[78,79] or alkaline[80,81] solutions), temperature,[82–84] high pressure,[85] and the addition of sodium azide,[86,87] urea[88,89] or ethanol,[90] in fibrillation induction have been researched. The study of *in vitro* HEWL´s fibrillation process has facilitated the development of drugs targeted against amyloidosis, and numerous studies now focus their attention on fibril formation inhibition.[91,92]

Apart from HEWL, other proteins have also been studied. For instance, the globular milk protein β–lactoglobulin can generate amyloid fibrils under certain conditions as low

20

pH (~2), low ionic strength (I<20 mM) and high temperature (>80 ºC)[93,94], with usually 2-10 mg mL^{-1} of protein concentration. Loveday *et al.*[95] studied the temperature effect on the fibrillation kinetics, concluding that in the temperature interval from 75 ºC till 120 ºC fibrillation kinetics is strongly affected by temperature, reducing the lag phase and accelerating the fibrillation, especially between 75 and 80 ºC. However, these results showed that temperature has little influence in the fibril morphology, except that prolonged heating at 120ºC fractures fibrils.[95] Loveday and co-workers have also studied the influence of pH and the addition of salts, such as NaCl and CaCl$_2$ in the fibrillation process of β–lactoglobulin.[96] Lowering pH below 2.0, the fibril formation is accelerated during the growth phase and it increases the fibrils formation yield, but has little effect on the duration of the lag phase. pH does not influence the β–lactoglobulin fibrils morphology which is characterized by long, semi-flexible and unbranched fibrils, with some spherical aggregates dispersed (**Fig. 12**). NaCl also accelerates fibril formation during the growth phase without shortening the lag phase. However, the use of CaCl$_2$ accelerates the fibrils growth and shortens the lag phase, being suggested that Ca^{2+} accelerates the nucleation by 'bridging' between two peptides via nucleophilic functional groups. It was also reported that NaCl and CaCl$_2$ alter the fibril morphology, which goes in accordance with another study probing fibrils stability.[97] Increasing the ionic strength of the fibrillation medium promotes conformational changes in the Aβ structure, as the fibril surface becomes more hydrophobic. Moreover, increased ionic strength influences the hydrogen bonding between external and internal layers showing that the energy gain from binding a new layer to the axial fibril ends is significantly greater at conditions of low ionic strength, leading to formation of long and thin fibrils.[97]
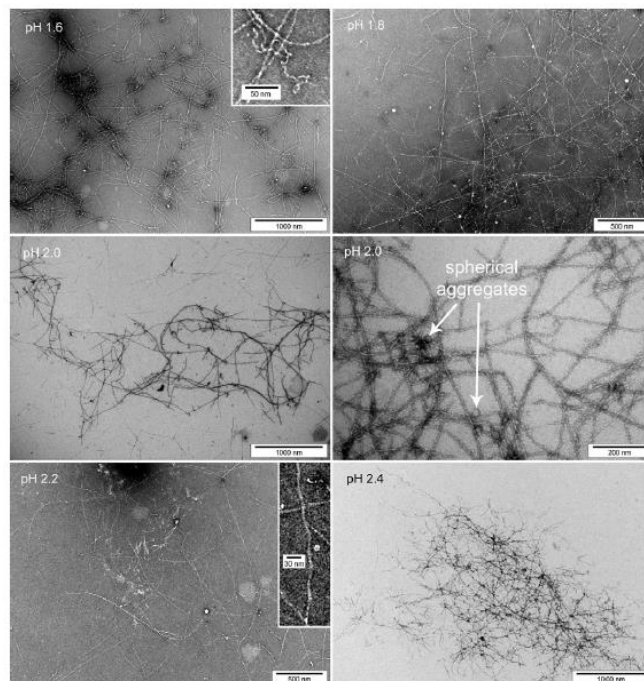
Fig. 12 - TEM images of β-lactoglobulin fibrils prepared at pH 1.6 - 2.4 by heating 1% (w/v) β-lactoglobulin solutions at 80ºC for 6h.[96]

Besides β–lactoglobulin, insulin has also been extensively studied for the preparation of amyloid fibrils.[98,99] For instance, Zako *et al.*[98] dissolved insulin (20 mg mL⁻¹) in 40 mM HCl, at pH 1.5, and then used a 20% acetic acid solution with 100 mM NaCl, at pH 1.6, to dilute it. The insulin solution was then fibrillated by heating at 70 ºC for 13 h, without stirring. ThT fluorescence was measured and fibrils were characterized by TEM (**Fig. 13**). In a similar study,[99] the incubation was taken at 60 ºC for 24 h showed that the 10 ºC increment, from 60 ºC up to 70 ºC, may accelerate the fibrillation of insulin. More recently, Carvalho *et al.*[100] explored a microwave assisted methodology which reduced the fibrillation of insulin from 13 h to 2 h.
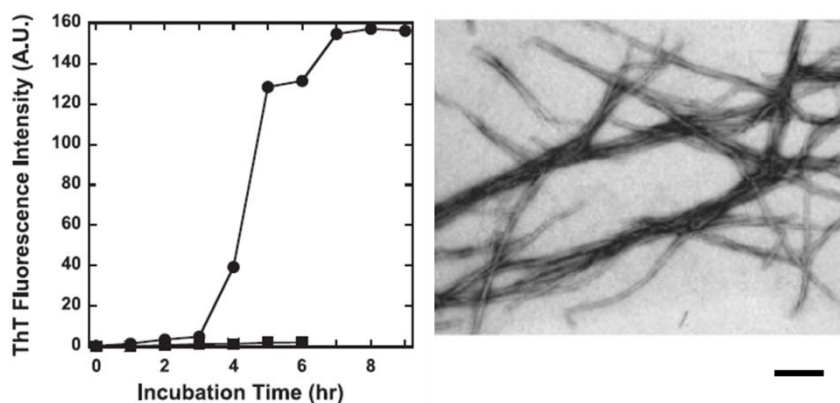
Fig. 13 - Fluorescence measurements of insulin fibrillation during 13 h and a TEM image of the fibrils formed (scale bar 200 nm).*adapted*[98]

Bovine serum albumin (BSA) is another protein that has been fibrillated *in vitro*. Arasteh *et al.*[101] dissolved BSA in 50 mM glycine-HCl solution, taking into account different variables like protein concentration, pH, temperature and time. The optimal fibrillation was obtained at protein concentration of 5 mg mL^{-1}, pH of 3.02 at 72 ℃ and up to 48 h. Most early studies were conducted under acid conditions. However, new insights on BSA fibrillation under alkaline conditions (pH = 8.9), were also reported.[102] It was concluded that at pH values close to the isoelectric point, amorphous aggregates are readily formed due to the lack of electrostatic repulsion. However, at pH values different from isoelectric point, the larger repulsion between molecules slows down the aggregation, leading to protein rearrangement in defined β-sheet amyloid fibrils.[102]

In a more recent study, Pan and Zhong[103] have used intrinsically disordered α-, β-, and k-caseins to study the formation of amyloid-like fibrils at pH = 2 and 90 ℃. No fibrils were observed for α-caseins, and acid hydrolysis was found to be the rate-limiting step of fibrillation of β- and k-caseins. Nanomechanic analysis of the obtained amyloid-like fibrils, using peak-force quantitative nanomechanical atomic force microscopy, showed a Young's modulus of 2.35 ± 0.29 GPa for β-casein and of 4.14 ± 0.66 GPa for k-casein. The β-casein fibrils dispersion had a viscosity more than 10 and 5 times higher than those of k-casein and β-lactoglobulin, respectively, at comparable concentrations.[103]

As already pointed out, most of these studies highly contributed to the understanding of the protein fibrillation process and consequently to the development of new treatments against amyloidosis. Concerning the potential use of these fibrils in the material field, one of the major limitations is the time required to obtain the fibrils, since most of the fibrillation procedures developed so far can take days, weeks and even months.[87,89,90] During the last years, different fibrillation procedures have been developed for the production of fibril-based materials and the fastest procedures usually take 8-15 h.[81,88] To the best of our knowledge, besides the use of microwave assisted methodology for insulin,[100] only one work[104] reported the production of lysozyme fibrils in less than 3h, through the use of guanidine hydrochloride as an amyloid inducer. However, the fibril dimensions in terms of length are a bit short (~300 nm) comparing to other studies where fibrils of around 1μm of length or even higher were obtained.[105–107]

An interesting breakthrough in the protein fibrillation was achieved using ionic liquids and it will be described in the next section.

1.3.1. Ionic Liquids for Protein Fibrillation

According to the commonly accepted definition, ionic liquids (ILs) are entirely composed of ions (organic cations and either organic or inorganic anions), which have melting points below the conventional temperature of 100 °C. Ionic liquids comprise an exceptional combination of intrinsic properties, such as negligible volatility, thermal stability, low flammability, high ion conductivity and what is more important their properties can be easily tuned by the judicious choice of cations and anions. As solvents, the most significant advantages include their non-volatility, good solvating properties, variable polarity range, which are normally associated with their environmentally "green" label.[108–110]

Ionic liquids have been used in several fields, including life sciences. They have been shown to stabilize and solubilize proteins, and to increase enzymatic activities.[109,111,112] Another interesting breakthrough on the application of ILs in this domain has been the promotion of proteins fibrillation. The use of ILs to adjust the fibrillation process and to stabilize different amyloid species opens perspectives of probing

protein conformational states and exploring new protein-solvent interactions. Both protic[113–117] and aprotic[116,118–120] families of ILs, have shown to be of value in the promotion of protein conformal states leading to the formation of fibrils. The use of aprotic ILs is reasoned based on their hydrogen bonding interacting capacity, while protic ILs use is based on their proton transfer ability, as a mean to control the effective acidity of the medium.

A couple of works have been done using model proteins such as hen egg white lysozyme (HEWL),[113,117,120] α-lactalbumin, trypsin and insulin.[120] For instance, Bae *et al.*[120] showed that diluted (5 wt.%) solutions of 1-*n*-butyl-3-methylimidazolium [C$_4$mim]-based ILs (with different anions) can effectively trigger amyloid fibril formation of α-lactalbumin, HEWL, trypsin and insulin. Briefly, protein solutions (1 mg mL^{-1}) were incubated in 20 mM glycine buffer (pH = 2.0) in the absence and presence of ILs at a ratio (v/v) of 1, 2 and 5%, with constant magnetic stirring at room temperature,[121] and amyloid fibril formation was monitored by the ThT fluorescence assay along the experiment. As shown in **Fig. 14**, the ILs [C$_4$mim][BF$_4$], [C$_4$mim][(CF$_3$SO$_2$)$_2$N] and [C$_4$mim][PF$_6$] were tested in the fibrillation of α-lactalbumin, and ThT measurements indicate that amyloid fibrils were effectively formed in 2-5 days.
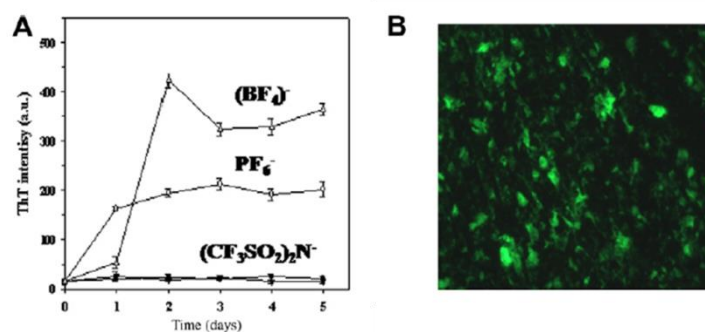
Fig. 14 - Amyloid fibril formation of α-lactalbumin with [C4mim]-based ionic liquids. (A) ThT fluorescence as a function of time of α-lactalbumin in the absence and presence of [C$_4$mim][BF$_4$], [C$_4$mim][(CF$_3$SO$_2$)$_2$N] and [C$_4$mim][PF$_6$]. (B) Fluorescence image of ThT-stained α-lactalbumin amyloid fibrils with [C$_4$mim][BF$_4$].*adapted*[120]

Although both the absence of any IL or the presence of [C$_4$mim][(CF$_3$SO$_2$)$_2$N] does not promote effective protein fibrillation, the use of [C$_4$mim][BF$_4$] and [C$_4$mim][PF$_6$]

ILs was successful in amyloid formation, as observed using ThT assays. In terms of the ILs anions ability to form amyloid fibrils, the order was shown to be BF_4^- > PF_6^- > $(CF_3SO_2)_2N^-$. Moreover, this study showed that the morphology and the properties of the aggregates can be modulated depending on the chemical structure of the IL and pH.[120]

The slow fibrillation process of α-synuclein, a small cytoplasmic protein, whose amyloid fibrils are known to be a critical step in Parkinson´s disease development, is a major obstacle to the development of therapeutic compounds to regulate its amyloid formation. In order to accelerate this process, Hwang *et al.*[118] used ILs to act as stimulators for α-synuclein fibrillation. Briefly, 5 and 10 wt.% solutions of ILs with different cations and anions were added to a α-synuclein solution (1.0 mg mL in 20 nM Tris-HCl, pH = 8), followed by continuously stirring at room temperature. Because of the slow process of formation of α-synuclein amyloid fibrils, these strategies can contribute to better understand the amyloid fibrils formation. Furthermore, using a series of ILs based on the imidazolium cation, with different alkyl chain lengths, combined with different anions, these authors concluded that the IL [C_4mim][$(CF_3SO_2)_2N$] (**Fig. 15** – IL-2) showed the most promising results, followed by its cation-ILs C_2mim$^+$ (**Fig. 15** – IL-1) and C_6mim$^+$ (**Fig. 15** – IL-3) respectively, while [C_4mim][BF_4] (**Fig. 15** – IL-9) seems to have no effect on the α-synuclein fibrillation. These results are contrary to the previous study conducted by Bae *et al.*[120], who suggested that protein fibrillation is strongly dependent on the chemical nature of the ILs and structure composition of the proteins.
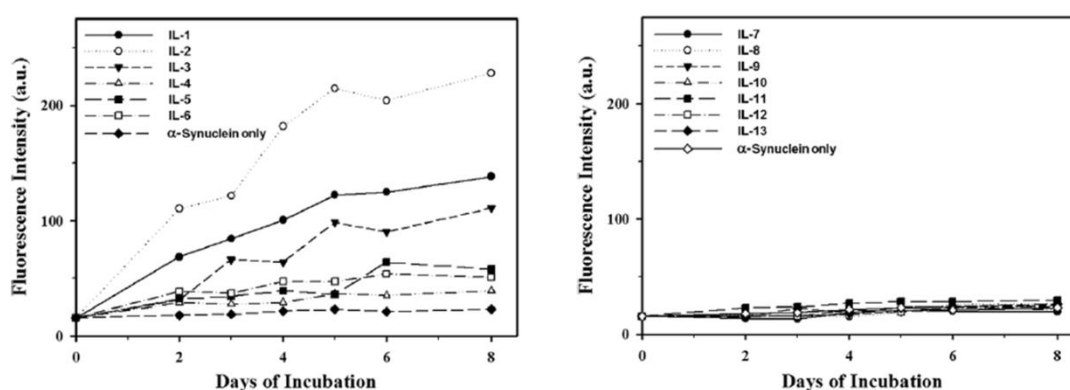
Fig. 15 - Kinetics of α-synuclein fibril formation using different ionic liquids and monitored by ThT fluorescence.[118]

On the other hand, Debeljuh *et al.* in a sequence of studies using Aβ(1-40)[114] and Aβ(16-22),[115] showed that solutions of some protic ILs, such as triethylammonium methanesulfonate (TeaMs), can promote protein fibrillation, as it can be seen by the presence of long flexible fibrils in TEM images in **Fig. 16**, supporting the existence of β-sheet secondary structures as measured by CD and ThT.
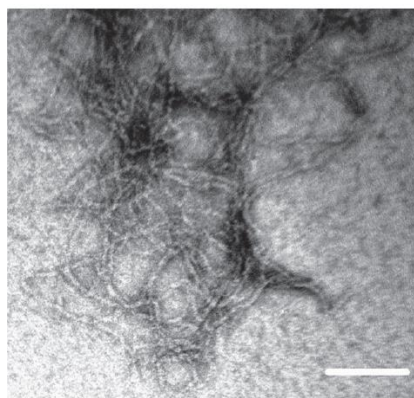
Fig. 16 - TEM image of amyloid fibrils from Aβ(1-40) induced by protic IL solution containing 10 wt.% TeaMs.[114]

In addition, Debeljuh and coworkers[114,115] have also shown that concentrated solutions of some protic ILs can induce α-helixes, another type of secondary structure of proteins, formation through the alteration of the natural hydrogen bonding in peptides. The mechanism by which these protic ILs can alter the hydrogen bonding nature of the peptide is the result of the unique hydrogen bond network system of the protic ILs. This ability of TeaMs to induce an α-helix structure are not limited to TeaMs alone, since studies using other similar ILs such as ethylammoniummesylate (EaMs), propylammoniummesylate (PropMs), ethylammonium nitrate (EaN) and triethylammonium trifluoromethanesulfonate (TeaTf) lead to the same conclusions.

Despite the potential of ILs to promote protein fibrillation, they can also be used to reduce amyloid formation. For example, Kalhor *et al.*[113] reported the use of very diluted solutions (µM) of protic ILs such as tetramethylguanidinium acetate to *in vitro* inhibit or reduce the amyloid formation of HEWL (**Fig. 17**). Partial unfolded HEWL is converted into intermediates and subsequently into protofibrils and amyloid fibrils. When the protein

is exposed to the IL, the oligomers are formed but part of them is specifically trapped by the IL, leading to fewer protofibrils, as illustrated in **Fig. 17**.
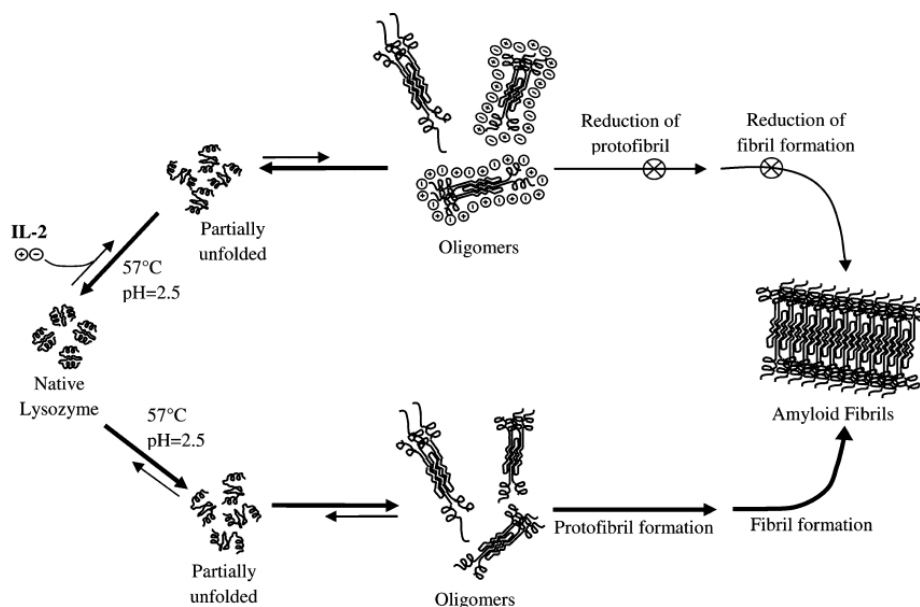
Fig. 17 – Schematic diagram of a proposed mechanism of HEWL fibril inhibition by tetramethylguanidinium acetate (IL-2).[113]

In a different vein, Byrne and Angell[117] used protic ammonium-based ILs with different anions to study the impact of these solvents on the ability to promote the re-dissolution of fibrillated HEWL, at room temperature, restoring a substantial part of the pristine protein enzymatic activity. The most remarkable result was obtained with the very fast re-dissolution of fibrils formed in an ethanol solution with EaN, restoring up to 72% of the protein bioactivity.

Although the exact mechanism of protein fibrillation in ILs is still debatable, it is generally accepted that the nonpolar to polar balance of these solvents is an important parameter in the disruption of the intramolecular hydrogen bonds, which are essential for β-sheets formation. Additionally, it will be fundamental to choose more "green ILs" among the many ILs available.

1.3.2. Potential use of DES for Protein Fibrillation

Very recently, deep eutectic solvents (DES) have been gaining much attention as versatile alternatives to ILs.[122] DES can be regarded as a new generation of solvents composed of a mixture of two or more compounds, where one of them is a salt. The formation of these new liquids at room temperature is due to the establishment of hydrogen bonds between a hydrogen bond donor (HBD) and a hydrogen bond acceptor (HBA), usually a halide anion present in the salt.[123–125] The most popular DESs used so far are those based on cholinium chloride (used as HBA) because of its low cost, low toxicity, biodegradability and biocompatibility, since it is considered an essential nutrient, which can be extracted from biomass, and often regarded as a part of the B-complex vitamins.[126] Cholinium chloride has been combined with several classes of HBD such as renewable polyols, carbohydrates, amides, amines, alcohols and carboxylic acids.[127] DES share many of the ILs appealing features, such as low volatility, high thermal stability and conductivity, wide liquid range and high solvation capacity[128–130] and possess other interesting advantages over ILs: they are usually easier to synthesize, since the components are easily mixed without any further purification; they have low production cost due to the low price of starting materials; and most of the synthesized DES are biodegradable, biocompatible and non-toxic.[130,131] In this way, DES are considered to be cheaper, efficient and greener solutions and they are finding many applications from metal finishing processes[132] up to, more recently, compound extraction and separation media for azeotropic mixtures,[133–136] with reported performances on par or even superior to conventional organic solvents and ILs. However, to the best of our knowledge, protein fibrillation using DES has never been researched before.

1.4. Applications of Protein Fibrils on the Development of Innovative Materials

From the materials perspective, protein nanofibrils are emerging as a unique and novel class of building nanoblocks for the development of innovative functional materials,

like films and scaffolds, because of their exceptional features as high strength and thermochemical stability.[24,137–140]

In fact, protein fibrils have already been extensively studied and used for several applications, such as templates for the synthesis or assembly of several metallic nanoparticles and nanowires,[141–143] as well as other inorganic (micro)nanophases, like hydroxyapatite,[e.g.144–148] fluorapatite,[149] calcium carbonate,[150,151] carbonate apatite,[152] silica[153] and cadmium selenide (CdSe) nanofibers.[154] These brands of functional hybrid nanomaterials found application in biosensors, electronic and energy devices, bioactive membranes and tissue engineering scaffolds, among others.[105]

For example, metal nanowires have been fabricated by assembling proteins such as the N-terminal region of the yeast prion Sup35. Conjugate colloidal gold particles were associated along the fibers using the exposed cysteine of a variant Sup35. Additional metal was deposited by reductive deposition of metallic silver and gold from salts, yielding silver and gold wires of around 100 nm in diameter (**Fig. 18**A).[155] In a different study, a very short peptide, composed of two phenylalanine residues, assembles to form amyloid-like nanotubes. These nanotubes were functionalised by reduction of ionic silver within the nanotubes followed by enzymatic degradation of the peptide backbone (**Fig. 18**B), yielding silver nanowires with around 20 nm in diameter.[156]
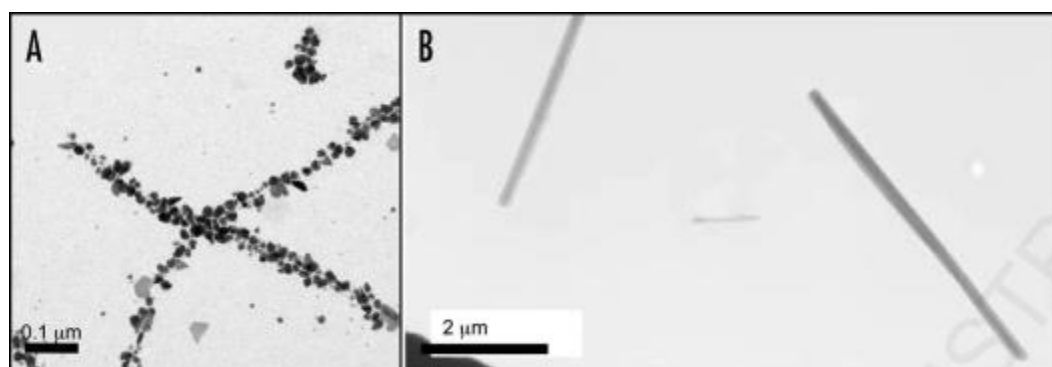
Fig. 18 - (A) Nanowires based on the N-terminal region of the yeast prion, Sup35. Nanogold was covalently linked to the engineered cysteine residues in the protein and conjugate colloidal gold and silver particles were associated along the fibers to form wires,[155] (B) assembly of diphenylalanine to form nanotubes that can be filled with silver to make nanowires.[156]

In a more recent study, amyloid−metal nanoparticle hybrids were developed as efficient active materials for wet catalysis and as membranes for continuous flow catalysis applications.[157] Specifically, amyloid fibrils from β-lactoglobulin were used as templates for the synthesis of gold and palladium metal nanoparticles from salt precursors. The resulting nanoparticle hybrids possess improved catalytic efficiency compared to their counterpart unattached particles, pointing out the role played by the amyloid fibril templates. Filter membranes could then be prepared from the metal nanoparticle-decorated amyloid fibrils by vacuum filtration (**Fig. 19**), and served as efficient flow catalysis active materials with a complete catalytic conversion achieved within a single flow passage of a feeding solution through the membrane.[157]
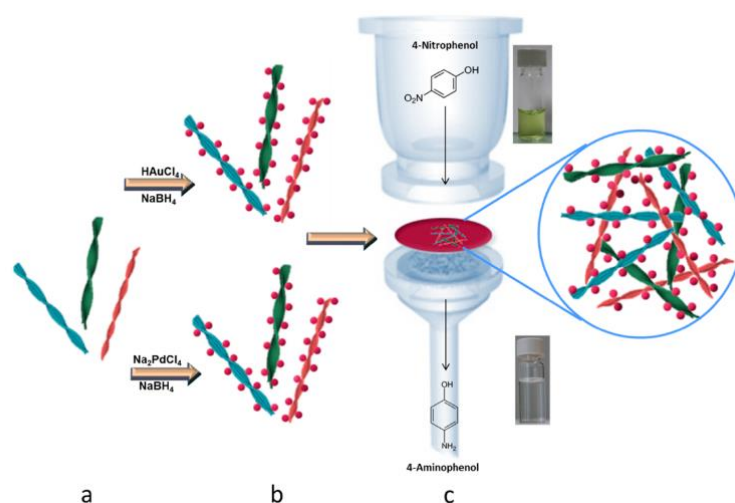
Fig. 19 - Schematic representation of metal nanoparticles-decorated amyloid fibrils and its preparation. (a) β-lactoglobulin amyloid fibrils. (b) Metal nanoparticles (gold and palladium) preparation on the surface of the fibrils by reducing corresponding salts using sodium borohydride. (c) Filter membrane of nanoparticle−amyloid fibrils as efficient flow catalysis active material.[157]

Additionally, a new class of hybrid materials, featuring organic semiconductors augmented by aggregating β-sheet peptide interfaces, have been proposed.[158] The peptides retain their β-sheet forming ability when additional amino acids and linker units were added to manipulate their solubility and coupling with perylene imides. The di-substituted material with peptides extending in the N to C direction away from the perylene core

exhibits strong coupling and long-range order, both attractive properties for electronic device applications.[158]

The combination of nanofibrillated proteins with graphene nanosheets is likewise an elegant strategy for the development of novel functional hybrid materials. Li *et al.*[93] combined graphene and protein fibrils to create responsive, biodegradable and lamellar nanostructures for the design of biosensors. The films were fabricated by vacuum filtration of the graphene dispersions with protein fibrils obtained from β-lactoglobulin.[93,94] The composites produced were highly conductive, can be degraded by enzymes and can reversible change shape in response to humidity variations. Their properties could be fine-tuned by varying the graphene-to-amyloid ratio (**Fig. 20**). In another study, graphene oxide (GO) nanosheets were hybridized through electrostatic interaction with lysozyme nanofibrils and it was constructed a biocompatible immobilization platform (amyloid-GO nanosheets) for enzymes without interfering their catalytic activity.[159] For instance, HRP (Horse- radish peroxidase) as a model enzyme was immobilized on the amyloid-GO nanosheets and a simple sensitive and selective colorimetric method for glucose-detecting was built. This method was considered to be simple, cost-effective and easy-to-make biosensors, and the integration of amyloid fibrils on GO nanosheets offers additional possibilities of their application in the designing and developing of novel biocatalysts.[159]
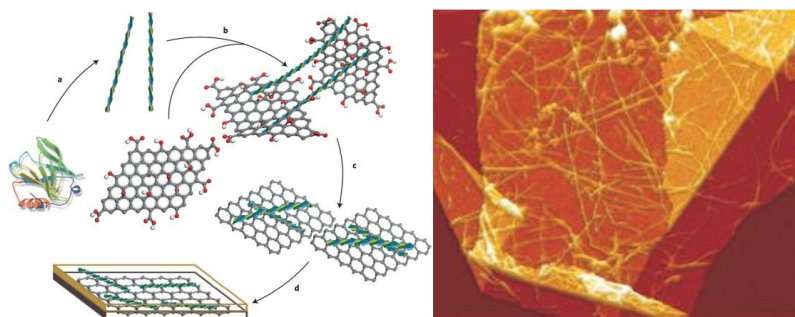
Fig. 20 - Schematic representation showing the fabrication of graphene-amyloid fibrils composite films and AFM image of the graphene-amyloid fibril suspension with 1:5 ratio.[93]

Bolisetty *et al.*[160] reported also a new class of hybrid membranes made from β-lactoglobulin amyloid fibrils and activated porous carbon to remove heavy metal ions and radioactive waste from water, in a more efficient way than current processes, reduction

three to five orders of magnitude per filtration and the process can be repeated numerous times. The performance of the membrane is enabled by the ability of the amyloids to selectively absorb heavy metal pollutants from solutions.[160]

In a completely different vein, several researchers have also explored the mechanical strength of protein nanofibrils as reinforcing elements in nanocomposites with synthetic matrices, namely, poly(L-lactic acid) PLLA,[161] poly(vinyl alcohol) PVOH,[99] and a silicone elastomer.[162] In general, and despite the different methodologies used, the obtained nanocomposites showed significant improvements in terms of mechanical properties. In more detail, a novel nanocomposite was prepared by adding lysozyme amyloid fibrils into a 5 wt.% solution of PLLA in chloroform. Films with 2, 3 and 5% fibrils were prepared. These mixtures were stirred for 48h and then film was casted to obtain fibril-reinforced PLLA composites (**Fig. 21**) with improved glass transition temperature (T_g), elongation at break and Young's modulus.[161] In a similar study, bovine insulin was converted into amyloid fibrils and then combined with PVOH to a final concentration of 0.6 wt.% of fibrils. This methodology reveals to preserve the amyloid fibril structure and to improve the properties of the resulting fibril-reinforced PVOH composite, being 15% stiffer than the PVOH control.[99] In another work, by combining lysozyme fibrils with a silicone elastomer, at a filling ratio of 10 wt.%, the resulting nanocomposite was at minimum two-fold stiffer than a carbon nanotube (CNT) elastomeric counterpart with the same filling ratio.[162]
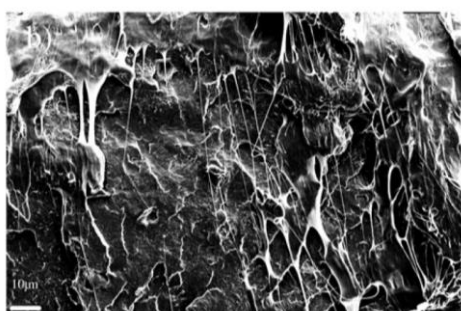
Fig. 21 - SEM image of a fracture surface PLLA film with 5 wt.% of amyloid fibrils.[161]

Using only protein matter, Claunch *et al.*[163] hydrolyzed wheat gluten into low molecular weight proteins that in part self-assemble into high Young's modulus fibers and the rest arrange around the fibers as a polymer matrix so that the total material produces a

fiber-reinforced polymer matrix composite, originating composites with a modulus of 266 MPa, at 37 ℃. In another study, Knowles *et al.*[164] prepared rigid nanostructured thin films from hen egg white lysozyme and bovine β-lactoglobulin fibrils. The films were well ordered and highly rigid, with a Young's *modulus* of up to 5–7 GPa, which is comparable to the highest values for proteinaceous materials found in nature.

Amyloid fibrils have also been explored for the development of composite hydrogels. For instance, Li and Mezzenga[165] reported the development of biocompatible pH-responsive fibrous hydrogels based on β-lactoglobulin amyloid fibrils hybridized and gelled by sulphonated multiwalled carbon nanotubes (MWNTs) (**Fig. 22**), with potential application in drug release, sensors and tissue engineering. The same research group described afterwards the preparation of similar biocompatible thermo-reversible hydrogel injectable scaffolds obtained by decoration of the amyloid fibrils with cross-linked poly(N-isopropyl-acrylamide) (PNiPAM).[166]
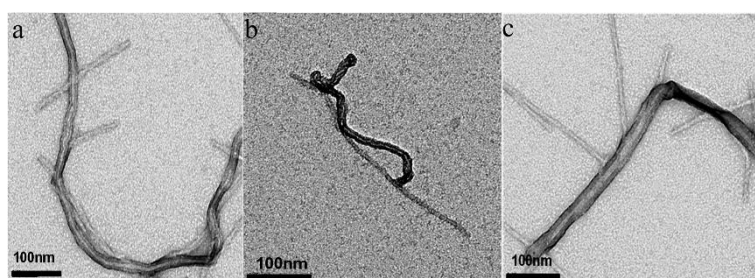
Fig. 22 - TEM images of hybrids consisting of sulphonated MWNTs and amyloid fibrils (*a* and *b*: covalent functionalization; *c*: non covalent functionalization).[165]

Zhang and co-workers developed novel self-complementary β-sheets using alternative oligopeptides that could self-assemble under physiological conditions to form membranes.[167–169] Using a 16-residue peptide and the addition of phosphate salt, the oligopeptide spontaneously assembles to form a macroscopic membrane.[167] This membrane presents thermal stability and does not dissolve in acidic or alkaline solutions, nor upon addition of guanidine hydrochloride, SDS/urea, or a variety of proteolytic enzymes. Because of this unique stability, simple composition, apparent lack of cytotoxicity, and easy synthesis in large quantities, such materials might be useful for biomaterial applications. For instance, these membranes are able to support mammalian cell attachment for prolonged

periods,[170] and to support neuronal cell attachments, differentiation and extensive neurite outgrowth.[171] Such support membranes, or scaffolds, can also be functionalized with different motifs to enhance the formation of confluent cell monolayers of human aortic endothelial cells,[172] or the osteoblast proliferation and migration in bone tissue regeneration.[173] These scaffolds were also coupled directly to short biologically active motifs including osteogenic growth peptides, and the coupled motifs in two different concentrations (10 and 70 wt.%) were further studied to enhance osteoblast proliferation. In the case of the scaffolds with 10% of the active motif, the cells were attached mostly on the surface (**Fig. 23**A) whereas with 70% the cells migrated into the scaffold (**Fig. 23**B), showing the potential use of functionalized fibrils in the composition of scaffolds.[173] More recently, β-lactoglobulin fibrils were cross-linked with butane tetracarboxylic acid and freeze-dried to obtain soft and elastic aerogels. By varying the fibril concentration and freezing gradient, it was possible to control the porosity and the elastic modulus with values from 20 up to 200 kPa. The obtained scaffolds were biocompatible and water stable, making them suitable for wet stable applications as purification membranes or 3D matrices for cell growth.[174] Fibrils from hen egg white lysozyme were also studied as cell growth network platforms.[175] Retinal pigmented epithelium (RPE) cells were cultured on lysozyme fibrils network platforms which provided a long-term viability and proliferation without a significant production of reactive oxygen species, turning these fibrils excellent candidates as building blocks for retinal tissue engineering materials.[175]
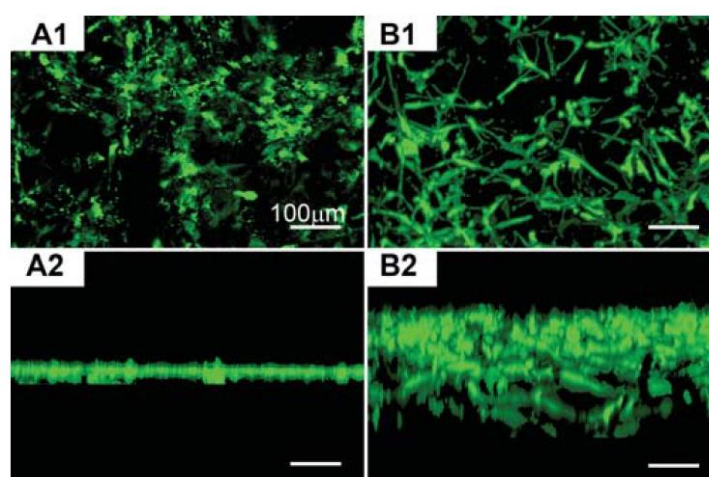
Fig. 23 - Reconstructed image of 3-D confocal microscope image of culturing on the different scaffolds functionalized with a specific motif in 10% (A1, A2) and 70% (B1, B2),

using calcein-AM staining. A1 and B1 are vertical view and A2 and B2 are horizontal view. The bar represents 100 mm.[173]

Sakono et al.[176] demonstrated that different morphologically amyloid fibrils from insulin can also be used as biomaterials for cell culture, in which insulin amyloid-coated dishes showed higher cell adhesion and cell proliferation ability compared to non-coated dishes. Furthermore, functionalised amyloid fibrils with bioactive ligands for cell adhesion, corresponding to residues 105-115 of the amyloidogenic protein TTR, were also developed revealing that amyloid fibrils can be used as promising bio-scaffolds to be applied in biomedical field.[177] The broad potential of this approach has been explored and illustrated by different studies where fibrils functionalised fibrils with fluorphores,[178] biotin,[179] cytochrome[180] and functional enzymes,[181] were successfully prepared. For instance, Baldwin and co-workers[179] assembled a protein composed of a functional cytochrome b562 with an amyloidogenic SH3 sequence. The assemblies have the amyloid-like core which display functional b-type cytochrome, opening a new perspective of binding functional proteins on an amyloid fibril scaffold.[179] Another step forward is the use of amyloid fibrils in the development of functionalised biomaterials with cell adhesive properties.[139,176] In fact, several bioactive ligands may be used for functionalisation of protein fibrils. One example is the classic Arginine-Glycine-Aspartic Acid (RGD) sequence. This sequence, originally found in the extra-cellular matrix protein fibronectin, is the minimal motif required for cell adhesion.[182]

In another vein, a new type of multi-layered microcapsules for controlled drug release, with tunable strength and permeability were designed by alternating layers of pectin and protein fibrils.[183] The mechanical stability of these microcapsules could be controlled by varying the number of layers or the density and length of the fibrils in the protein layers, producing microcapsules with superior mechanical stability than other available multi-layered capsules. Moreover, Maji et al.[184] suggested the use of amyloid fibrils in the formulation of long-acting drugs. A TEM image of amyloid fibrils of a long-acting gonadotropin-releasing hormone (GnRH) analog is illustrated in **Fig. 24**, with the end of a fibril highlighted. The concept is based on its structural composition as a sequence of β-sheet peptides aligned along the fibril axis by hydrogen bonding, and it was tested with a family of long-acting analogs of GnRH showing that the peptides at the end of the fibril can be released in a slow and controlled way.[184]

36
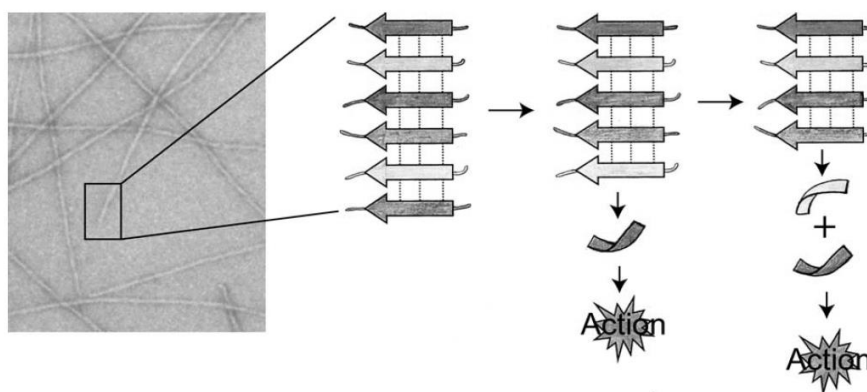
Fig. 24 - TEM image of amyloid fibrils and schematic representation of a long-acting GnRH analog.[184]

Besides this approach where fibrils could release functional peptides from the fibril termini after administration, allowing a controlled release of a monomeric drug (**Fig. 25**A),[185] peptide oligomeric intermediates may similarly be used for auto-delivery of the drugs as suggested for insulin[186] (**Fig. 25**B). Gupta *et al.*[186] harnessed the inherent property of insulin to aggregate into an oligomeric intermediate on the pathway to amyloid formation, to generate a form that exhibits controlled and sustained release of insulin for extended periods. Administration of a single dose of this insulin oligomer, known as the supramolecular insulin assembly II (SIA-II), to experimental animals, rendered diabetic by streptozotocin or alloxan, released the hormone capable of maintaining physiologic glucose levels for 100 days.[186] Amyloid fibrils might also be utilized as vehicles for drug delivery (**Fig. 25**C),[185] wherein the drug molecules (orange spheres) could be entrapped within amyloid networks (violet network) ensuring the slow release of the drugs after administration. **Fig. 25**C shows that the drug release occurs at the target site and that the drug molecule binds to specific receptors on the cell surface to perform its action.
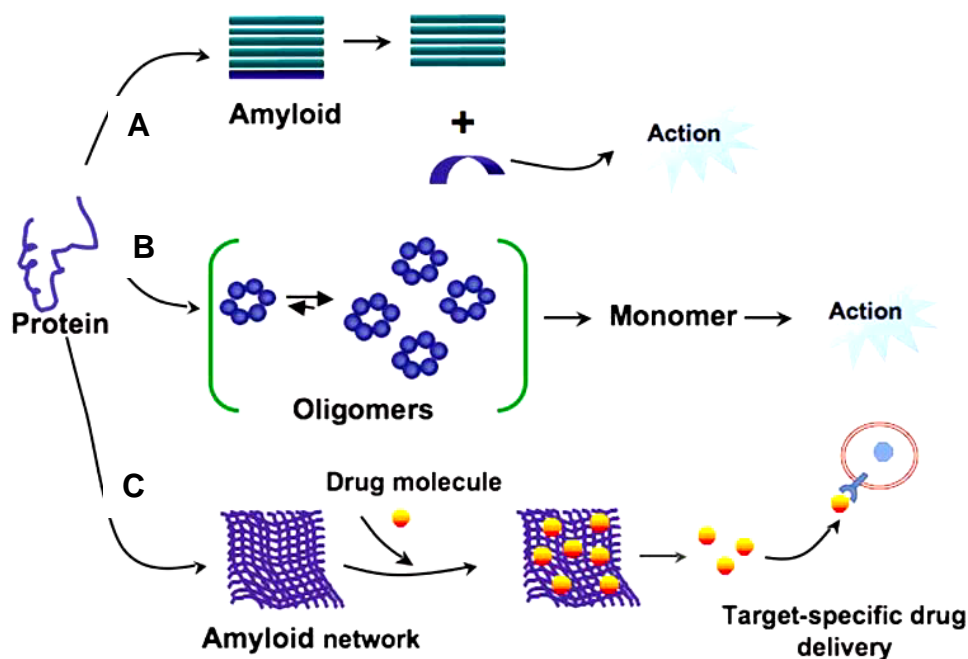
Fig. 25 - Schematic representation of the application of amyloid fibrils for drug delivery.[185]

Recently, Kabay *et al.*[187] developed a controlled drug release platform made of protein fibrils from bovine serum albumin with ampicillin sodium salt. This platform was produced by electrospinning with average diameters of 130-180 nm. Infra-red spectroscopy has demonstrated that the fibers composing the platform could entrap large amounts of ampicillin inside, which was confirmed by the antimicrobial capacity against *Escherichia coli* and *Staphylococcus aureus*.[187]

In a completely distinct vein, Hendler *et al.*[188] described a quite sophisticated bottom–up methodology for the preparation of multifunctional orderly-doped fibrils with desired properties made of protein-dopant/ligand complexes. In summary, in this work a series of β-lactoglobulin protein complexes, with various shaped ligands having different electronic and photo-physical properties, were prepared and structurally characterized. The resulted non-covalent complexes of β-lactoglobulin can function as building blocks for the construction of highly-doped fibrillar structures. These structures exhibited a minimal perturbation in their architecture, as compared to the fibrils formed by β-lactoglobulin. These innovative functional materials could find application as diagnostic materials and optoelectronics components.[188]

These multiple applications in very broad range of areas evidence how versatile the use of amyloid fibrils might be, regarding their unique and interesting properties. However, there is still a vast array of innovative studies to be conducted concerning the potential of protein fibrils, and specially functionalised amyloid fibrils for the design of new materials. Since the purpose is focused on the material science field, these amyloid fibrils will be reported as protein nanofibers in all the following chapters.

1.5. Aim

The main goal of this project was to use alternative solvents, namely ionic liquids and deep eutectic solvents, in the production of protein nanofibers and to develop new functional materials based on these protein nanofibers combined with polysaccharides. Beforehand dissolved, hen egg white lysozyme (HEWL) as a model protein, undergo fibrillation promoted by ionic liquids and deep eutectic solvents in the pursuit for novel and fast fibrillation methods to obtain long and thin nanofibers (Chapter 2). Furthermore, some polysaccharides, such as pullulan and nanofibrillated cellulose were selected as starting polymeric matrices. The idea was to prepare novel materials by combining the different polysaccharides with protein nanofibers and evaluating the mechanical and functional properties of the novel materials (Chapter 3).

<div align="right">

2.

</div>

Production of Protein Nanofibers

Protein nanofibers are undoubtedly promising building nanostructures to be studied and applied in the material science field. Most of the current procedures to obtain these nanofibers are time-consuming and thus there is a need to search for novel and fast procedures. Bear in mind that the use of ionic liquids presents major advantages such as their tunnability, which is immediately translated in a huge number of ILs that can be explored to fibrillate proteins into nanofibers. The formation of protein nanofibers using ILs follows established procedures that normally include a step of dissolution of the proteins followed by the fibrillation stage, promoted by the addition of a specific IL. Very recently, deep eutectic solvents (DES) have been gaining much attention as versatile alternatives to ILs,[122] and they will also be considered as fibrillation solvents. This part of the work originated 3 papers that correspond to the 3 sub-chapters that are highlighted bellow.

2.1. Potential use of different ionic liquids to promote a faster lysozyme fibrillation

Silva, NHCS; Pinto, RJB; Ferreira, R ; Correia, I ; Freire, CSR; Marrucho, IM (2017) *Potential use of different ionic liquids to promote a faster lysozyme fibrillation*, submitted.

2.2. Production of lysozyme nanofibers using a deep eutectic solvent

2.3. Tuning lysozyme nanofibers dimensions using deep eutectic solvents for improved reinforcement ability

2.1.

Potential use of different ionic liquids to promote a faster lysozyme fibrillation

Nuno H. C. S. Silva,[a,b] Ricardo J. B. Pinto,[a] Rita Ferreira,[c] Isabel Correia,[c]

Carmen S. R. Freire,[a] Isabel M. Marrucho[d]

[a] CICECO Aveiro Institute of Materials and Chemistry Department, University of Aveiro, Campus de Santiago, 3810-193 Aveiro, Portugal

[b] Instituto de Tecnologia Química e Biológica António Xavier, Universidade Nova de Lisboa, Av. República, Ap. 127, 2780-901 Oeiras, Portugal

[c] QOPNA, Department of Chemistry, University of Aveiro, Campus de Santiago, 3810-193 Aveiro, Portugal

[d] Centro de Química Estrutural, Instituto Superior Tecnico, Universidade de Lisboa, Avenida Rovisco Pais, 1049-001 Lisboa, Portugal

Abstract

Protein nanofibers are gaining much attention due to their unique mechanical strength, thermal stability and functional properties, thus promoting the research on new preparation methodologies. Most fibrillation processes developed so far are time consuming, usually taking from 8 h to 15 h, which represents a major drawback in their use. The use of alternative solvents, such as ionic liquids (ILs), as fibrillation agents has been recently reported with considerable reduction in the fibrillation time. This fact encouraged us to study the fibrillation of hen egg white lysozyme (HEWL) in the presence of several ILs from the two different families, those based on imidazolium and cholinium cations combined with different anions derived from organic acids. The properties of the obtained protein nanofibers were studied using UV-vis and fluorescence spectroscopy, electrophoresis, circular dichroism and electron microscopy.

All ILs used were shown to fibrillate HEWL within a few hours, generally achieving conversion ratios over 70-80%. Typically, worm-like nanofibers were obtained, with 0.3-1 µm of length and 15-40 nm of width, depending on the ILs used. Furthermore, the presence of the acetate anion increases the ability of HEWL to form β-sheet structures. These results show that the use of specific ILs can accelerate the formation of long and thin HEWL fibrils that can be used in multiple applications in the bionanotechnological field.
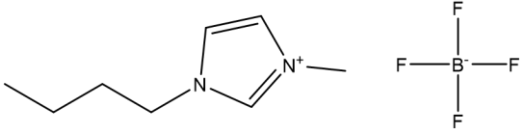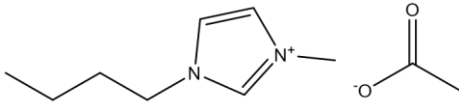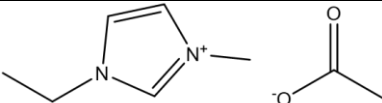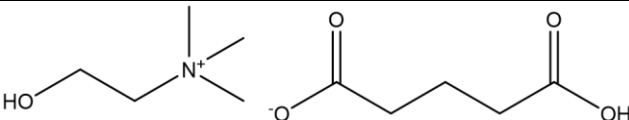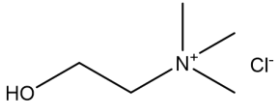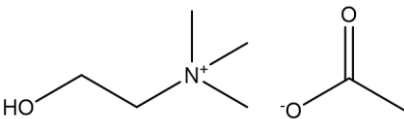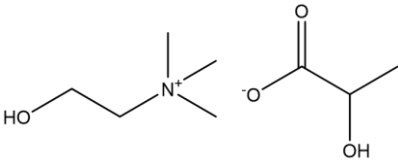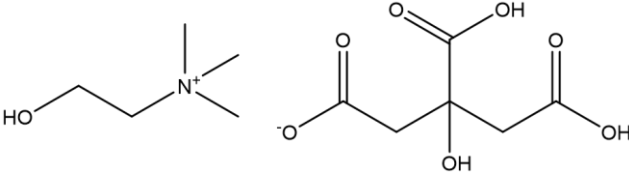
Introduction

Until recently, the study of protein nanofibers, mostly known as amyloid fibrils, assembly mechanism and structure has been clearly associated with the need to understand protein misfolding disorders, including several neurodegenerative disorders, such as Alzheimer's, Parkinson's, Huntington diseases, amyotrophic lateral sclerosis and also other diverse systemic disorders such as type 2 diabetes.[189] Amyloid fibrils are highly ordered, unbranched, self-assembling, insoluble protein fibers of aligned cross-β structures, which are due to the misfolding of variable size proteins. Despite the clear association of protein nanofibers with protein misfolding disorders, many other functional amyloids are at the basis of vital phenomena such as cell adhesion,[177] cytoprotection,[190–192] regulation[193] and secretory granules.[23,24] In fact, amyloid fibrils seem to be ubiquitous in the biological kingdom since they can be found in plants,[194] fungi,[195] and bacteria[196,197] as well as in mammals.[140,177,193] In addition, amyloid fibrils share structural similarities and assume singular mechanical properties comparable to spider silk.[28] The growing interest that protein nanofibers have been getting in the bionanotechnology field and their emergence as a unique class of building nanoblocks for the preparation of innovative functional nanocomposites is due to their exceptional features, such as high strength and thermochemical stability. In fact, protein nanofibers can be combined with other polymers as reinforcing elements of synthetic matrices, namely poly(lactic acid) PLLA,[161] poly(vinyl alcohol) PVOH,[99] or cellulose to form reinforced blend fibers.[198] These nanofibers have also been explored as templates for the controlled synthesis of metal nanotubes.[156] For instance, protein nanofibers, resulted from the self-assembly of a short peptide, were functionalised with silver. After an enzymatic degradation of the peptide backbone, silver nanotubes with 20 nm of diameter were obtained.[156] In a different line, Li and Mezzenga[165] reported the development of biocompatible pH-responsive fibrous hydrogels based on fibrils hybridized and gelled by sulphonated multiwalled carbon nanotubes, with potential application in drug release, sensors and tissue engineering. These functional hybrid nanomaterials find application in many fields as biosensors, electronic and energy devices, bioactive membranes and tissue engineering scaffolds.[105]

Several proteins have been used to produce protein nanofibers.[76] Among them, insulin,[99,100] β-lactoglobulin[96,199] and lysozyme[77,84] have been the most used. Hen egg white lysozyme (HEWL) has been extensively used and the influence of different fibrillation conditions as pH,[78,79] temperature,[82–84] and the mixture with another compounds[87,88] and solvents,[90] have been thoroughly investigated. In particular, the time needed to obtain these nanofibers has been a challenging issue, since the fastest fibrillation procedures take several hours and even days.[81,88] Ionic liquids (ILs) and deep eutectic solvents (DES) have also been investigated within the fibrillation process, showing that these families of alternative solvents can be explored to obtain stable protein nanofibers.[114,115,118,120,200] For instance, Debeljuh *et al.*[114,115] showed that some protic ILs, such as triethylammonium methanesulfonate, in concentrations below 50 wt%, can promote protein fibrillation of some Alzheimer´s disease peptides, generating long flexible fibrils after one week of incubation. Although the exact mechanism of protein structure induction is still debatable, it is generally accepted that the nonpolar to polar balance of these solvents is an important parameter in the disruption of the protein intramolecular hydrogen bonds, which are essential for beta sheets formation.[20] Furthermore, Bae *et al.*[120] demonstrated that the presence of specific ILs creates a hydrophobic ionic media that induces the formation of amyloid fibrils of α-lactalbumin. Diluted (5 wt%) solutions of 1-butyl-3-methyl imidazolium ([C$_4$mim])-based ILs combined with different anions, like tetrafluoroborate [BF$_4$]$^-$, hexafluorophosphate [PF$_6$]$^-$ and bis(trifluoromethanesulfone)imide [(CF$_3$SO$_2$)$_2$N]$^-$ were used to promote amyloid fibrils in a couple of days.[120] Although no protein fibrillation occurred in the presence of [C$_4$mim][(CF$_3$SO$_2$)$_2$N], the use of [C$_4$mim][BF$_4$] and [C$_4$mim][PF$_6$] was effective in the formation of protein nanofibers. In addition, the morphology and properties of the aggregates could be modulated depending on the chemical structure of the IL and pH. In the present work, the use of ILs for protein fibrillation was explored. Two different families of cations were used: 1-alkyl(C4,C2)-3-methyl imidazolium-based ILs which are the most widely studied ILs and cholinium-based ILs, that are considered as a newer generation of non-toxic, biocompatible and cheaper ILs. These two families of cations were combined with different anions derived from organic acids. The only exception is the use of [BF$_4$]$^-$ anion, which was reported before to be highly efficient in protein fibrillation[120] and it is used here for comparison. The chemical structures and acronyms of the ILs used in this work as possible promoters of HEWL fibrillation are depicted in Table 1. The protein fibrillation was analysed and

46

characterized through different techniques. UV-vis spectroscopy and sodium dodecyl sulphate polyacrylamide gel electrophoresis (SDS-PAGE) were used to confirm the fibrillation of the native protein and conversion efficiency into protein nanofibers. Fluorescence microscopy was used to measure the presence of β-structures. Furthermore, the secondary structure of HEWL protein in suspension was determined by Circular Dichroism (CD). CD has been used in studies of protein folding and stability assays, intermolecular interactions and ligand binding studies. Proteins can form diverse aggregates of various sizes and morphologies (amorphous aggregates, oligomers, protofibrils, amyloid fibrils, among others) which have distinct properties and effects depending on the external conditions. Thus, it is very important to study the secondary structure of the HEWL nanofibers since it provides fundamental information for their application. Electron microscopy, both scanning and transmission, permit us to study and characterized the nanofibers produced in terms of morphology and dimensions.

Table 1. Chemical structures and acronyms of the ILs used in this work.

ILs		Chemical Structures
[C$_4$mim][BF$_4$]	1-butyl-3-methyl-imidazolium tetrafluoroborate	
[C$_4$mim][Ac]	1-butyl-3-methyl-imidazolium acetate	
[C$_2$mim][Ac]	1-ethyl-3-methyl-imidazolium acetate	
[Ch][Glu]	cholinium glutarate	
[Ch]Cl	cholinium chloride	
[Ch][Ac]	cholinium acetate	
[Ch][Lac]	cholinium lactate	
[Ch][Cit]	cholinium citrate	

Experimental Details

Preparation of Protein Nanofibers

For each IL, lysozyme from hen egg white (Fluka, ~70000U/mg), was dissolved (2 mg/mL) in an aqueous solution of 10 mM HCl at pH = 2 with 20 mM glycine (Sigma-

Aldrich, ≥98,5%) with 5% (v/v) of the respective IL. The samples were incubated at controlled temperature of 70 ± 3 ºC using an oil bath, and magnetic stirring. Triplicates of each sample were carried out so that standard deviations can be calculated. The obtained protein nanofibers were separated from the ILs solution by centrifugation at 15000 rpm, during 45 min, using a Megafuge 16R centrifuge (Thermo Scientific). The supernatant was discarded, and the obtained nanofibers were washed twice with Milli-Q ultrapure water.

UV-vis analysis

The concentration of HEWL in the supernatant of the incubated samples was determined by UV spectroscopy at 276 nm, using a UV-1800 spectrophotometer (Shimadzu, Kyoto, Japan), and a previously established calibration curve, where $Abs_{276nm} = 2.39[HEWL]_{mg/mL} - 0.0012$ ($R^2=0.9994$).

Fluorescence analysis (ThT assays)

Thioflavin T (ThT) (Sigma-Aldrich) was used to quantify the presence of misfolded protein aggregates. The ThT assay measures changes in fluorescence intensity of ThT upon binding to protein nanofibers. To evaluate the progress of the formation of protein fibrils with time a solution of 2.5 mM Thioflavin T – ThT (Sigma-Aldrich) in 10 mM phosphate buffer, pH = 7.4, was used. 30 µL aliquots of the incubated solution were taken at specific time intervals and 3 mL the Thioflavin T – ThT solution was added. Fluorescence measurements were carried out at 25 ºC using quartz cells on a Horiba Jobin Yvon Fluoromax-3 fluorimeter. The excitation wavelength used was 440 nm and the emission was measured at 482 nm, with both slits of 5 nm. The percentage of fluorescence was calculated according to the maximum fluorescence intensity value (100% fluorescence) registered for each assay.

SDS-PAGE

10 µL of each sample was diluted 1:2 in loading buffer (4% sodium dodecyl sulphate (SDS), 15% glycerol, 20% mercaptoethanol, 0.125 M Tris pH 6.8, 1 mg.mL bromophenol blue) and then separated by electrophoresis following the procedure described by Laemmli.[201] The stacking gel consisted of 4% acrylamide: *N,N'*-methylene-bis-acrylamide (37.5:1), 0.1 M Tris-HCl (pH 6.8), 0.1% SDS (sodium dodecyl sulfate). The separating gels were composed of 15% acrylamide-bis (37.5:1),

0.375 M Tris-HCl (pH 8.8) and 0.1% SDS. Polymerization was initiated with 0.05% *N,N,N',N'*-tetramethylethylenediamine and 0.05% ammonium persulfate. The gel was run in a Mini-Protean system (Bio-Rad) at 180 V (constant voltage) for 1 h. After stained with Coomassie Blue, the gel was scanned in Molecular Imager Gel Doc XR+System (Bio-Rad) and analysed with Image Lab software (v4.1, Bio-Rad). Data were observed as optical density of gel bands (arbitrary units), and the results were expressed as percentage of HEWL prepared in MilliQ.

Circular Dichroism (CD)

Circular dichroism (CD) spectra were recorded in the far UV range from 250 to 190 nm with quartz Suprasil® CD cuvettes (0.1 cm) at room temperature (*ca*. 25ºC) using a JASCO J-720 spectropolarimeter (JASCO, Hiroshima, Japan) with a 180–700 nm photomultiplier (EXEL-308). The initial samples were diluted with Millipore water until a spectrum with appropriate intensity could be obtained. Each CD spectrum is the result of three cumulative runs. The following parameters were used in data acquisition: data pitch - 0.1 nm; bandwidth - 2.0 nm; time response – 2 s and scan speed – 100 nm/min.

Scanning transmission electron microscopy (STEM)

STEM images were obtained using a field emission gun (FEG) SEM Hitachi SU70 microscope operated at 15 kV. Samples were prepared by immersing a carbon-coated copper grid into the protein nanofibers suspension, and then allowing the solvent to evaporate overnight. The average dimensions of the nanofibers were determined by analysis of STEM images using the ImageJ program (at least 100 nanofibers were analysed in each case).

Transmission electron microscopy (TEM)

Transmission electron microscopy (TEM) was performed with a Hitachi H-9000 microscope operating at 300 kV. The samples for TEM were prepared by depositing an aliquot of the suspension of lysozyme nanofibers onto a carbon-coated copper grid and then allowing the solvent to evaporate.

Results & Discussion

HEWL fibrillation using ionic liquids

The HEWL fibrillation using several ILs was firstly evaluated by the ThT assay. The chemical structures and acronyms of the ILs are presented in Table 1. In this work, HEWL was added to 5% (v/v) aqueous solutions of each IL. Samples were taken at specific time intervals and the formation of protein nanofibers was indirectly measured by the fluorescence of ThT dye. Fig. 1 shows the results for the fibrillation of HEWL in the presence of each one of the ILs, expressed as the intensity of the thioflavin T fluorescence (482 nm), as a function of time.
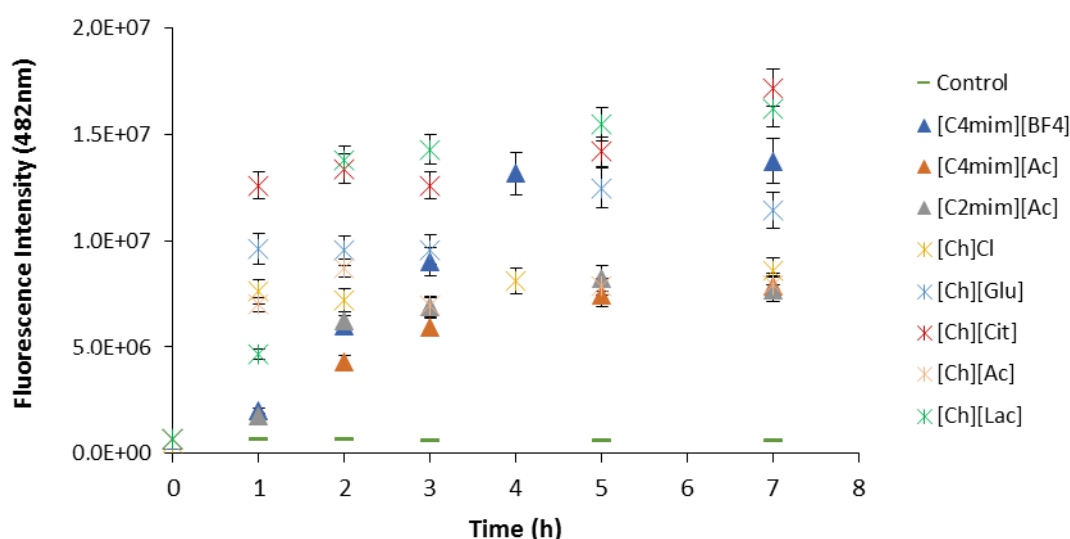
Fig. 1 - ThT fluorescence intensity as a function of time for β-structures produced for each one of the IL used. The experiments were carried out using 5% (v/v) solutions of ILs at 70 ºC and pH = 2.

Generally, there is an increase in the ThT fluorescence intensity values with time for all the ILs used, reaching in 5 h more than 90% of the maximum fluorescence intensities registered for each case. After 5 h, no significant increase in the ThT fluorescence intensity was observed until the end of the experiment (24 h). Comparing the results obtained for the two families of cation cores, in general all the cholinium-based ILs promote higher fluorescence intensities than the imidazolium-based ILs, at any given time. Cholinium-based ILs reached the maximum values of ThT fluorescence intensities in 1-2 h, while for imidazolium-based ILs 3-4 h are needed to reach a similar

value. Compared to other fibrillation strategies described in literature, using the addition of urea[88,89] or ethanol,[90] these results clearly show that ILs are very effective in promoting protein fibrillation. A direct comparison between the two families of cation cores can be established using [C$_2$mim][Ac] and [Ch][Ac]. Although no major differences can be observed between fluorescence intensity for the assays of these two ILs at 5 h, in the first hour of fibrillation [Ch][Ac] promotes higher fibrillation (88.3 ± 4.3% in respect to the maximum obtained at 7 h) than [C$_2$mim][Ac] (22.6 ± 1.1%). Probably, the presence of the OH group in the cholinium cation might be responsible for the different behaviour observed for these two ILs since it is known that this group can establish hydrogen bonds with diverse solutes.[202] However, a marked decrease in the fluorescence intensity between 1-3 h can be observed when [Ch][Ac] is used, possibly indicating the dissolution of disaggregation of the formed fibrils. Although this behaviour was only observed here for [Ch][Ac], it was also reported before for guanidine hydrochloride.[104] All these facts seem to indicate that, despite the different mechanism of fibrillation and the relative stability of the protein fibrils formed, the anion plays the major role in protein fibrillation.

For the imidazolium-based ILs the following rank was obtained [C$_4$mim][BF$_4$] > [C$_4$mim][Ac] ≅ [C$_2$mim][Ac], showing that no major differences are observed in HEWL fibrillation with the increase of the alkyl side chain length of the cation. On the other hand, the important effect of the anion in the fibrillation can clearly be seen since very different fibrillation results were obtained for [C$_4$mim][BF$_4$] (14 x 10^6 a.u. at 7 h) and [C$_4$mim][Ac] (7.88 x 10^6 a.u. at 7 h). In what concerns the cholinium-based ILs, the following rank was observed [Ch][Cit] ≅ [Ch][Lac] > [Ch][Glu] > [Ch]Cl ≅ [Ch][Ac]. The major differences here observed can be attributed to the differences in the anions. The three most effective cholinium-based ILs are derived from a tri-acid ([Cit]$^-$), a di-acid ([Glu]$^-$) and a monoacid functionalised with an extra OH group ([Lac]$^-$). The presence of extra groups that can establish hydrogen bonds seems to be crucial on the fibrillation efficiency. It should be remarked that the use of a buffer guaranties that no pH effect is taking place and that the effects here observed are all due to specific interactions between the ILs and the HEWL.

Another important parameter is the conversion ratio from native HEWL into β-sheet structures (expectable protein nanofibers) in the final suspension. The conversion ratio was determined indirectly by UV spectroscopy at 276 nm, taking in consideration

the absorption of native protein at this wavelength. A calibration curve for different concentrations of native HEWL was determined at 276 nm, and the conversion ratios were calculated by the difference between the initial and final concentrations of HEWL present in solution. Table 2 presents the conversion ratios obtained for all the conditions tested in this work. Generally, the use of cholinium-based ILs yields higher conversion ratios than imidazolium-based ILs. The direct comparison established before between [Ch][Ac] and [C$_2$mim][Ac] clearly illustrates this fact. A comparison between these results and those obtained for the ThT assay for these two ILs shows that, despite the fact that [Ch][Ac] has much higher conversion ratios than [C$_2$mim][Ac], it does not lead to efficient formation of protein nanofibers since both ILs lead to similar fluorescence intensity, indicating that probably only small oligomeric structures, not detected by this test, might be formed. [Ch]Cl, [Ch][Cit] and [Ch][Lac] have conversion rations over 90%, showing that more than 90% of the native HEWL was misfolded and possibly arranged into protein nanofibers. Again, when [Ch]Cl is used, despite the high conversion ratios obtained, low results were observed in the fluorescence ThT assay. This can indicate that [Ch]Cl possibly leads to the formation of other non β-structures aggregates, which are not detected by ThT dye. Circular dichroism spectroscopy can be very useful for this purpose, as will be discussed below. [C$_4$mim][BF$_4$] was the imidazolium-based IL which presented the highest conversion ratio (71.5 ± 1.4 %), while the [C$_4$mim][Ac] achieved the lowest conversion ratio of all the ILs used. [C$_4$mim][BF$_4$] has a conversion ration lower than 50%, meaning than there is more non-fibrillated protein than protein nanofibers.

Table 2. Conversion ratios of native HEWL into possible β-sheet structures and ThT fluorescence intensity measurements at 7 h.

Samples	Conversion %	ThT Assays
[C$_4$mim][BF$_4$]	71.5 ± 1.4	14.0 x 10^6
[C$_4$mim][Ac]	48.1 ± 2.6	7.88 x 10^6
[C$_2$mim][Ac]	59.0 ± 2.1	7.71 x 10^6
[Ch]Cl	97.3 ± 0.5	9.54 x 10^6
[Ch][Glu]	72.7 ± 1.3	11.0 x 10^6
[Ch][Ac]	84.3 ± 0.9	17.1 x 10^6

[Ch][Cit]	96.5 ± 0.5	7.63×10^6
[Ch][Lac]	92.5 ± 0.8	16.2×10^6

*Intensity of thioflavin T fluorescence measured at 7h.

In order to complement the UV-vis spectrometry results, SDS-PAGE was used. The objective was to verify if non-fibrillated protein was still in the medium. As it is shown in Fig. 2, the controls (HEWL in milliQ; HEWL at pH 2) present gel bands under the standard 18.2 kDa, corresponding to the native HEWL, which has a molecular weight of 14.3 kDa.[77] This band corresponding to the native HEWL is narrower for all the samples, meaning that a certain amount of native HEWL was converted into protein aggregates. The widths of bands resulting from the use of each IL are in agreement with the conversion ratios determined by UV spectroscopy. Gel bands with higher optical densities (OD) were registered for lower conversion ratios. The use of [C$_4$mim][Ac], [C$_2$mim][Ac] and [Ch][Glu], with conversion ratios lower than 75%, presented OD around 90%, while [Ch][Ac] with a conversion ratio slightly higher than 80% presented a lower OD of 73.45%. The only exception is the band associated to [C$_4$mim][BF$_4$], that is smaller than expected for the respective conversion ratio. However, many other small bands can also be observed under 14.3 kDa, suggesting that the use of [C$_4$mim][BF$_4$] denatures the protein into small peptides.
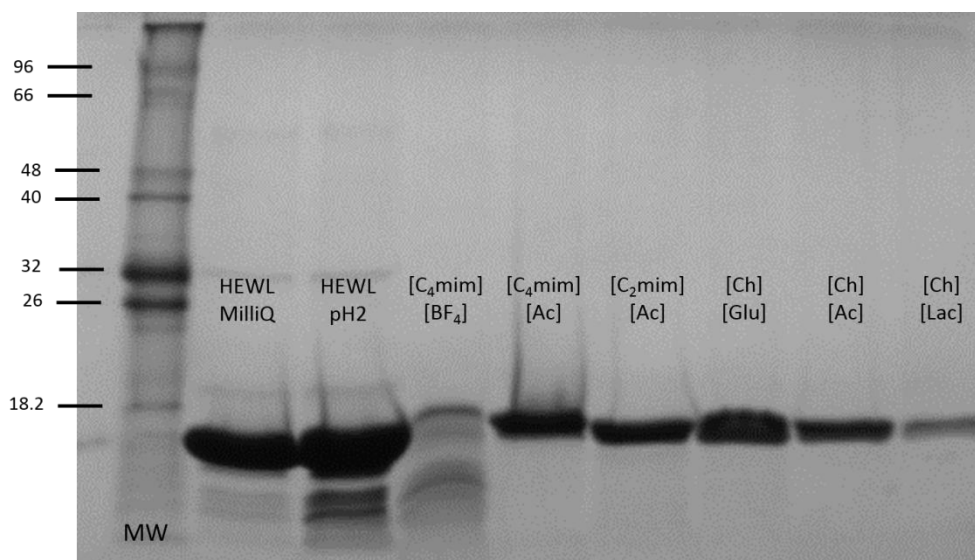
Fig. 2 - SDS-PAGE of the supernatants of the HEWL fibrillation medium for all ILs used with conversion rates lower than 95%.

In the same perspective, the use of ILs with conversion ratios over than 90% presented the lowest ODs (<45%). The SDS-PAGE of the supernatant of HEWL fibrillation using [Ch]Cl and [Ch][Cit] are depicted in Fig. 3. Almost invisible bands with tenuous marks can be observed, confirming the high conversion ratios determined indirectly by UV spectroscopy at 276 nm. The lowest OD (12.1%) was registered when using [Ch]Cl, which presents the highest conversion ratio (97.3 ± 0.5 %).
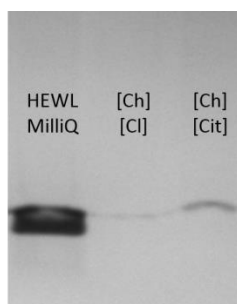
Fig. 3 - SDS-PAGE of the supernatants of HEWL fibrillation medium, for the ILs with conversion rates over than 95%, [Ch]Cl and [Ch][Cit].

HEWL nanofibers secondary structure

Circular dichroism has been extensively used to evaluate the secondary structure of proteins as different secondary structural elements, such as α-helix and β-sheets, correspond to different patterns in CD spectra.[203] This is due to the fact that protein CD spectrum can be considered as a linear combination of the spectra of its individual secondary structural elements present in the protein. On the other hand, different structural elements have characteristic structural spectra. For example, proteins with high α-helical content show negative bands at 208 and 222 nm and a positive band at 192 nm; the presence of a negative band at *ca.* 216 nm implies the presence of β-sheets, as well as a positive band at 195 nm; while unordered structures such as random coil are characterized by low ellipticity above 210 nm and a negative band at 200 nm.[204]

In this work, CD spectroscopy was used to analyse the secondary structure of HEWL protein induced by the presence of different IL diluted aqueous solutions. The CD spectra of all samples recorded in the far UV are presented in Fig. 4.

Spectra for the control protein and for the protein diluted in Millipore water were also measured and are presented in Fig 4D. Both spectra display strong negative bands in the range from 200 to 260 nm, with the signal intensity at 208 nm greater than that at

222 nm, which is characteristic of a protein containing α–helixes, β–sheets and unordered structures such as random coils.
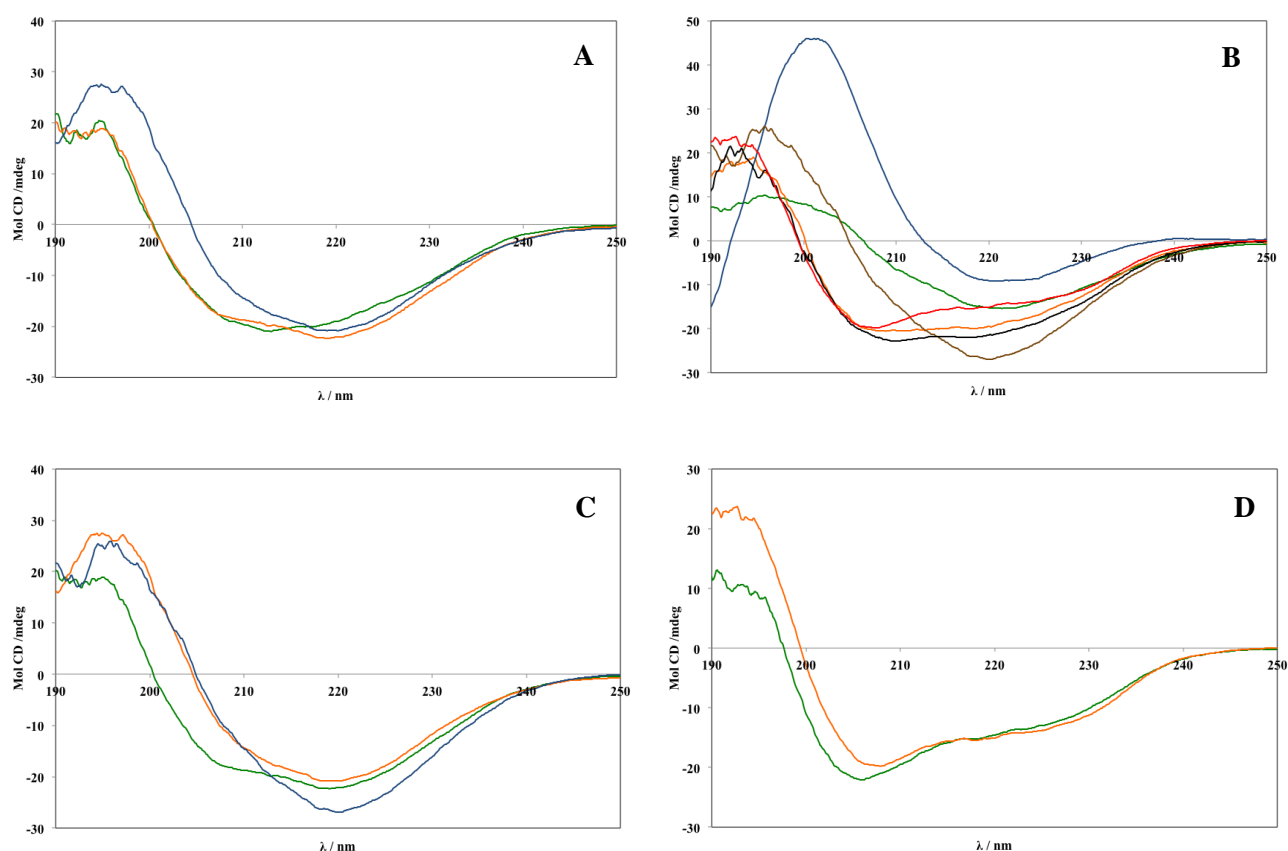
Fig. 4 - CD spectra measured in the far UV range: A) [C$_2$mim][Ac] (blue), [C$_4$mim][BF$_4$] (green) and [C$_4$mim][Ac] (orange); B) [Ch]Cl (orange), [Ch][Glu] (green), [Ch][Cit] (blue), [Ch][Ac] (brown), [Ch][Lac] (black); C) [C$_2$mim][Ac] (orange), [C$_4$mim][Ac] (green), [Ch][Ac] (blue); D) HEWL in Millipore H$_2$O (orange) and HEWL control (green).

Regarding the effect of different anions in imidazolium-based ILs, presented in Fig. 4A, both [C$_2$mim][Ac] and [C$_4$mim][Ac] CD spectra show similar bands in the 218-220 nm region indicating that they have similar amounts of β-sheets. However, the more pronounced band at 210 nm present in the [C$_4$mim][Ac] CD spectrum suggests the presence of a small amount of α-helixes in HEWL in the presence of this IL. [C$_4$mim][BF$_4$] seems to be the IL which induces the smallest amount of β-sheets. These results seem to indicate that the main role of ILs in fibrillation is associated to the

presence of carboxylic acid functionality and that the increase in the cation chain does not have a significant impact in this process. The comparison of the results obtained for the 3 ILs containing acetate anions, [C$_2$mim][Ac], [C$_4$mim][Ac] and [Ch][Ac], shown in Fig. 4C, further corroborate this conclusion. It can be observed that the 3 spectra are typical of proteins containing β-sheets and [Ch][Ac] seems to be the IL inducing the highest percentage of β-sheets, due to the presence of a very well defined negative band around 220 nm. The effect of the different anions of the cholinium-based ILs in secondary structure HEWL fibers can be observed in Fig. 4B. The cholinium-based ILs bearing acetate and glutarate anions have a high percentage of β-sheets while [Ch][Lac] and [Ch]Cl have a pronounced percentage of random coil and a smaller percentage of β-sheets, due to the presence of a larger band around 210 nm, besides the band at 220 nm. According to this data and in what concerns the effect of [Ch]Cl in the secondary structure of HEWL, by the presence of this larger and undefined band around 210 nm, CD spectra supports the formation of non-β structures when using [Ch]Cl, which agrees with the results obtained in the previous sections where simultaneously the highest conversion ratio and the lowest results in the fluorescence ThT assay were obtained for this IL. Furthermore, the use of [Ch][Cit] leads to a totally different CD spectrum. The negative band at *ca*. 220 nm seems to have a contribution from another band centred at ca. 225 nm and there is a strong positive band centred at 200 nm. The spectrum of the protein nanofibers produced using [Ch][Cit] resembles those observed for K2Q42K2 polyQ fibrils,[203] and therefore it can be concluded that this IL has the highest ability to induce the formation of β-structures. These results indicate again the importance of the carboxylic acid functionality in the fibrillation process, since all ILs with the anion acetate promoted mainly the formation of β-structures, and [Ch][Cit], bearing a tri-carboxylic acid anion, is the IL with the highest ability to induce fibrillation into β-forms.

Characterization of HEWL nanofibers

Even though ILs are efficient in producing β-sheet amyloid structures, the protein nanofibers morphology is a key factor in their application in materials field. In fact, protein nanofibers can assume different morphologies, depending on the fibrillation mechanism, especially on the nucleation phase.[20] Protein nanofibers are usually polymorphic, meaning that fibrils formed by a given peptide or protein can have

multiple distinct morphologies depending on the fibrillation conditions.[56] Typically three different kinds of aggregates, namely spherical-like, worm-like and rod-like, can be observed.[94] In the pursuit of new material elements to impart overall better materials properties, it is known that rod-like aggregates show a superior mechanical strength than other aggregates, especially due to their fine and elongated fibrillar shape.[94] In this context, STEM is very useful not only to confirm the formation of protein nanofibers but also to analyse their morphology. The STEM images of HEWL nanofibers induced by the presence imidazolium and cholinium-based ILs are presented in Fig. 5 and Fig. 6, respectively. It can be observed that, despite obvious differences in size and shape of the nanofibers, both families of ILs induce elongated fibrillar shape HEWL nanofibers.
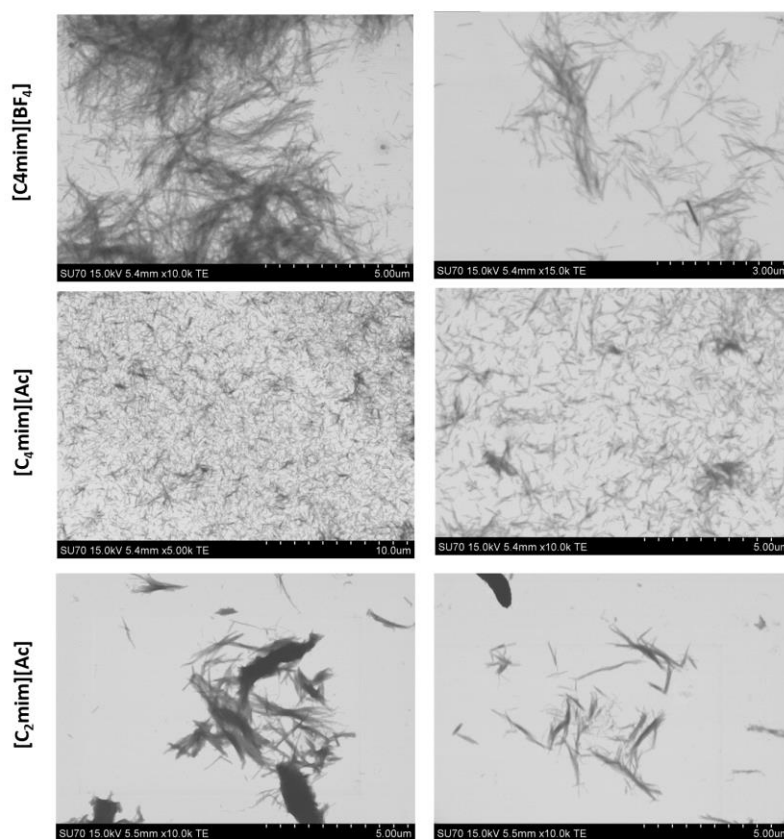
Fig. 5 - STEM images of HEWL nanofibers induced by different imidazolium-based ILs, at 70ºC, pH = 2.
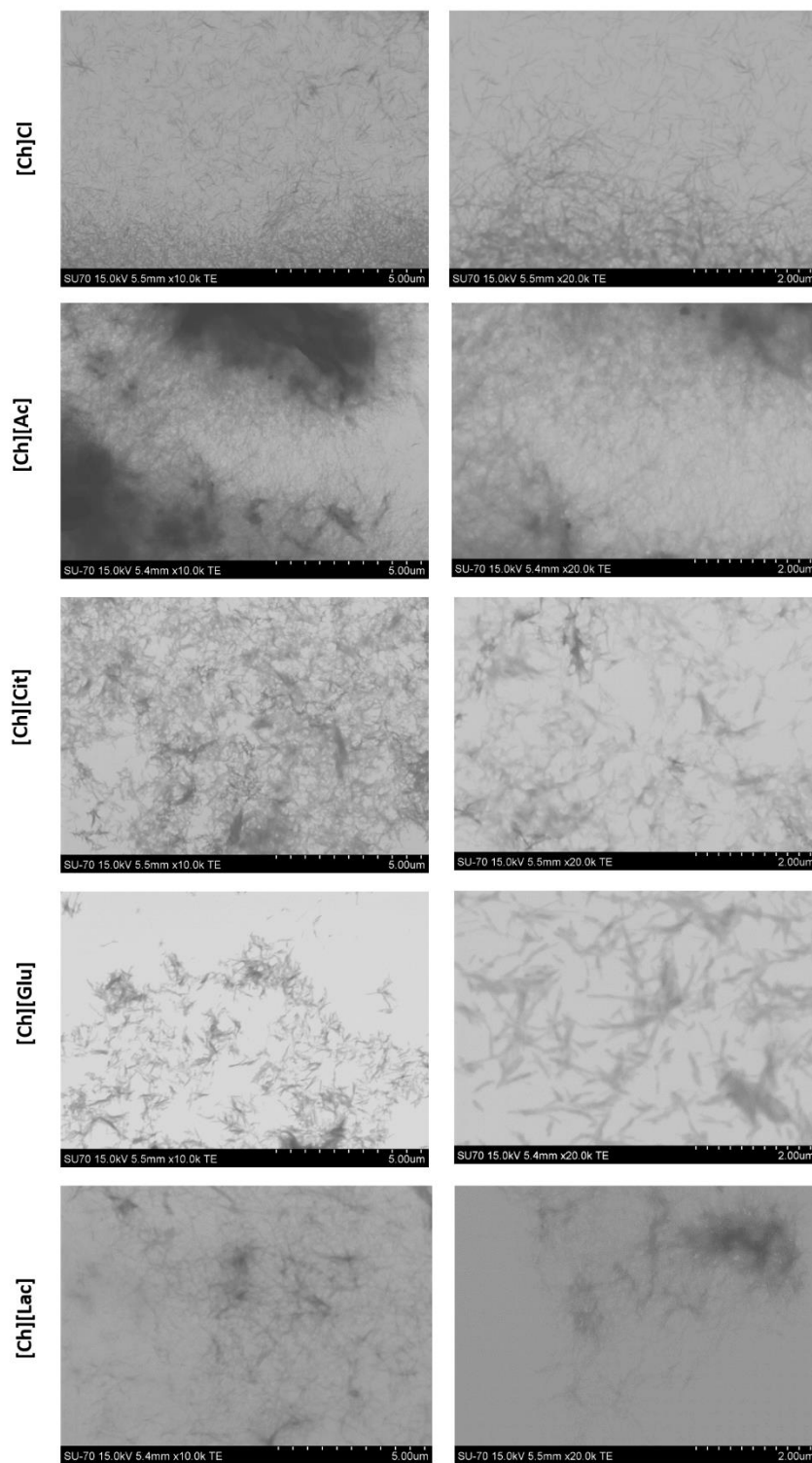
Fig. 6 - STEM images of HEWL nanofibers induced by different cholinium-based ILs, at 70ºC, pH = 2.

The average dimensions in length and width of the nanofibers were determined by analysis of the STEM images using the ImageJ program. At least 100 nanofibers

were analysed for each one of the ILs. Fig. 7 shows box charts corresponding to the average length and width of the different protein nanofibers obtained, respectively.
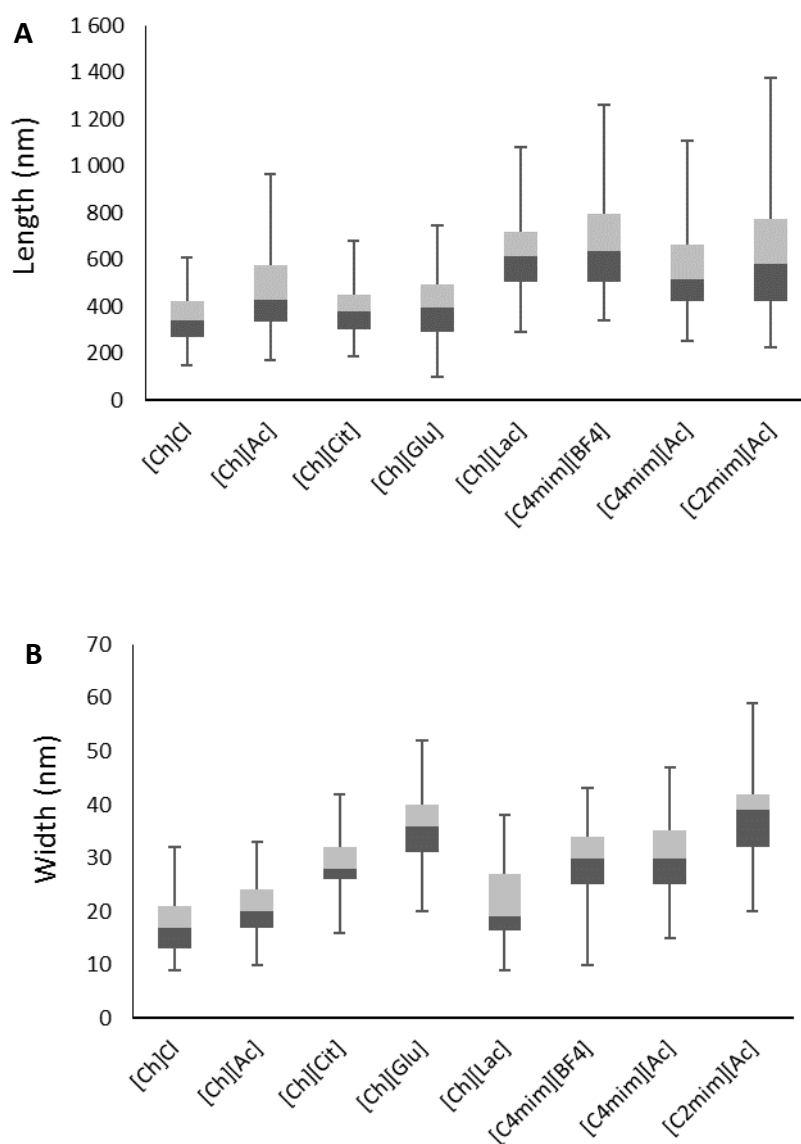
Fig. 7 - Box charts of the fibril dimensions: A - length (nm) and B - width (nm).

Generally, the use of imidazolium-based ILs yields longer nanofibers than cholinium-based ILs. Nanofibers produced using imidazolium-based ILs have average lengths of 635 ± 31.8 nm ([C$_4$mim][BF$_4$]), 517 ± 35.8 nm ([C$_2$mim][Ac]) and 584 ± 29.2 nm ([C$_4$mim][Ac]), with maximum lengths obtained over than 1100 nm. These values are much higher than the average lengths obtained for the cholinium-based ILs, which are of 341 ± 17.1 nm, 377 ± 18.8 nm and 396 ± 19.8 nm for [Ch]Cl, [Ch][Cit]

and [Ch][Glu], respectively, where the maximum values of length registered do not overpass the 800 nm. Exceptionally, [Ch][Ac] and [Ch][Lac] generate longer nanofibers, with 430 ± 21.5 nm and 616 ± 30.8 nm, achieving maximum length values nearly 1000 nm, which are closer to those obtained when using imidazolium-based ILs. A higher resolution TEM image of a HEWL nanofiber obtained using [Ch][Lac] is shown in Fig. 8.
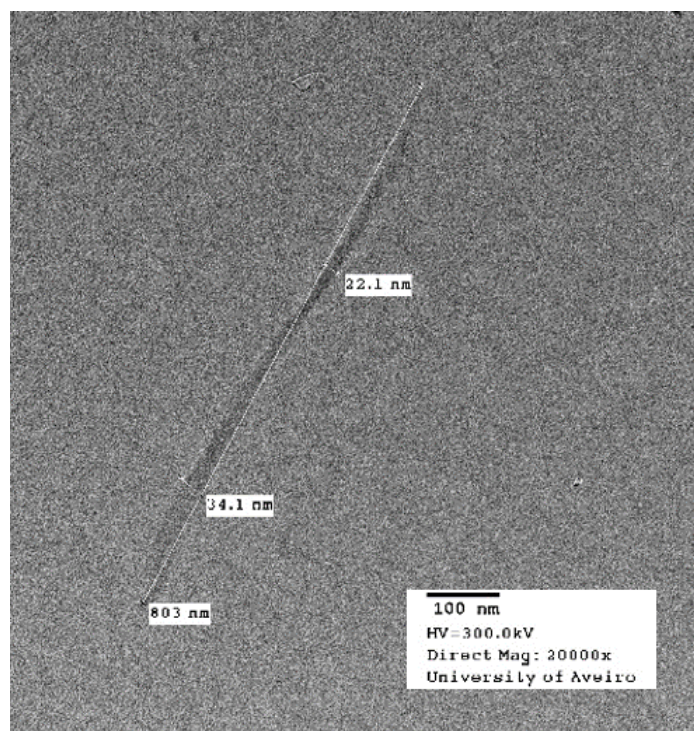
Fig. 8 - TEM image of a protein nanofiber obtained using [Ch][Lac], at 70°C, pH = 2.

Interestingly, when using cholinium-based ILs bearing anions derived from mono-carboxylic acids, such as acetate or lactate, longer nanofibers can be generated, suggesting that the carboxylic acid group can have an important role on the fibrillation process, in particular on the length of the nanofibers. The same inference was observed regarding the use of a DES based on cholinium chloride and acetic acid to induce HEWL fibrillation,[200] reported in the following section *2.2 Production of lysozyme nanofibers using a deep eutectic solvent*, where longer nanofibers with an average length of 900 ± 30.2 nm were generated by the DES, comparing to those generated using cholinium chloride alone (341 ± 17.1 nm). Curiously, when using cholinium-based ILs bearing anions derived from di- and tri- carboxylic acids, such as glutarate and citrate, the same effect is not observed.

In terms of width, cholinium-based ILs bearing anions derived from di- and tri-carboxylic acids, such as glutarate and citrate, seems to increase the width of the HEWL nanofibers produced, with average values of 36 ± 1.8 nm and 28 ± 1.4 nm, respectively. These values are higher than those obtained for the other cholinium-based ILs, [Ch]Cl (17 ± 0.85 nm), [Ch][Ac] (20 ± 1.0 nm) and [Ch][Lac] (19 ± 1.0 nm). Considering now the ILs based on the imidazolium cation, it can be observed that the use of [C_2mim][Ac] seems to generate longer but more dispersed length nanofibers. Higher magnifications suggest that the nanofibers obtained using [C_2mim][Ac] are a set of many fine and elongated nanofibers compacted together in a larger nanofiber, as it can be seen in Fig. 9. However, taking into account the large standard deviations obtained, the average width of the HEWL nanofibrils is similar for all the imidazolium-based ILs, [C_2mim][Ac] (39 ± 1.9 nm), [C_4mim][Ac] (32 ± 1.6 nm) and [C_2mim][BF_4] (32 ± 1.6 nm).
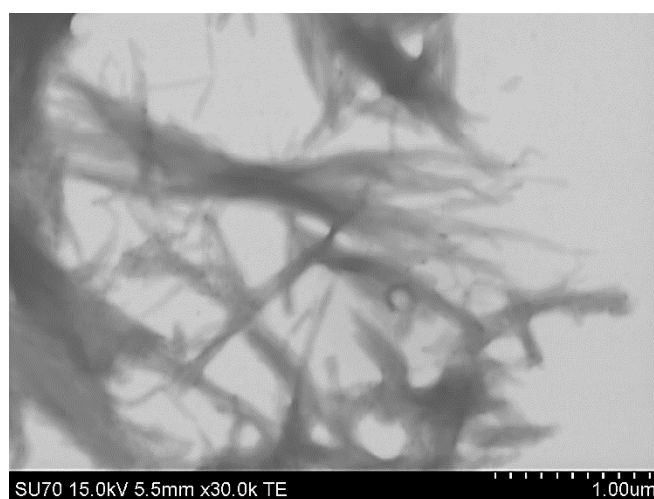
Fig. 9 - STEM images of HEWL nanofibers induced by [C_2mim][Ac], at 70ºC, pH = 2.

In sum, it can be concluded that the different ILs studied in this work, based on imidazolium and cholinium cations, promoted faster fibrillation ratios, when compared with previous methodologies described for the same protein,[82,200,205,206] with conversion ratios over than 80% being obtained within 1-2 h when using ILs based on cholinium cation. Furthermore, the nanofibers obtained were very thin and elongated, with widths ranging typically between 20-30 nm and lengths between 200-800 nm. Using ILs based on imidazolium, maximum lengths over than 1000 nm were achieved. In fact, the use of ILs can be certainly explored to produce protein nanofibers, avoiding time consuming

processes, and obtaining the so-called worm-like morphology with an interesting aspect ratio to be applied in the vast material science field.

Conclusions

This study unveils the potential of using ILs to promote the fast and efficient fibrillation of HEWL. The most remarkable result obtained is the fast fibrillation of HEWL, which reaches more than 80% in the first hour and 95% of the total protein in 5 h for some of the studied cholinium-based ILs. Additionally, all ILs used in this study were able to fibrillate HEWL within a few hours and most of them with conversion ratios over than 70-80%. Although ILs based on the imidazolium cation presented the smallest conversion ratios, the longest nanofibers were obtained using these ILs. Interestingly, ILs based on cholinium cation combined with anions derived from mono-carboxylic groups also promote the production of longer nanofibers. Using circular dichroism spectroscopy, it could be concluded that the presence of acetate anions in the IL increases the formation of β-sheet structures in HEWL, and in general, the cholinium-based ILs yielded improved results. In terms of the anions used to prepare cholinium-based ILs, citrate, containing three carboxylic acids yielded the best results.

This work is another step forward in the understanding of protein fibrillation mechanism in alternative solvents, since it is here demonstrated the use of ILs can not only accelerate the fibrillation process, but also tune nanofiber dimensions, especially in terms of length, depending on the anion-cation combination used. This can be very important depending on the envisaged applications.

2.2.

Production of lysozyme nanofibers using a deep eutectic solvent

Nuno H. C. S. Silva,[a,b] Ricardo J. B. Pinto,[a] Carmen S. R. Freire,[a] Isabel M. Marrucho[b]

[a] CICECO and Chemistry Department, University of Aveiro, Campus de Santiago, 3810-193 Aveiro, Portugal

[b] Instituto de Tecnologia Química e Biológica António Xavier, Universidade Nova de Lisboa, Av. República, Ap. 127, 2780-901 Oeiras, Portugal

Abstract

Amyloid fibrils have recently gained a lot of attention due to their morphology, functionality and mechanical strength, allowing for their application in nanofiber-based materials, biosensors, bioactive membranes and tissue engineering scaffolds. The *in vitro* production of amyloid fibrils is still a slow process, thus hampering the massive production of nanofibers and its consequent use. This work presents a new and faster (2-3 h) fibrillation method for HEWL using a deep eutectic solvent based on cholinium chloride and acetic acid. Nanofibers with dimensions of 0.5-1 µm in length and 0.02-0.1 µm in thickness were obtained. Experimental variables such as temperature and pH were also studied, unveiling their influence in fibrillation time and nanofibers morphology. These results open a new scope for protein fibrillation into nanofibers with applications ranging from medicine to soft matter and nanotechnology.

Introduction

Protein misfolding and aggregation into amyloid fibrils has been gaining a lot of attention because of its association with several pathological disorders, such as Alzheimer's and Parkinson's diseases, which affect a large number of people worldwide.[207] Such structures are typically defined as unbranched protein fibers of aligned cross-β structures which are easily detected in vitro using fluorescence dyes as Thioflavin T, and morphologically observed by electron microscopy.[23,208] However, their singular mechanical properties, comparable to dragline silk and much greater than most biological filaments,[28] protein fibrils started to be studied in a range of potential technological applications, in particular their use in the fabrication of nanofiber-based materials.

Several proteins have been used to unveil the mechanism of amyloid fibrils formation.[76] Hen egg white lysozyme (HEWL) has been widely used as a model protein in aqueous solution, and the influence of a variety of conditions,[77] including pH of the media (using acidic[78,79] or alkaline[80,81] solutions), temperature,[82–84] high pressure,[85] and the addition of sodium azide,[86,87] urea[88,89] or ethanol,[90] in fibrillation induction have been researched. Although the exact mechanism of protein structure induction by different solvents is still debatable, it is generally accepted that the nonpolar to polar balance of the solvents used in fibrillation is an important parameter in the disruption of the protein intramolecular hydrogen bonds allowing the formation of β dimers, which presence has been confirmed by circular dichroism. The protofilaments are formed by stacking of the dimers with their long axis (nearly) perpendicular leading to the formation of the nanofibers.[209–211] These studies contributed to the understanding of protein fibrillation process and consequently to the development of new drugs targeted against amyloidosis.

Due to their singular mechanical properties, comparable to dragline silk and much greater than most biological filaments,[28] a range of potential technological applications of protein fibrils rely on their efficient preparation and use in the fabrication of nanofiber-based materials. For instance, amyloid-hydroxyapatite composites have been developed as reinforced materials to mimic bone tissues[107,145,147] and other bioactive nanomaterials based on protein nanofibers were synthesized for

applications in sensing, neuronal tissue engineering, and electrostimulated stem cell differentiation.[106,212] Furthermore, such fibrils have been used as templates for the synthesis or assembly of several metallic nanoparticles and nanowires,[141–143] as well as other inorganic (micro)nanophases, like fluorapatite,[149] calcium carbonate,[150,151] carbonate apatite,[152] silica,[153] and CdSe nanofibers.[154] These functional hybrid nanomaterials find application in biosensors, electronic and energy devices, bioactive membranes and tissue engineering scaffolds, among many others.[105,213] Due to their exceptional features, such as high strength and thermochemical stability, protein nanofibers are indeed emerging as a unique and novel class of building nanoblocks for the construction of innovative functional nanocomposites. Despite the fact that most of the amyloid fibrils used for these applications are being produced by denaturing methods, there are also functional amyloid fibrils being produced by bacteria which are used as building blocks for bionanomaterials and nanotechnologies.[214,215] For example, Zhong *et al.*[214] reported the development of a strong and multi-functional underwater adhesives obtained from fusing mussel foot proteins (Mfps) of *Mytilus galloprovincialis* with CsgA proteins, the major subunit of *Escherichia coli* amyloid curli fibres. Although the kinetics to produce the amyloid fibrils by bacteria is relatively fast, the process is complex and expensive.

One of the major limitations in the production of fibrils for the fabrication of intelligent materials is the time required to obtain these fibrils, since most of the fibrillation procedures developed so far can take days, weeks and even months. Only one work,[104] reported the production of lysozyme fibrils in less than 3 h, through the use of guanidine hydrochloride as an amyloid inducer. However, the fibril dimensions in terms of length are a bit short (~300 nm) comparing to other studies approaching material-based fibrils which goes around and even higher than 1 μm.[105–107] During the last years, different fibrillation procedures have been developed for the production of material-based fibrils, usually taking 8-15 h.[81,88]

More recently, the use of ionic liquids (ILs) has been shown to alter the fibrillation process and to stabilize different amyloid species, opening new perspectives of probing protein conformational states and exploring new protein-solvent interactions.[114,115,118,120] Bae *et al.*[120] demonstrated that the presence of specific ILs creates a hydrophobic ionic media that induces the formation of amyloid fibrils of α-lactalbumin. Diluted (5 wt.%) solutions of 1-butyl-3 methyl imidazolium ([C4mim])-

based ionic liquids, combined with different anions, in 20 mM glycine buffer (pH = 2) at room temperature were used and amyloid fibrils were observed after few days with the use of [C$_4$mim][BF$_4$] and [C$_4$mim][PF$_6$].[120] These authors show that the morphology and properties of the aggregates could be modulated depending on the chemical structure of the IL and pH. Although the exact mechanism of protein structure induction is still debatable, it is generally accepted that the nonpolar to polar balance of these solvents is an important parameter in the disruption of the intramolecular hydrogen bonds, which are essential for beta sheets formation.

Very recently deep eutectic solvents (DES) have been gaining much attention as versatile alternatives to ILs.[122] DES can be regarded as a new generation of ionic solvents composed of a mixture of two or more compounds, where one of them is a salt. The formation a new liquid compound at room temperature is due to the establishment of hydrogen bonds between a hydrogen bond donor (HBD) and a hydrogen bond acceptor (HBA), usually a halide anion present in the salt.[123–125] The most popular DESs synthesized so far are those based on cholinium chloride (used as HBA) because of its low cost, low toxicity, biodegradability and biocompatibility, since it is considered an essential nutrient, which can be extracted from biomass, and often regarded as a part of the B-complex vitamins.[126] Cholinium chloride has been combined with several classes of HBD such as renewable polyols, carbohydrates, amides, amines, alcohols and carboxylic acids.[127] Cholinium and other ammonium cations, for example betaine, combined with convenient anions, such as saccharinate, lactate, and hexanoate, have been largely explored in the search for natural, biocompatible, renewable and "drinkable" solvents.[128] DES share many of the ILs appealing features, such as low volatility, high thermal stability and conductivity, wide liquid range and high solvation capacity[128–130] and possess other interesting advantages over ILs: they are easier to synthesize, since the components are easily mixed without any further purification; they have low production cost due to the low price of starting materials; and most of the synthesized DES are biodegradable, biocompatible and non-toxic.[130,131] DES are also considered to be cheaper, efficient and greener solutions, and, in this way, are finding many applications from metal finishing processes[132] up to, more recently, compound extraction and separation media for azeotropic mixtures,[133–136] with reported performances even superior to conventional organic solvents and ILs. Regarding protein fibrillation, partial denaturation caused by solvent environment or changes in

68

temperature or pressure is pre-requisite for fibril formation. To the best of our knowledge, protein fibrillation using DES has only been researched in terms of protein stability studies. The stability of HEWL in different choline chloride-based deep eutectic solvents has been studied and showed the accumulation of discrete, partially folded intermediates that displayed a high content of secondary structure and disrupted tertiary structure when using non-diluted and 10%-diluted urea:choline chloride (2:1) at 70ºC.[216]

In this work, one widely used DES based cholinium chloride, and a simple acid, acetic acid (Fig. 1), in a proportion of 1:1, ([Ch]Cl:Ac) was studied as a possible promoter of HEWL fibrillation. As mentioned by several authors,[126,217] DES having organic acids as HBD do not present melting points on DES, but instead less transition temperatures are observed. The influence of experimental variables such as temperature (room temperature (RT), 50, 70ºC) and pH (2, 5) in the process of fibrillation induction was also researched, as well as the role of DES in the production of protein nanofibers.
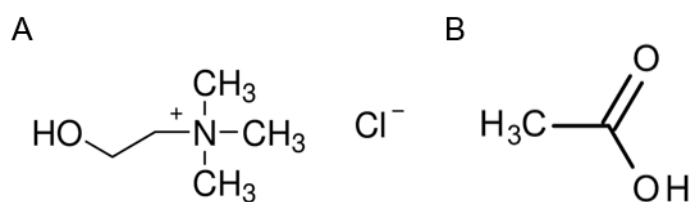
Fig. 1 - Chemical structure of (A) cholinium chloride ([Ch]Cl) and (B) acetic acid.

Experimental Details

Preparation of the DES

As proposed by Florindo *et al.*,[217] the preparation of [Ch]Cl:Ac was performed by first mixing the two components, cholinium chloride (Sigma-Aldrich, ≥98%) and acetic acid (Sigma-Aldrich, ≥99,7%) in a 1:1 mole proportion, and then grinding them in a mortar with a pestle at room temperature until a homogeneous liquid is formed.

Preparation of Protein Nanofibers

Lysozyme from hen egg white (Fluka, ~70000U mg^{-1}), was dissolved (2mg mL^{-1}) in an aqueous buffer solution of 10 mM HCl at pH = 2 with 20 mM glycine (Sigma-Aldrich,

≥98,5%) with 1, 5 and 10% (v/v) of the DES. The samples were incubated at different temperatures (RT, 50°C and 70°C), under magnetic agitation. The assays at 50 and 70°C were conducted using an oil bath. For the test at pH = 5, a 0.1 M phosphate buffer solution was used. Triplicates of each sample were carried out so that standard deviations can be calculated. The protein nanofibers were separated from the solution with the DES after centrifugation at 15,000 rpm, during 45 min, using a Megafuge 16R centrifuge (Thermo Scientific). The supernatants were exchanged with Milli-Q ultrapure water. This separation step was repeated 2 times.

UV-vis analysis

The concentration of HEWL was calculated by UV spectroscopy at 276 nm, using a UV-1800 spectrophotometer (Shimadzu, Kyoto, Japan), of the supernatants obtained after centrifugation of the incubated samples, at 15000 rpm for 45 min, using a Megafuge 16R centrifuge (Thermo Scientific) and a previously established calibration curve, where $Abs_{276nm} = 2.39[HEWL]_{mg/mL} - 0.0012$ (R^2=0.9994). Controls using [Ch]Cl and acetic acid were prepared according to the amounts of individual components in the DES, 3.5% (m/v) of [Ch]Cl and 1.5% (v/v) of acetic acid.

Fluorescence analysis (ThT assays)

For the time-course assay, 30 µL aliquots were taken from the incubated solution at desired time intervals, and added to a 3 mL solution containing 2.5 mM Thioflavin T – ThT (Sigma-Aldrich), in 10 mM phosphate buffer, pH = 7.4. Fluorescence measurements were carried out at 25°C using quartz cells on a Horiba Jobin Yvon Fluoromax-3 fluorimeter. The excitation wavelength was 440 nm and the emission was measured at 482 nm, with both slits of 5 nm. The percentage of fluorescence was calculated according to the maximum fluorescence intensity value (100% fluorescence) registered for each assay.

Scanning transmission electron microscopy (STEM)

STEM images were obtained by using a field emission gun (FEG) SEM Hitachi SU70 microscope operated at 15 kV. Samples were prepared by immersing a carbon-coated copper grid into the protein nanofibers suspension, and then allowing the solvent to evaporate overnight. The average dimensions of the nanofibers were determined by

analysis of STEM images using the ImageJ program (at least 100 nanofibers were analyzed for each experiment).

Results & Discussion

Effect of temperature and pH on the fibrillation process of HEWL

Literature shows that temperature and pH are two experimental variables that play a major role in protein fibrillation processes. The available studies[82,205,206,218] indicate that high temperature (60-70ºC) and low pH (1.6-2) are important factors that favour the partial unfolding of native HEWL, and consequently their refolding in β-sheet conformation, leading to the formation of protein nanofibers. Since we are working with aqueous solutions of DES (1, 5 and 10% (v/v)), there is the need to ascertain if the individual components of DES would yield the same effect. According to literature, DES in diluted aqueous solutions can act as two separated solutes.[219,220] Therefore, assays were carried out for [Ch]Cl and acetic acid (Ac) individually, at 70ºC and pH = 2, with the same individual concentrations as those used in 5% (v/v) aqueous solution of DES. Also, a fibrillation assay using a solution with both [Ch]Cl and acetic acid (Ac) in the same proportion as in a 5% (v/v) aqueous solution of DES was considered. The formation of protein nanofibers was indirectly measured by the fluorescence of thioflavin T when binding to β-sheet amyloid structures. The intensity of thioflavin T fluorescence as a function of time for [Ch]Cl, Ac and [Ch]Cl with Ac is depicted in Fig. 2.
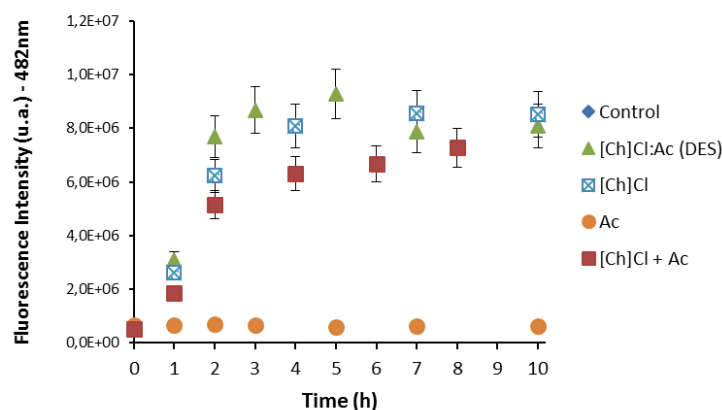
Fig. 2 - ThT fluorescence intensity as a function of time for HEWL fibrillation using a [Ch]Cl:Ac solution of 5% (v/v) at 70ºC and pH2, and its individual components

separately ([Ch]Cl; Ac) and together ([Ch]Cl + Ac) in the same proportion and concentration as when used in the DES.

It can be clearly seen that the addition of the ionic liquid [Ch]Cl promotes high fluorescence intensity, similar to that obtained when an aqueous solution of 5% (v/v) DES is used, while there is no increase of the fluorescence intensity when acetic acid alone is used. In fact, it can be observed that similar fluorescence intensity is obtained for aqueous solutions of DES, [Ch]Cl and the DES at similar concentrations. This is a clear indication that, at 5% (v/v) solution, both components of DES separate in aqueous solution and that [Ch]Cl has a major role in the fibrillation process, while Ac works only as an adjuvant.

Fig. 3 displays the results for the fibrillation of HEWL expressed as the intensity of the thioflavin T fluorescence as a function of time at different experimental conditions. The effect of the [Ch]Cl:Ac concentration in the promotion of HEWL fibrillation is evaluated in Fig. 3A. These assays took place at 70ºC and acidic conditions, using 10 mM HCl buffer solution which confers a pH = 2. The pH was measured along the experiments without significant changes being noticed. Three different [Ch]Cl:Ac concentrations, 1, 5 and 10% (v/v) were used. It can be observed that the intensity of fluorescence significantly changes with the amount of [Ch]Cl:Ac used, indicating that this parameter plays an important role in the fibrillation process. While the lowest concentration of [Ch]Cl:Ac (1% (v/v)) showed no significant fluctuations in the fluorescence intensities in comparison with the control (0% [Ch]Cl:Ac), at higher [Ch]Cl:Ac concentrations (5 and 10% (v/v)) the fibrillation process is favoured, as supported by the substantial raise in the fluorescence intensity. Nevertheless, the assay containing 5% (v/v) of [Ch]Cl:Ac displayed a higher fluorescence intensity than that with 10% (v/v) of [Ch]Cl:Ac, suggesting that the former [Ch]Cl:Ac concentration is the ideal for an optimal fibrillation of HEWL. There are several studies in the literature also reporting the existence of an ideal concentration of salts and other fibrillation agents.[104,221] For example, Fujiwara et al.[221] showed that albumin fibrillation is induced up to certain concentration of salt, while only amorphous aggregates were found at higher concentrations. Vernaglia et al.[104] also studied the effect of guanidine hydrochloride concentrations in the lysozyme fibrillation process. Three distinct regimes were observed: at low concentrations, the structure of lysozyme

72

was very stable and no fibrils were observed; at intermediate concentrations, lysozyme was partially unfolded and fibrils were rapidly formed; at high concentrations guanidine hydrochloride was capable of dissolving and dis-aggregating the formed fibrils.
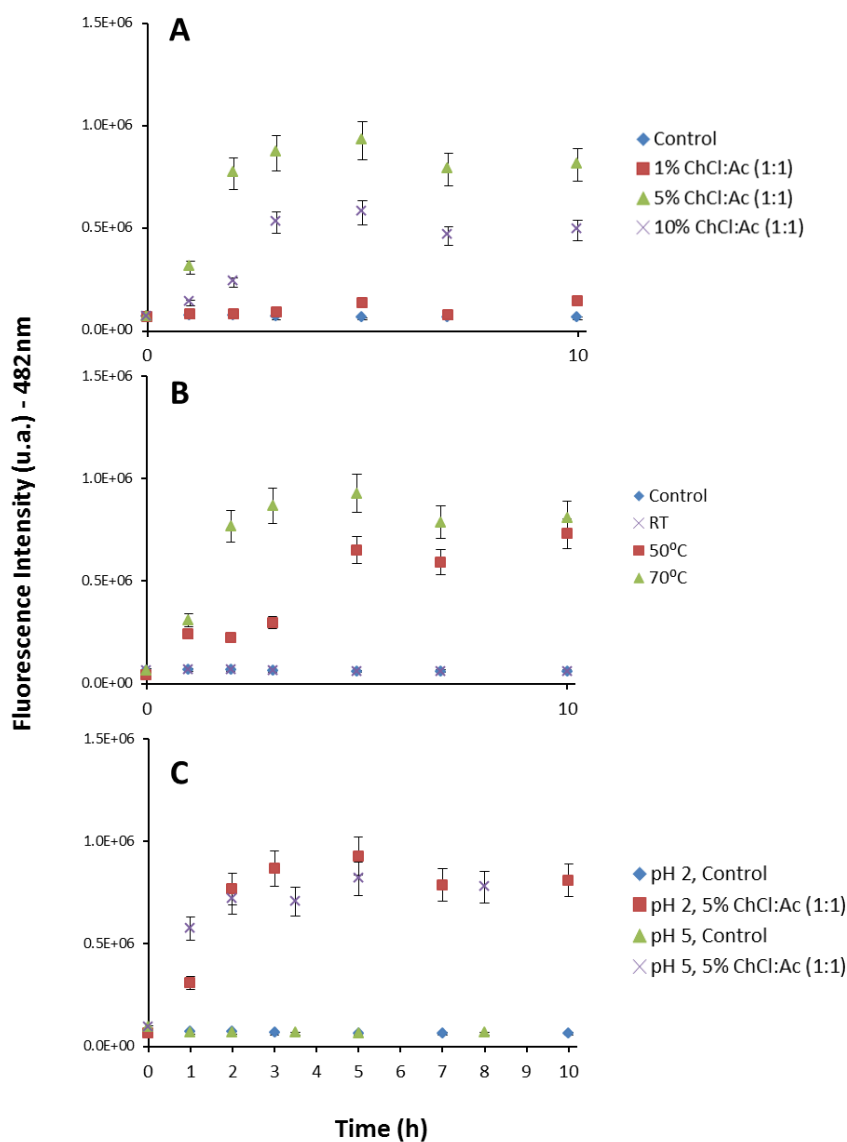
Fig. 3 - ThT fluorescence intensity as a function of time for HEWL varying: (A) [Ch]Cl:Ac concentration, keeping the temperature at 70ºC and the pH = 2; (B) temperature, keeping the [Ch]Cl:Ac concentration at 5% (v/v) and the pH = 2; and (c) pH, keeping the [Ch]Cl:Ac concentration at 5 % (v/v) and the temperature at 70ºC.

Although our studies do not allow us to infer on direct causes leading to the decrease in fluorescence intensity in the assays at 10% (v/v) of [Ch]Cl:Ac, the solubilization of fibrils might be a possible explanation. In this line with the different shape of the curve for higher concentrations of [Ch]Cl:Ac, there is a formation of a small quasi-plateau region for low incubation times. This type of behaviour has been attributed in the literature to the formation of small oligomeric structures that need more time to develop into fibrils due to their enhanced solubility.[222,223] Also to be noted, is the short time required to get nanofibers when using acidic aqueous solutions with 5 and 10% (v/v) of [Ch]Cl:Ac: in only 3 h both assays achieved more than 90% of the maximum fluorescence intensities registered for each case.

The effect of temperature in the fibrillation of HEWL when the [Ch]Cl:Ac concentration (5% (v/v)) and pH (pH = 2) were kept constant is depicted in Fig. 3B. It can be concluded that temperature also plays a leading role in the fibrillation of HEWL with the maximum fibrillation achieved for the highest temperature (70ºC) in a 2h incubation period. Decreasing the temperature from 70ºC down to 50ºC more than duplicates the time needed (5 h) to reach the maximum fluorescence intensity. In fact, it is clear from the observation of Fig. 3B that the mechanism through which fibrillation occurs changes with temperature: at 50ºC we obtain the classical sigmoidal growth profile also known as a "nucleated growth" mechanism,[20,70] i.e., there exists an initial lag phase where the fluorescence intensity remains almost constant due to nucleation followed by an exponential phase which ends up in a final equilibrium region,[71–73] while at 70ºC a faster and continuous formation of protein nanofibers can be observed. Furthermore, the assay carried out at room temperature shows that almost no fibrillation occurs, within a ten days period and, according to Fig. 4, three months are necessary for fibrillation to take place at room temperature. It is well known that hydrogen bonding is weakened as the temperature rises. It is well known that hydrogen bonding is weakened as the temperature rises. At low temperatures, the helical structure of the protein is tightly bound through hydrogen bonding making more difficult the solvent access to amino acid residues that are responsible for protein conformational structure.
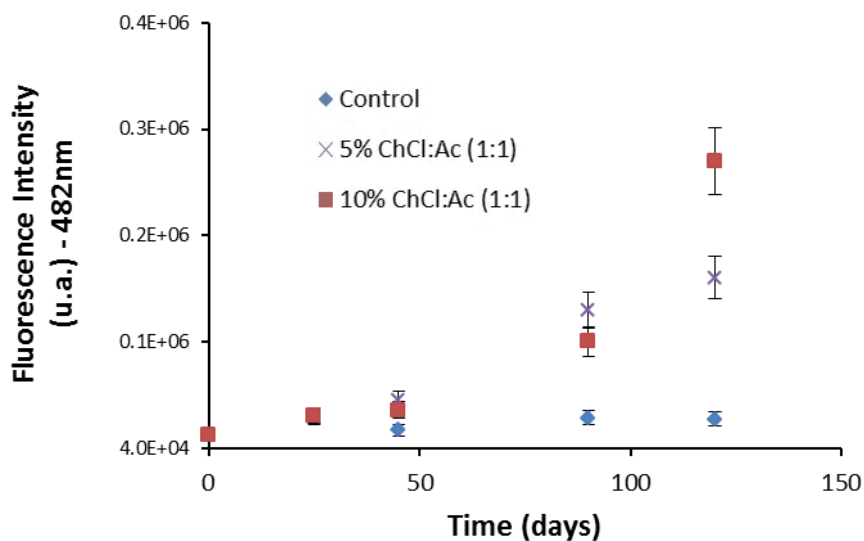
Fig. 4 - ThT fluorescence intensity as a function of time for HEWL nanofibers formation, at room temperature and pH = 2.

Another parameter usually studied in protein fibrillation is the pH. The effect of pH was researched using solutions at two pH values (2 and 5) and at a fixed [Ch]Cl:Ac concentration of 5% (v/v) and a temperature of 70ºC (Fig. 3C), which were previously found to be the best conditions to promote HEWL fibrillation. At both pH values, and in the presence of fixed [Ch]Cl:Ac concentration, the fibrillation occurs within 2-3 h, revealing no significant differences in the kinetics behaviour. In the absence of [Ch]Cl:Ac, there is no evidence of HEWL fibrillation, which leads to the conclusion that independently of the pH used, the presence of [Ch]Cl:Ac is critical for fibrillation to occur. Consequently, Fig. 3C clearly demonstrates that pH of DES solutions does not play a relevant role in HEWL fibrillation, allowing working at milder conditions than it was possible with other solvents.[78,87] These results are intriguing since most of literature shows that pH usually plays an important role in fibrillation.

In conclusion, Thioflavin-T fluorescence studies indicate that temperature and [Ch]Cl:Ac concentration are the key parameters controlling the fibrillation of HEWL, with a maximum amount of nanofibers formed at 70ºC and 5 (v/v)% of DES, while milder pH conditions can be used, since fibrillation with [Ch]Cl:Ac is not significantly affected by pH. A major breakthrough provided by this study is undoubtedly the acceleration of protein fibrillation, which can be especially significant when their use in material fabrication is envisaged. In a study led by Mishra *et al.*[82], HEWL unfolding

was followed by partial acid hydrolysis, and mature amyloid fibrils were then added as seed. In terms of the fibrillation mechanism, and taking into account the classical sigmoidal profile discussed before, this procedure reduced the lag phase from 70-80h down to 30-40 h. A quick glance to our results in Fig. 3 shows that the use of [Ch]Cl:Ac seems to have a similar effect, reducing the lag phase. However, HEWL fibrillation strategy here proposed through the use of [Ch]Cl:Ac is much faster than that using amyloid fibril seeds. The same effect has been seen using other denaturant solvents, like urea and guanidine hydrochloride. In fact, Kumar *et al.*[88] have showed a faster formation of amyloid fibrils using urea at 2 and 4 M, at 60°C during 15 h. The same was observed using guanidine hydrochloride.[104] These studies predict that the lag phase is mainly controlled by the ionic interactions, which agrees with our observations.

Conversion ratio of native HEWL into nanofibers

Once the ThT fluorescence assay is positive, thus indicating the β-sheet structure formation, it is important to determine the conversion ratio from native HEWL into β-sheet structures (possibly nanofibers) in the final solution. This conversion ratio was determined indirectly by UV spectroscopy at 276 nm, taking in consideration the absorption of native protein at this wavelength. A calibration curve for different concentrations of native HEWL was determined at 276 nm, and the conversion ratios were calculated by the difference between the initial and final concentrations of HEWL in solution. Table 1 presents the conversion ratios obtained for all the conditions tested. It can be seen that most of the conversion ratios are over 90%, indicating that more than 90% of native HEWL was misfolded and possibly arranged into nanofibers. However, the assays conducted at room temperature for 4 months at a constant pH = 2 displayed conversion ratios of 10.8% and 19.6%, when 5% and 10% (v/v) [Ch]Cl:Ac were used, respectively. These results also indicate that temperature has an essential role in catalysing the protein misfolding process, probably through the weakening of the intramolecular hydrogen bonding interactions, and consequent in the HEWL fibrillation in [Ch]Cl:Ac aqueous solutions. Furthermore, all assays conducted without ChCl:Ac showed conversion ratios lower than 2%, highlighting the importance of ChCl:Ac in the HEWL unfolding and subsequent fibrillation.

Table 1. Conversion ratios from native HEWL into possible β-sheet structures and ThT fluorescence intensity results.

Assay conditions			Conversion %	ThT Assay	
T (ºC)	pH	% (v/v) [Ch]Cl:Ac		Fluorescence*	Time*
70	2	1	87.5 ± 0.4	1.34×10^6	5h
		5	94.9 ± 0.5	7.69×10^6	2h
		10	97.5 ± 0.5	5.28×10^6	3h
		[Ch]Cl	92.7 ± 0.5	8.09×10^6	4h
		[Ch]Cl + Ac	91.8 ± 0.5	6.30×10^6	4h
	5	5	99.7 ± 0.1	7.18×10^6	5h
50	2	5	99.8 ± 0.1	9.28×10^6	2h
RT	2	5	10.8 ± 0.1	2.00×10^6	120d
		10	19.6 ± 0.1	3.10×10^6	120d

*Intensity of fluorescence and time required to achieve 90% of the maximum ThT fluorescence intensity value.

Morphology of the protein nanofibers

Protein nanofibers can assume different morphologies, specially depending on the nucleation phase.[20] In fact, protein nanofibers are usually polymorphic, meaning that fibrils formed by a given peptide or protein can have multiple distinct morphologies depending on the conditions under which the fibrils aggregate.[56] Different kind of aggregates were reported by Jung *et al.*[94] and they are mainly categorized as spherical-like, worm-like and rod-like. In the pursuit of new material elements with better properties, like mechanical strength, the rod-like aggregates are the most suitable, due to their fine and elongated fibrillar shape.

In this context, transmission electronic microscopy (TEM) is a very useful technique to confirm the formation of protein nanofibers and analyse their morphology. The STEM images of the nanofibers obtained in this work using ChCl:Ac aqueous solutions under different experimental conditions are presented in Fig. 5 and Fig. 6. It can be observed that in all assays, fine and elongated nanofibers, corresponding to the so called rod-like shape, were obtained. The only exception seems to be the control with

[Ch]Cl, with shorter nanofibers were obtained, as it can be seen in Fig. 6. Since the dimensions of the obtained protein nanofibers are very important for the foreseen applications, the average dimensions in length and thickness of the nanofibers were determined by analysis of the STEM images using the ImageJ program and at least 100 nanofibers were analysed in each case. In Fig. 6, we compare the nanofibers obtained using an aqueous solution of 5 (v/v)% [Ch]Cl:Ac DES with those obtained when aqueous solutions of 3.5 (m/v)% [Ch]Cl was used. Although similar thioflavin T fluorescence assay results were obtained for both experiments, the nanofibers obtained when [Ch]Cl was used are much smaller than those obtained using [Ch]Cl:Ac DES, especially in terms of length. Maximum fibril length values of around 0.6 µm were obtained when using the IL, which is basically half of the maximum values obtained using the DES. This result suggests that the acid group of DES has an important role on the fibrillation process, contributing for longer nanofibers.
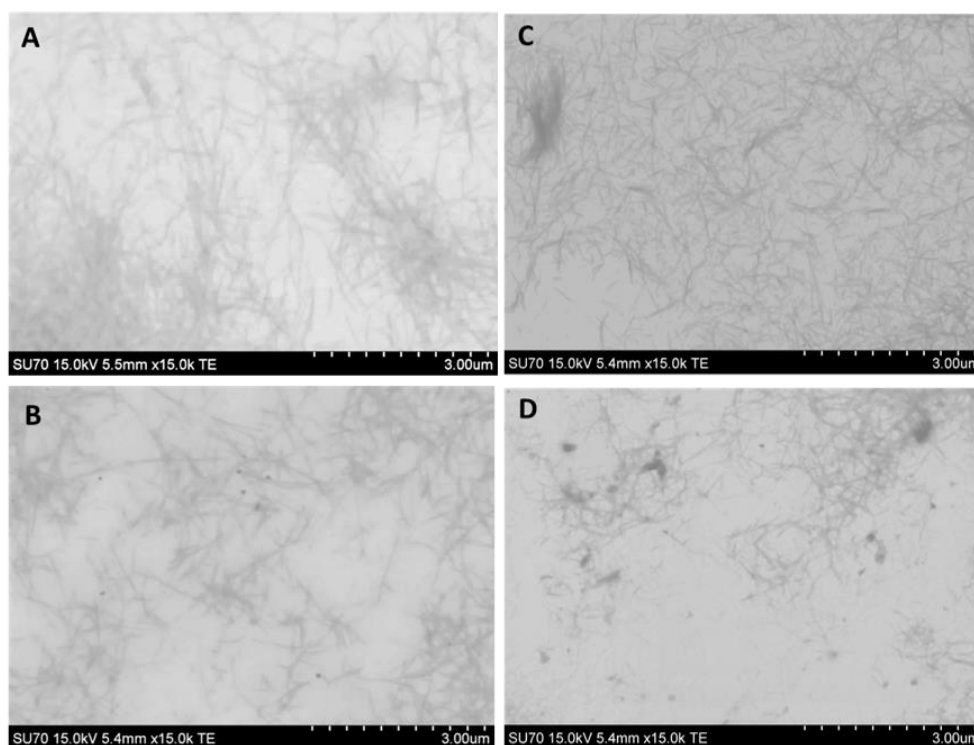
Fig. 5 - STEM images of protein nanofibers formed by inducing HEWL fibrillation using 5% (v/v) [Ch]Cl:Ac, under different conditions. (A) 70ºC, pH = 2. (B) 50ºC, pH = 2. (C) 70ºC, pH = 5. (D) RT, pH = 2.
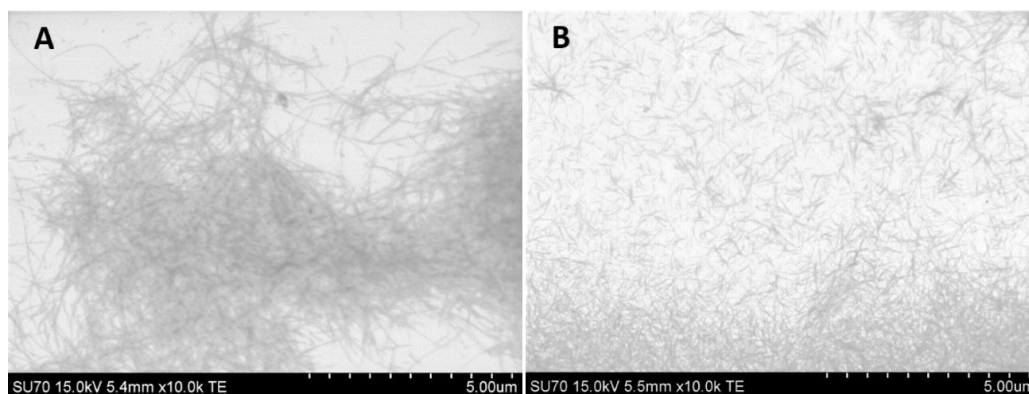
Fig. 6 - STEM images of protein nanofibers formed by inducing HEWL fibrillation using 5% (v/v) [Ch]Cl:Ac and 3.5% (m/v) [Ch]Cl, at 70ºC and pH = 2.

Furthermore, Fig. 7 shows box charts corresponding to length and thickness of HEWL nanofibers, respectively. HEWL fibrillation at 70ºC and pH = 2, using 5% (v/v) [Ch]Cl:Ac, provided the longest nanofibers with an average length of 0.9 ± 0.3 µm. As we decrease the temperature to 50ºC, keeping the pH conditions (pH = 2), shorter (0.6 ± 0.2 µm) and slightly thinner (0.03 ± 0.01 µm) nanofibers were obtained. The same tendency, smaller lengths and diameters can also be observed when temperature is further lowered down to room temperature and still maintaining these pH conditions. Curiously, and although Thioflavin T fluorescence assays show no significant changes in terms of the fibrillation period and the fluorescence intensity values, pH seems to have a relevant effect on nanofibers dimensions as well. Comparing nanofibers produced at 70ºC and two different pH conditions (2 and 5), more neutral pH generates shorter (0.5 ± 0.2 µm) and thinner nanofibers (0.023 ± 0.005 µm) than acidic pH conditions where a length of 0.9 ± 0.3 µm and a thickness of 0.04 ± 0.01 µm were observed. According to Juarez *et al.,*[224] a lower pH induces further structural changes in secondary structure favouring electrostatic repulsive interactions, which makes the molecules more soluble, disfavouring their aggregation to a great extent, and thus longer nanofibers are formed. In conclusion, despite the similar results observed in terms of the fibrillation period and the ThT fluorescence intensity values for both pHs, at 70ºC using 5% (v/v) [Ch]Cl:Ac, there are some differences in the morphology of the nanofibers obtained, especially regarding the length of the nanofibers obtained.
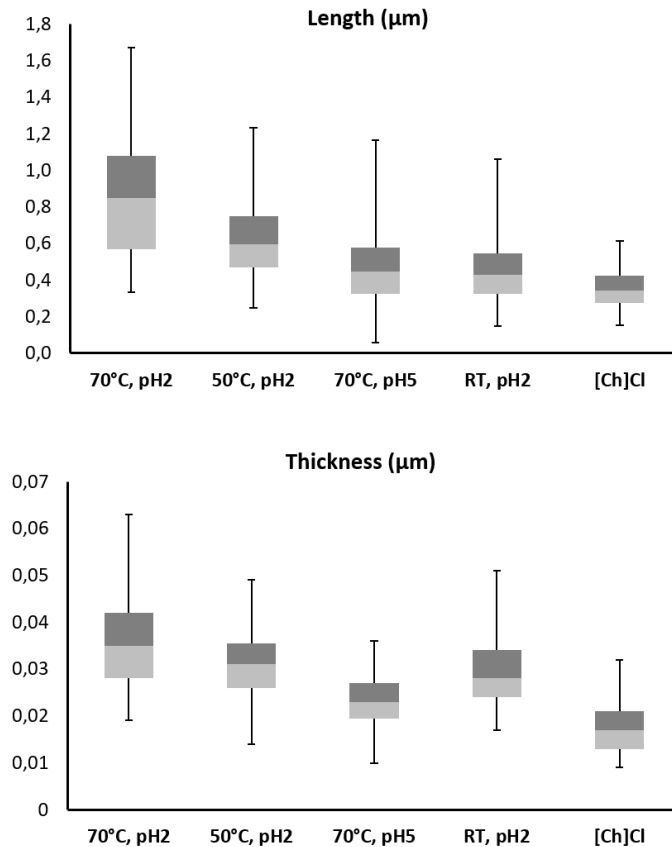
Fig. 7 - Box charts with fibril dimensions in length (µm) and thickness (µm).

Comparing the results obtained in this work with those from literature data, and despite the small differences observed depending on temperature and pH conditions, the nanofibers dimensions obtained using [Ch]Cl:Ac, as well as morphologies observed in the TEM images, are all very similar to those described in literature for HEWL,[82,205,206] β-lactoglobulin[95] and albumin,[225] with average dimensions of 0.5-1 µm in length and 0.02-0.1 µm in thickness.

Conclusions

This study describes a novel, efficient and timesaving fibrillation method for HEWL using aqueous solutions of a deep eutectic solvent based on cholinium chloride and acetic acid, in a 1:1 proportion. The thioflavin-T fluorescence assay was used to infer on the influence of experimental variables such as DES concentration, temperature and pH. An optimal concentration of 5 (v/v)% of DES for HEWL fibrillation was determined. Temperature also has a key role in the acceleration of the fibrillation,

greatly reducing the lag-phase, without changing the fibrillation kinetics. This behaviour was linked to the disruption of protein intramolecular hydrogen bonds at higher temperatures. STEM was used to determine the length and the thickness of the produced nanofibers. Both temperature and pH significantly influence nanofibers dimensions, in terms of length and thickness. Longer and thicker nanofibers were obtained at high temperatures and lower pH values. Considering the time effectiveness of HEWL fibrillation using [Ch]Cl:Ac, the incubation time was reduced from 8-15 h down, when other solvents are used, to 2-3 h, with nanofibers dimensions of 0.5-1 µm in length and 0.02-0.1 µm in thickness. It is foreseen that this protein fibrillation method will clearly impact on the use of protein nanofibers in the vast material science field, especially in the development of nanosized reinforcing elements for bionanocomposites preparation with applications ranging from medicine to soft matter and nanotechnology.

2.3.

Tuning lysozyme nanofibers dimensions using deep eutectic solvents for improved reinforcement ability

Nuno H. C. S. Silva,[a,b] Carla Vilela,[a] Ricardo J. B. Pinto,[a]

Carmen S. R. Freire,[a] Isabel M. Marrucho[c]

[a] CICECO Aveiro Institute of Materials and Chemistry Department, University of Aveiro, Campus de Santiago, 3810-193 Aveiro, Portugal

[b] Instituto de Tecnologia Química e Biológica António Xavier, Universidade Nova de Lisboa, Av. República, Ap. 127, 2780-901 Oeiras, Portugal

[c] Centro de Química Estrutural, Instituto Superior Técnico, Universidade de Lisboa, Avenida Rovisco Pais, 1049-001 Lisboa, Portugal

Abstract

Deep eutectic solvents (DESs), a novel generation of solvents, have recently been described as efficient and timesaving fibrillation agents for proteins. In this context, the present work aims at assessing the effect of the hydrogen bond donor (HBD) of cholinium chloride ([Ch]Cl):carboxylic acid based DESs on the dimensions (length and width) of lysozyme nanofibers (LNFs). Mono-, di- and tri-carboxylic acids (acetic, lactic, levulinic, malic and citric acids) were used to prepare different DES formulations, which were successfully used on the fibrillation of lysozyme. The results showed that the carboxylic acid (*i.e.* the HBD) plays an important role on the fibrillation efficiency and on the length of the ensuing LNFs with aspect-ratios always higher than those obtained by fibrillation with [Ch]Cl only. The longest LNFs were obtained using lactic acid as the HBD with an average length of 1004 ± 334 nm and width of 31.8 ± 6.8 nm, and thus an aspect-ratio of *ca.* 32. The potential of these protein nanofibers as

reinforcing additives was evaluated by preparing pullulan (PL)-based nanocomposite films containing LNFs with different aspect-ratios, resulting in highly homogenous and transparent films with improved mechanical performance.

Introduction

Protein nanofibers, also known as amyloid fibrils, are typically defined as unbranched protein fibers of aligned cross-β structures[23,76] that, due to their exceptional mechanical properties and thermochemical stability, have recently gained increasing interest in the development of innovative functional nanomaterials[76,226] for different applications, including biosensors, scaffolds, drug carriers and nanocomposite materials.[226] In this latter domain of research, the protein nanofibers' unique combination of size, aspect-ratio, chemical composition and mechanical strength,[226] translates into materials with significantly improved mechanical performance. For example, protein nanofibers have been combined with synthetic matrices, such as poly(lactic acid),[161] poly(vinyl alcohol)[99] and silicone elastomer,[227] to produce nanocomposites with notable mechanical properties. However, the major weakness associated with the application of protein nanofibers in the large scale production of nanocomposite materials is the time required to obtain these nanofibers, since most of the fibrillation procedures are laborious and time-consuming.[81,88] Nevertheless, the recent development of timesaving fibrillation methods for the production of insulin amyloid nanofibrils using a microwave assisted synthesis,[228] and lysozyme nanofibers (LNFs) using a new generation of solvents, *viz.* deep eutectic solvents (DESs),[200] will certainly contribute to propel their widespread use.

Among the existing proteins, hen egg white lysozyme (HEWL) has been extensively investigated as a source of protein nanofibers with several studies reporting the influence of various conditions in its fibrillation.[77] The use of different fibrillation agents (*e.g.*, ethanol,[229] guanidine hydrochloride,[230] urea,[88,89] ionic liquids (ILs)[120] and DES[200]) originates nanofibers with divergent sizes and concomitantly different aspect-ratios. The aspect-ratio of the nanofibers, defined as the ratio between the length and width, is an important factor in materials design since it plays a fundamental role on the mechanical performance of the ensuing materials.[226] For example, Vernaglia *et al.*[230] reported the use of guanidine hydrochloride diluted in potassium phosphate as a fibrillation inducer and produced LNFs with an average length of 100 nm and width of 13 nm, which results in a low aspect-ratio (*ca.* 7.7) compared to other studies where fibrils around 1 μm[105–107] with similar widths were reported. Recently, Silva *et al.*[200] obtained LNFs with dimensions of 0.5–1.0 μm in length and 0.02–0.1 μm in width *via*

fibrillation with a DES based on cholinium chloride ([Ch]Cl) and acetic acid in a molar proportion of 1:1 (see chapter *2.2. Production of lysozyme nanofibers using a deep eutectic solvent*). Accordingly, [Ch]Cl (*i.e.* hydrogen bond acceptor (HBA)) is a key component for protein fibrillation, while the carboxylic acid (*i.e.* hydrogen bond donor (HBD)) seems to have a notable impact on the length of the resulting nanofibers.[200]

Bearing these results in mind, the aim of the present work is to further investigate the effect of the carboxylic acid component of [Ch]Cl-based DES on the fibrillation of HEWL. More specifically, the nature of the carboxylic acid will be evaluated as a strategy to tune the dimensions (aspect-ratio) of the nanofibers. Hence, [Ch]Cl-based DES formulations with different carboxylic acids, namely acetic, lactic and levulinic acids (monoacids), malic acid (diacid) and citric acid (triacid), were tested as fibrillation media for HEWL. Furthermore, the obtained protein nanofibers with different aspect-ratios were used as reinforcing elements in pullulan (PL)-based nanocomposite films and their optical and mechanical properties were assessed.

Experimental Details

Chemicals

Acetic acid ($\geq$ 99.7%, Sigma-Aldrich), lactic acid ($\geq$ 99.7%, Sigma-Aldrich), malic acid ($\geq$ 99.7%, Sigma-Aldrich), citric acid ($\geq$ 99.7%, Sigma-Aldrich), levulinic acid ($\geq$ 99.7%, Sigma-Aldrich), cholinium chloride ([Ch]Cl, $\geq$ 98%, Sigma-Aldrich), glycerol ($\geq$ 99.5%, Sigma-Aldrich), glycine ($\geq$ 98.5%, Sigma-Aldrich), hen egg white lysozyme (HEWL, Sigma-Aldrich, ~70000 U mg^{-1}), pullulan powder (PL, 98%, MW 272 kDa, B&K Technology Group), Thioflavin T (ThT, Sigma-Aldrich) were used as received. Other chemicals and solvents were of laboratory grades. Ultrapure water (type 1, 18.2 MΩ•cm at 25°C) was obtained from a Simplicity® Water Purification System.

Preparation of the DES

The [Ch]Cl:acid based DES were prepared according to the method reported by Florindo *et al.*[217] in which the two components, *i.e.*, [Ch]Cl and the selected acid, were mixed and then grinded in a mortar with a pestle at room temperature until the formation of a homogeneous liquid. The selected acids (Fig. 1) were acetic, lactic, malic

and citric acids in a 1:1 equimolar concentration, and levulinic acid in a 1:2 molar proportion (Table S1).
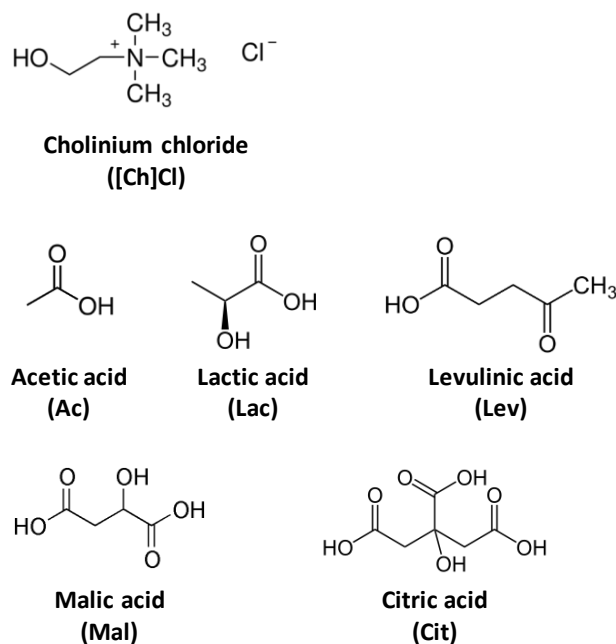
Fig. 1 - Chemical structures of cholinium chloride ([Ch]Cl) and of the carboxylic acids that compose the DESs used in this study.

Production of lysozyme nanofibers (LNFs)

HEWL was dissolved (2 mg mL^{-1}) in an aqueous solution of 10 mM HCl at pH = 2 with 20 mM glycine with 5% (v/v) of the respective DES. The samples were incubated at 70 °C in an oil bath under magnetic stirring. The LNFs were separated from the DES aqueous solution by centrifugation at 15000 rpm during 45 min (Thermo Scientific Megafuge 16R centrifuge). The supernatants were exchanged with Milli-Q ultrapure water. This purification step was repeated twice, and the nanofibers were kept in Milli-Q ultrapure water at 4°C until further use. Triplicates of each sample were carried out and tests with [Ch]Cl alone, as well as with the individual acids, were carried out as control. For the preparation of pullulan films, the nanofibers were freeze-dried and kept in an exicator.

Preparation of films of PL and LNFs

A 6% PL aqueous solution with 10% glycerol (in relation to the mass of PL) was prepared. Then, 5% of freeze-dried LNFs were added and homogenized by magnetic stirring overnight. LNFs produced using [Ch]Cl, [Ch]Cl:Ac, [Ch]Cl:Lac and

[Ch]Cl:Lev were used as reinforcing elements. PL/LNFs films were obtained via solvent casting of the obtained aqueous suspensions, at 30°C in a ventilated oven overnight, using acrylic plates (5×5 cm^2) as moulds. Pure PL films containing only glycerol were also prepared for comparison purposes.

Fluorescence analysis (ThT assays)

For the time-course assay, 30 μL aliquots were taken from the incubated solution at desired time intervals, and added to a 3 mL solution containing 2.5 mM Thioflavin T – ThT, in 10 mM phosphate buffer at pH 7.4. Fluorescence measurements were carried out at 25°C using quartz cells on a Horiba Jobin Yvon Fluoromax-3 fluorimeter. The excitation wavelength was 440 nm and the emission was measured at 482 nm, with both slits of 5 nm. The percentage of fluorescence was calculated according to the maximum fluorescence intensity value (100% fluorescence) registered for each assay.

UV-vis quantification of non-fibrillated HEWL

The concentration of HEWL in the supernatants was measured by UV-vis spectroscopy at 276 nm using a UV-1800 spectrophotometer (Shimadzu, Kyoto, Japan). The supernatant was obtained after the first centrifugation of the incubated samples, and a previously established calibration curve: $\text{Abs}_{276nm} = 2.39[\text{HEWL}]_{mg/mL} - 0.0012$ (R^2=0.9994) was used.

Scanning transmission electron microscopy (STEM)

STEM images were obtained using a field emission gun (FEG) SEM Hitachi SU70 microscope operated at 15 kV. Samples were prepared by immersing a carbon-coated copper grid into the LNFs suspension, and then allowing the solvent to evaporate overnight. The average dimensions of the LNFs were determined by analysis of STEM images using the ImageJ program (at least 100 protein nanofibers were analysed for each experiment).

UV-vis analysis

The transmittance spectra of the PL-based films were acquired with an UV-Vis Spectrophotometer (Shimadzu UV-1800) equipped with a quartz window plate with 10 mm diameter, with the holder in the vertical position. Spectra were recorded at room temperature in steps of 1 nm, in the range 200–700 nm.

Mechanical assays

Tensile tests were performed on an Instron 5966 Series machine, using a load cell of 500 N, operating at a deformation rate of 10 mm min^{-1}, under ambient conditions. At least 5 specimens were tested for each PL-based film sample. Young's modulus, tensile strength and elongation at break were calculated using the Bluehill 3 material testing software.

Results & Discussion

Production of LNFs using different [Ch]Cl-based DESs

The fibrillation of HEWL was performed using different DES formulations in order to assess the effect of the carboxylic acid (HBD) of [Ch]Cl:carboxylic acid based DESs on the dimensions of the protein nanofibers as a strategy to tune their aspect-ratio. Several mono-, di- and tri-carboxylic acids, namely acetic (Ac), lactic (Lac), levulinic (Lev), malic (Mal) and citric (Cit) acids (Fig. 1), were selected to act as HBD. The molar proportion of all [Ch]Cl:carboxylic acid DESs was 1:1, with the exception of the DES containing levulinic acid, which was 1:2 in order to form an eutectic mixture. The formation of protein nanofibers was indirectly assessed by measuring the fluorescence intensity of thioflavin T upon binding to β-sheet structures, as well as by determining the amount of non-fibrillated HEWL by UV-vis spectroscopy at 276 nm. The obtained LNFs with the different DES formulations were further characterized regarding their morphology and dimensions (length and width) by STEM analysis.

Fig. 2 shows the fluorescence intensity of thioflavin T versus time for HEWL in aqueous solutions of the five [Ch]Cl-based DESs.
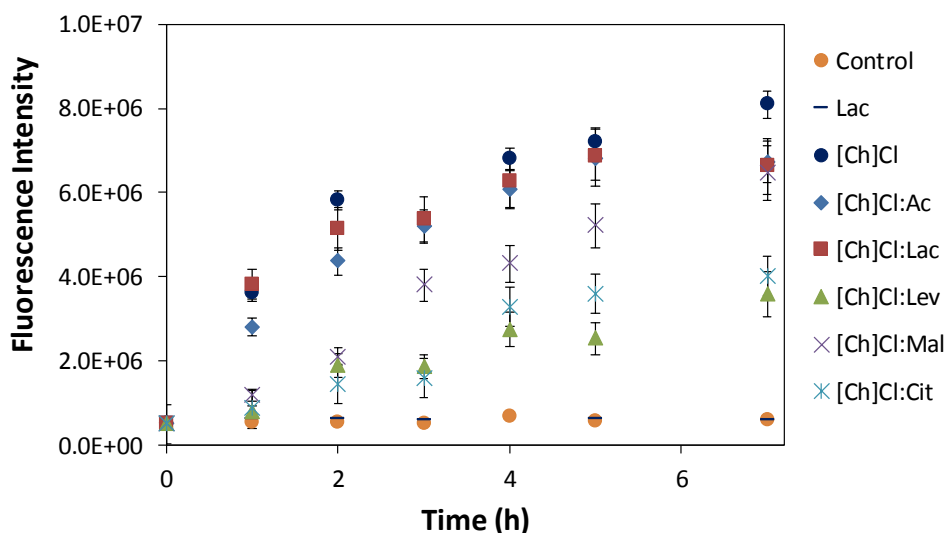
Fig. 2 - ThT fluorescence intensity as a function of time for *β*-sheet structures formed in the aqueous solutions of the different DESs (fibrillation conditions: 5% (v/v) DESs, 70 °C, pH = 2).

Fibrillation could be observed immediately after the addition of the HEWL solution to the different DESs aqueous solutions, and an increase in the ThT fluorescence intensity with time was observed for all five [Ch]Cl-based DESs. The highest fluorescence intensity values, corresponding to the highest fibrillation rate, were registered when using aqueous solutions of lactic (6.63×10^6) and malic (6.46×10^6) acids, which are very similar to those obtained with aqueous solution of [Ch]Cl:Ac (6.73×10^5). For the DESs aqueous solutions of both citric and levulinic acids, half of the final ThT fluorescence intensity was reached only after 4 h of incubation, while for the other DESs this value was obtained within the first 1–2 h. The fact that some DESs promote higher ThT fluorescence intensities than others is probably related with the total amount of [Ch]Cl. Depending on the carboxylic acid and its molar mass, the amount of [Ch]Cl used to prepare the 5% (v/v) of DES aqueous solution is different, as it can be observed in Table 1.

Table 1. Composition of DES used and the molar mass of the correspondent acids.

Sample	M_{acid} (g mol^{-1})	$m_{[Ch]Cl}$ (mmol g^{-1} DES)	m_{acid} (mmol g^{-1}DES)
[Ch]Cl	-	7.2	-
[Ch]Cl:Ac (1:1)	60.05	5.0	5.0
[Ch]Cl:Lac (1:1)	90.08	4.3	4.3
[Ch]Cl:Lev (1:2)	116.12	2.7	5.5
[Ch]Cl:Mal (1:1)	134.02	3.6	3.6
[Ch]Cl:Cit (1:1)	192.13	3.0	3.0

Using a higher amount of [Ch]Cl, as in the case of [Ch]Cl:Ac (5.0 mmol g^{-1} DES), [Ch]Cl:Lac (4.3 mmol g^{-1} DES) and [Ch]Cl:Mal (3.6 mmol g^{-1} DES), originates higher fluorescence intensities (above 6.40×10^6) after 7 h of incubation. In turn, when using [Ch]Cl:Lev (2.7 mmol g^{-1} DES) or [Ch]Cl:Cit (3.0 mmol g^{-1} DES) the fluorescence intensities for the same incubation time barely surpassed 4.02×10^6. In fact, the control assay with [Ch]Cl only registered the highest fluorescence intensity at 7 h (8.09×10^6). On the other hand, the assay with just lactic acid, as an example (Fig. 2), did not show any evidence of β-structures. A similar conclusion was taken for the tests involving the other individual carboxylic acids as summarized in Table 2.

Table 2. ThT fluorescence intensity measurements of the control and the assays using the acids only, after 7 h of incubation.

Samples	ThT Assay
Control	5.37×10^5
Acetic acid	5.81×10^5
Lactic acid	5.69×10^5
Levulinic acid	5.42×10^5
Malic acid	5.56×10^5
Citric acid	5.47×10^5

According to this data, it is reasonable to admit that the lysozyme fibrillation is directly driven by the quantity of [Ch]Cl used in the fibrillation medium, which can possibly be due to the capacity of [Ch]Cl to form hydrogen bonds in solution and to leverage the interaction with the protein, leading to convert lysozyme into β-structures. In this line, the concentration of [Ch]Cl ,together with other experimental conditions:[20] *e.g.* high temperature and low pH, plays an important role in the protein fibrillation process. Therefore, it was expected to obtain equal fluorescence intensities for all DESs solutions with the same content in [Ch]Cl. To confirm this assumption, three DESs with the same (1:1) proportion and the same molar concentration, *i.e.* [Ch]Cl:Lac (3.0% (v/v)), [Ch]Cl:Mal (3.6% (v/v)), [Ch]Cl:Cit (4.3% (v/v)), and thus with the same molar fraction of [Ch]Cl (0.13 mmol mL^{-1}), were investigated on the fibrillation of HEWL (Table 3).

Table 3. Mass and molar fractions of the components of the [Ch]Cl:Lac, [Ch]Cl:Mal and [Ch]Cl:Cit DESs used in the complementary assays to ascertain the role of [Ch]Cl in HEWL fibrillation.

Samples	M_{ChCl} (g mol^{-1})	$m_{[Ch]Cl}$ (g assay^{-1})	n_{ChCl} (mmol mL^{-1})	m_{acid} (g assay^{-1})	n_{acid} (mmol mL^{-1})	m_{DES} (g assay^{-1})	% (v/v) DES
[Ch]Cl:Lac	139.62	0.74	0.13	0.47	0.13	1.21	3.0
[Ch]Cl:Mal	139.62	0.74	0.13	0.70	0.13	1.43	3.6
[Ch]Cl:Cit	139.62	0.74	0.13	1.00	0.13	1.74	4.3

However, the fluorescence intensities obtained were different from each other dependent on the nature of the DES used, as illustrated in Fig. 3. This leads to the conclusion that, although the acid group of the DES does not promote fibrillation by itself, its chemical structure plays a fundamental role in the efficiency of the fibrillation process.
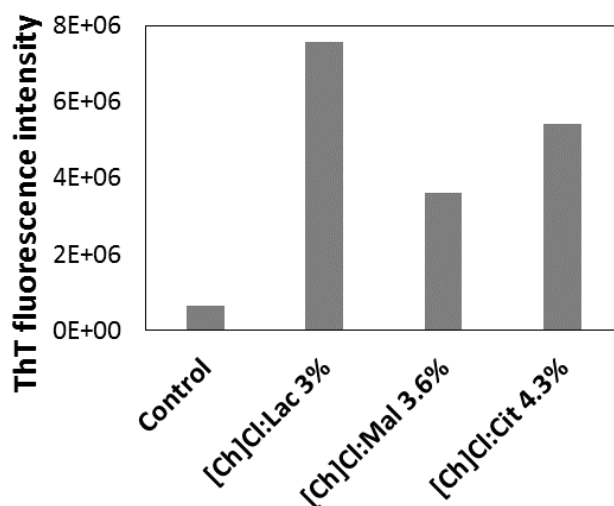
Fig. 3 - ThT fluorescence intensity measurements of the assays using [Ch]Cl:Lac, [Ch]Cl:Mal and [Ch]Cl:Cit with the same molar fraction of [Ch]Cl (0.13 mmol mL^{-1}), after 7 h of incubation.

Table 4 presents the conversion ratio of HEWL into β-sheet structures (possibly nanofibers) obtained with the different 5% (v/v) DESs solutions. It is can be seen that the conversion ratios for [Ch]Cl:Ac and [Ch]Cl:Lac are above 90%, indicating that more than 90% of HEWL was misfolded and possibly arranged into nanofibers. Moreover, a conversion ratio of about 80% was achieved using [Ch]Cl:Mal as fibrillation agent, whereas [Ch]Cl:Cit and [Ch]Cl:Lev originated lower conversion ratios of nearly 70%. Worth noting is the fact that these results are in close agreement with the ThT fluorescence intensity data (Table 4).

Table 4. Conversion ratios of HEWL and ThT fluorescence intensity measurements after 7 h of incubation.

Samples	Conversion (%)	ThT Assay
[Ch]Cl	94.5 ± 0.4	$(8.09 \pm 0.32) \times 10^6$
[Ch]Cl:Ac	93.7 ± 0.5	$(6.73 \pm 0.37) \times 10^6$
[Ch]Cl:Lac	93.4 ± 0.5	$(6.63 \pm 0.39) \times 10^6$
[Ch]Cl:Lev	70.0 ± 0.7	$(3.58 \pm 0.18) \times 10^6$
[Ch]Cl:Mal	80.8 ± 0.6	$(6.46 \pm 0.32) \times 10^6$
[Ch]Cl:Cit	69.3 ± 0.7	$(4.02 \pm 0.21) \times 10^6$

The STEM micrographs of all LNFs obtained in this study are presented in Fig. 4, where thin and elongated nanofibers are visible, corresponding to the so-called worm-like shape.[56] It is clearly evident that, besides the effect on HEWL fibrillation, the carboxylic acid present in the [Ch]Cl-based DESs has a fundamental role on the dimensions (length and width) of the nanofibers. In fact, the LNFs produced with the different DESs formulations present higher dimensions than those produced with [Ch]Cl (aqueous solution) only. Notably, [Ch]Cl:Ac and [Ch]Cl:Lac seem to produce the longest nanofibers, whereas [Ch]Cl:Lev and [Ch]Cl:Cit generate slightly shorter nanofibers (although still much longer than those produced using [Ch]Cl), confirming the importance of the carboxylic acid component of the DES on the production of longer LNFs, as will be discussed below.

Fig. 5 depicts the distribution of the length and width of the obtained protein nanofibers, determined from the STEM micrographs. According to the box charts, the use of an aqueous solution of [Ch]Cl as fibrillation agent originates LNFs with a maximum length of 611 nm, whereas the use of any of the five [Ch]Cl-based DESs (containing different carboxylic acids) yields LNFs with maximum length values above 1000 nm. In fact, the maximum length value (2086 nm) was obtained for the LNFs produced by the aqueous solutions of [Ch]Cl:Lac. In terms of average values (Table), the longest LNFs were produced when aqueous solutions of [Ch]Ch:Ac and [Ch]Cl:Lac were used, with average lengths of 887 ± 310 nm and 1004 ± 334 nm, respectively. Nanofibers with slightly lower average lengths were produced using aqueous solutions of [Ch]Cl:Mal, 827 ± 331 nm, followed by the ones generated by [Ch]Cl:Lev and [Ch]Cl:Cit with average length values lower than 500 nm (492 ± 175 and 490 ± 152 nm, respectively). Nevertheless, these values are still higher than those obtained for the control (350 ± 104 nm) where no acid was present (Table 5), thus confirming the relevance of the carboxylic acid to tune the length of the lysozyme nanofibers.

Regarding the width of the LNFs (Fig. 4), values ranging from 10 up to 50 nm were obtained for the different [Ch]Cl-based DES. Among the carboxylic acids, levulinic and citric acids seem to promote the production of thinner nanofibers (*ca.* 20 nm) when compared to acetic, lactic and malic acids (*ca.* 30 nm). The most significant conclusion is that the presence of the acid groups in HBD of DES, as well as the

94

chemical structure of the acids used, are very important parameters in tuning the length and width of the nanofibers.
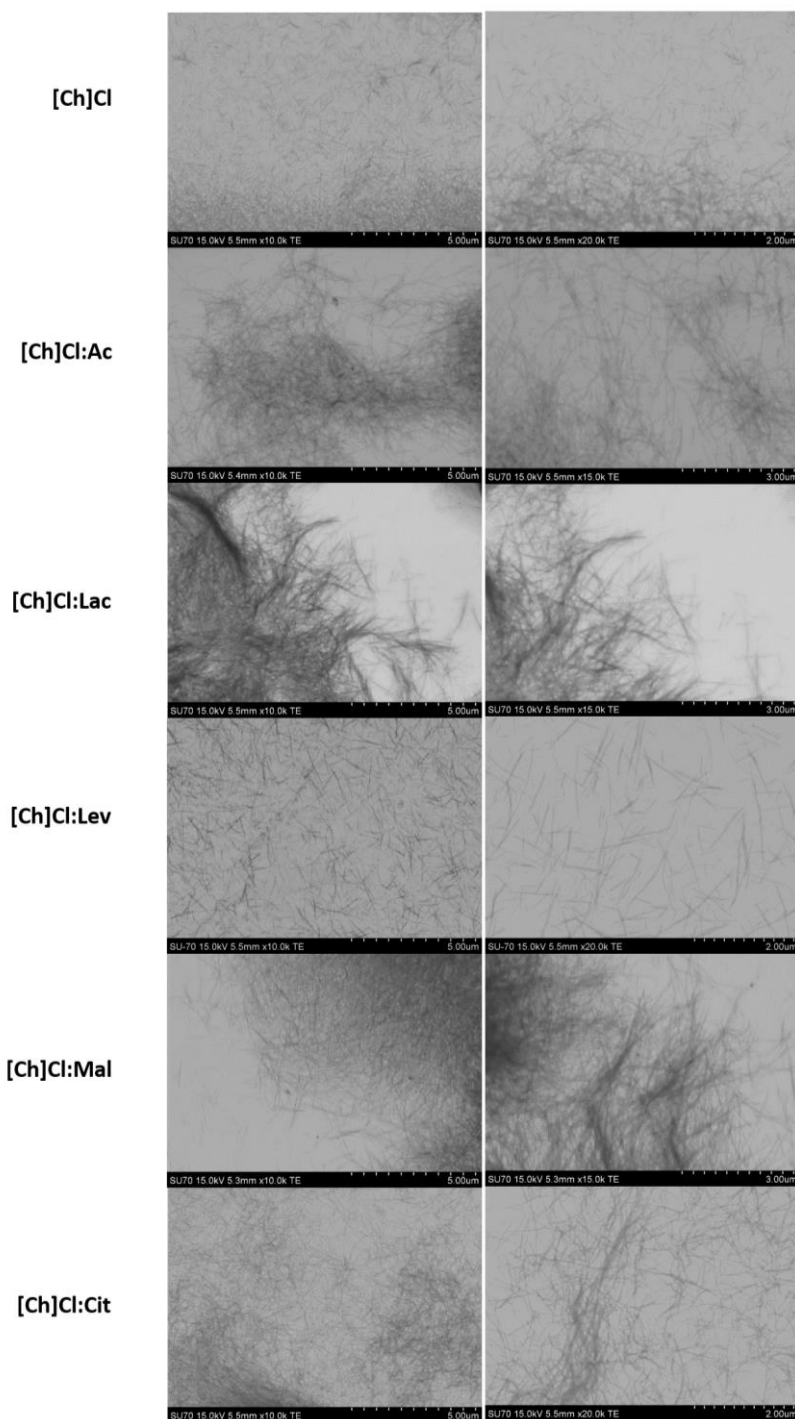
Fig. 4 - STEM images of LNFs formed using 5% (v/v) of DESs and [Ch]Cl aqueous solutions, at 70 °C, pH = 2. The STEM images of [Ch]Cl are from our previous work,[200] and they are presented here for comparison.
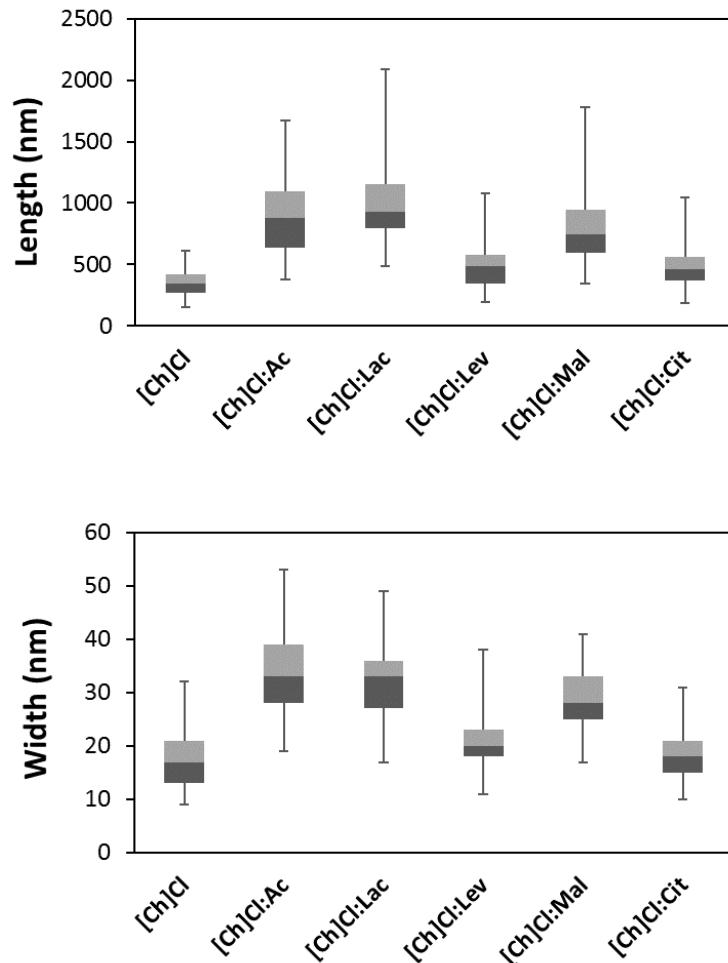
Fig. 5 - Box charts with LNFs dimensions of length (nm) and width (nm). The results of [Ch]Cl were taken from our previous work,[200] and they are presented here for comparison.

The aspect-ratios of the LNFs obtained with the different [Ch]Cl-based DESs as fibrillation agents are presented in Table 5. According to the data, all nanofibers have higher aspect-ratios (23.7–31.6) than those obtained using aqueous solutions of [Ch]Cl (19.8). In fact, the nanofibers produced using [Ch]Cl:Lac registered the highest aspect-ratio with a value of 31.6, suggesting that they are probably the ones with the higher reinforcing ability for composite materials, followed by the LNFs obtained when using aqueous solutions of [Ch]Cl:Mal, [Ch]Cl:Cit and [Ch]Cl:Ac with 28.9, 26.6 and 26.4, respectively.

Table 5. Average length and width, and the corresponding aspect-ratio of the LNFs produced with different [Ch]Cl-based DES formulations (aqueous solutions).

Samples	Length (nm)	Width (nm)	Aspect-ratio
[Ch]Cl	350 ± 104	17.7 ± 5.4	19.8
[Ch]Cl:Ac	887 ± 310	33.6 ± 7.8	26.4
[Ch]Cl:Lac	1004 ± 334	31.8 ± 6.8	31.6
[Ch]Cl:Lev	492 ± 175	20.8 ± 4.4	23.7
[Ch]Cl:Mal	827 ± 331	28.6 ± 5.3	28.9
[Ch]Cl:Cit	490 ± 152	18.4 ± 4.7	26.6

Assessment of the reinforcement potential of the LNFs produced by different DESs

The potential of the protein nanofibers as reinforcing elements was studied by preparing pullulan (PL)-based nanocomposite films containing LNFs with different aspect-ratios. PL was selected as matrix because it is a biodegradable, non-toxic, water-soluble and filmogenic non-ionic exopolysaccharide with a long history in food and pharmaceutical applications.[231,232] So, freeze-dried LNFs obtained via fibrillation with [Ch]Cl, [Ch]Cl:Ac, [Ch]Cl:Lac and [Ch]Cl:Lev were dispersed in a PL aqueous solution, and the corresponding nanocomposite films with 5 wt.% of nanofibers were obtained through solvent casting. All films were plasticized with glycerol (selected based on previous studies[233–235]) to reduce brittleness, and were characterized regarding their optical and mechanical properties. Fig. 6 shows that the ensuing thin nanocomposite films were very homogeneous, highly transparent and glossy, which are important characteristics of a material for application in *e.g.* the packaging and biomedical fields.
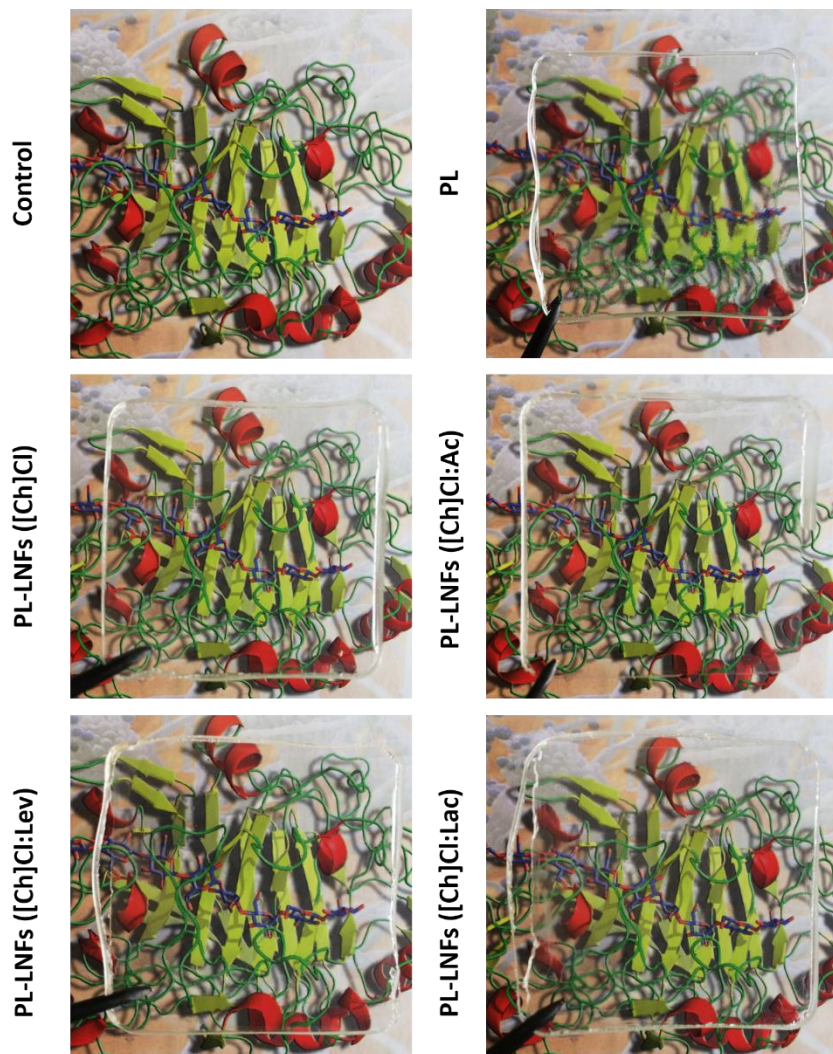
Fig. 6 - Photographs of the nanocomposite films of PL and LNFs, confirming their homogeneity and transparency. The control is the picture without any film.

The optical properties of the PL-based nanocomposite films were evaluated by determining their transmittance in the range between 200 and 700 nm, as presented in Fig. 7. The UV-visible spectra show that all PL-based films are optically transparent, with transmittance values of nearly 90% in the visible range (400−700 nm),[236] confirming that the transmittance was not affected by the incorporation of the LNFs produced with the different DESs. In the ultraviolet range (200–400 nm), there is an absorption peak around 276–280 nm, which can be linked to the presence of the protein nanofibers, since all aromatic amino acids, such as tyrosine, phenylalanine and tryptophan, absorb UV light.[237] Tryptophan is usually responsible for most of the absorbance of ultraviolet light at 280 nm, and lysozyme has almost 5% of this amino acid in its singular chain (6 tryptophans in 129 total amino acids).[238] As a consequence,

these PL-based films with LNFs present low transmittance values in the UV region when compared with pure PL films, which means that the PL-LNFs nanocomposite films display higher ultraviolet light barrier properties, particularly in the short-wavelength spectrum.
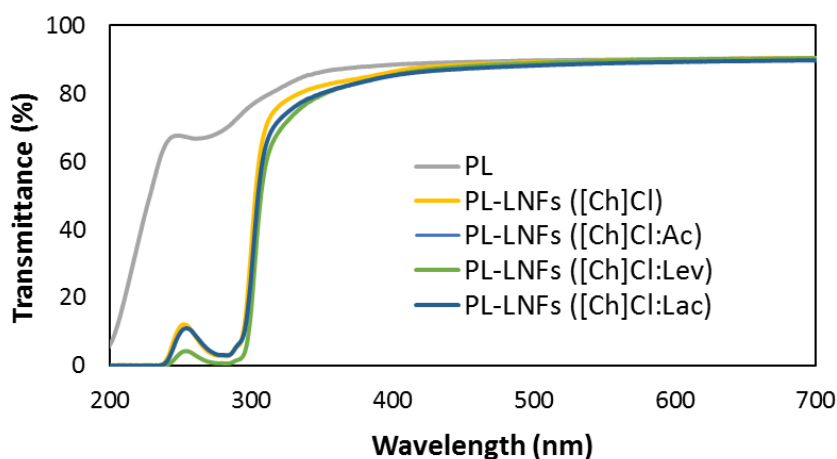
Fig. 7 - UV-vis spectra of the nanocomposite films based on PL and LNFs.

The mechanical properties of the PL-based nanocomposite films containing 5 wt.% of LNFs with different aspect-ratios were evaluated by typical tensile experiments. The Young's modulus, tensile strength and elongation at break, determined from the stress-strain curves, are presented in Fig. 8. The plasticized PL film without LNFs showed a Young's modulus of 1587 ± 68 MPa, tensile strength of 36.6 ± 3.2 MPa and elongation at break of 6.67 ± 1.21%, in agreement with previously published data.[239,240] Overall, the incorporation of LNFs in the PL films promoted an increase in the Young's modulus and tensile strength, as well as a decrease in the elongation at break, all of which are influenced by the aspect-ratio of the nanofibers (Fig. 7). As expected, the use of shorter LNFs with an aspect-ratio of 19.8 ([Ch]Cl, Table 2) promoted an increase of *ca*. 18% in the Young's modulus (1868 ± 127 MPa, PL-LNFs([Ch]Cl)), whereas longer LNFs with aspect-ratios of 26.4 ([Ch]Cl:Ac) and 31.6 ([Ch]Cl:Lac) led to an augment of about 34% (2131 ± 151 MPa, PL-LNFs([Ch]Cl:Ac)) and 36% (2157 ± 82 MPa, PL-LNFs([Ch]Cl:Lac)), respectively. Additionally, the tensile strength of the PL-based nanocomposites followed the same trend as that observed for the Young's modulus. All PL-LNFs nanocomposite films show tensile strength values higher than the pure PL film (36.6 ± 3.2 MPa), reaching maximum values of 41.5 ± 5.0 MPa (PL-LNFs([Ch]Cl:Lac)) and 42.3 ± 3.4 MPa (PL-

LNFs([Ch]Cl:Ac)) for the nanocomposites containing LNFs with aspect-ratios of about 31.6 and 26.4, respectively. Regarding the elongation at break, this parameter is reduced from 6.67 ± 1.21% for pure PL films to values in the range 2.13–2.66% (Fig. 8) for the nanocomposites films, which corresponds to a reduction of about 60%. This is obviously ascribed to the stiffness of the protein nanofibers.

The results obtained from the tensile tests clearly confirm that the LNFs with higher aspect-ratio, namely the ones produced with [Ch]Cl:Ac and [Ch]Cl:Lac (Table 2), have a stronger impact on the nanocomposites properties than those produced with just [Ch]Cl. Moreover, the LNFs are indeed an effective reinforcing element for PL films even at a low loading of protein nanofibers (5 wt.%), because of their high and tunable aspect-ratios.
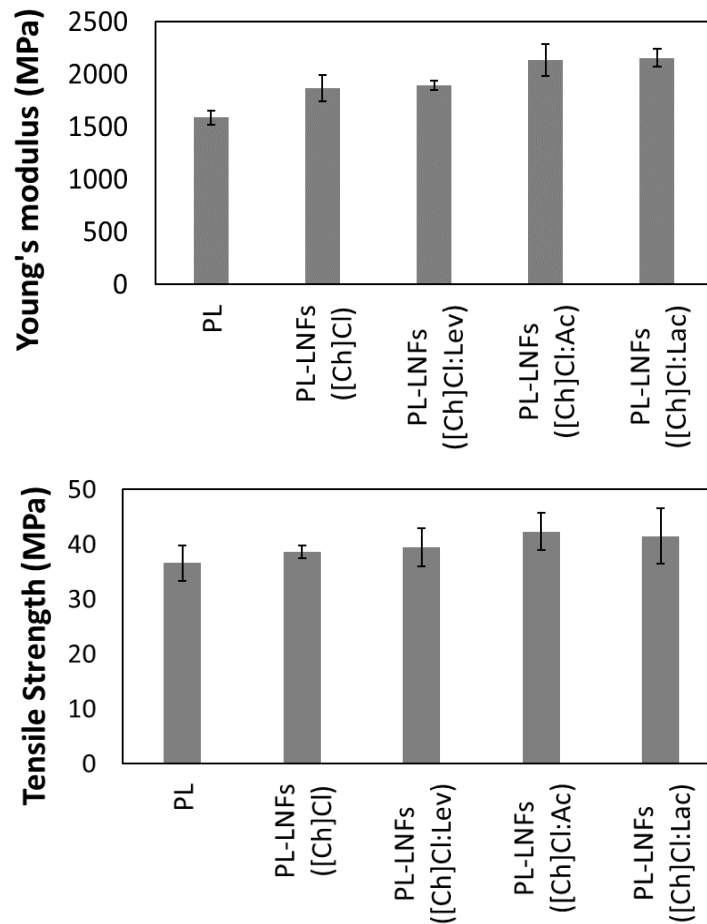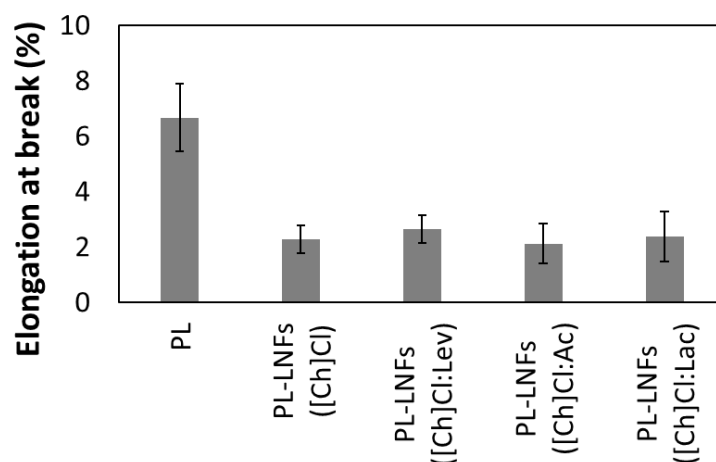
Fig. 8 - Young's modulus, tensile strength and elongation at break of the PL-based nanocomposite films reinforced with 5 wt.% of LNFs produced using different DES formulations. The aspect-ratio of the LNFs increase in the following order: [Ch]Cl < [Ch]Cl:Ac < [Ch]Cl:Lac < [Ch]Cl:Lev (Table 5).

Conclusions

DESs based on cholinium chloride ([Ch]Cl, the HBA) and different carboxylic acids (the HBD) are efficient fibrillation agents of HEWL allowing to produce protein nanofibers with different dimensions (length and width). In fact, the aspect-ratio of LNFs can be tuned by varying the type of carboxylic acid (mono-, di- and tri-carboxylic acids: acetic, lactic, levulinic, malic and citric acids). The longest LNFs were obtained using lactic acid ([Ch]Cl:Lac) with an average length of 1004 ± 334 nm and width of 31.8 ± 6.8 nm, and hence an aspect-ratio of 31.6. Furthermore, the incorporation of only 5 wt.% of protein nanofibers with different aspect-ratios in a pullulan matrix originated homogeneous, glossy and transparent nanocomposite films with substantially improved mechanical properties. The LNFs with the higher aspect-ratio led to an increase of about 36% for the Young's modulus and 15% for the tensile strength, confirming their higher reinforcing capacity. These promising results emphasize the potential of protein nanofibers with tailorable dimensions (using [Ch]Cl:carboxylic acid based DESs as timesaving fibrillation agents) as reinforcing elements for the development of nanocomposites with upgraded mechanical performance.

3.
Development of innovative materials based on protein nanofibers

The main objective of this part of the thesis was the development of novel functional protein nanofibers-polysaccharide based materials for potential application as packaging materials and biosorbents for water purification. The preparation of the nanocomposites was performed by distinct methodologies, depending on the polysaccharide used. For instance, pullulan based films were prepared by film casting of water suspensions containing pullulan and protein nanofibers due to its high filmogenic ability (following the preliminary results described in chapter *2.3 Tuning lysozyme nanofibers dimensions using deep eutectic solvents for improved reinforcement ability*), and NFC membranes were prepared by vacuum filtration from an aqueous based suspension containing cellulose and protein nanofibers. The obtained materials were then analysed in terms of transparency, thermal stability, morphology and mechanical performance, and the evaluation of potential functional properties were further carried out.

This work originated 2 papers that corresponds to the sub-chapters highlighted in the following pages.

3.1. Pullulan-based nanocomposite films for functional food packaging: exploiting lysozyme nanofibers as antibacterial and antioxidant reinforcing additives
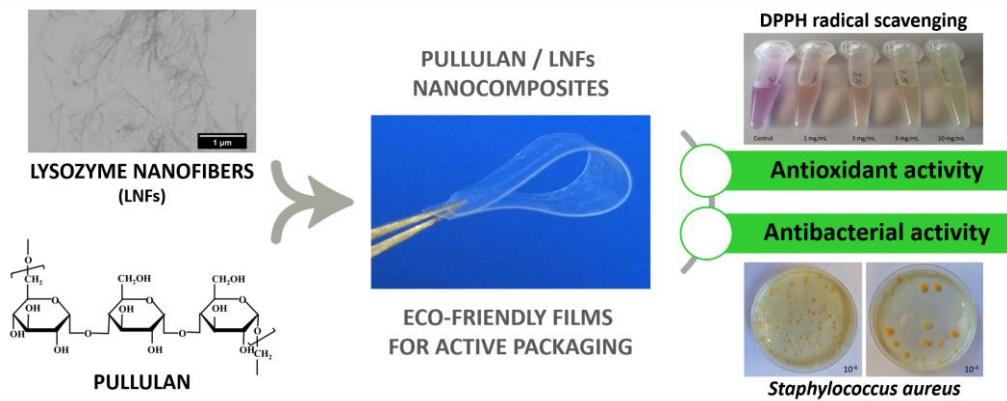
Silva, NHCS; Vilela, C; Almeida, A; Marrucho, IM; Freire, CSR (2018) *Pullulan-based nanocomposite films for functional food packaging: exploiting lysozyme nanofibers as antibacterial and antioxidant reinforcing additives*, FOOD HYDROCOLLOIDS, 77, 921-930.

3.2. Innovative membranes based on nanocellulose and protein nanofibers for the removal of mercury (II) from natural waters
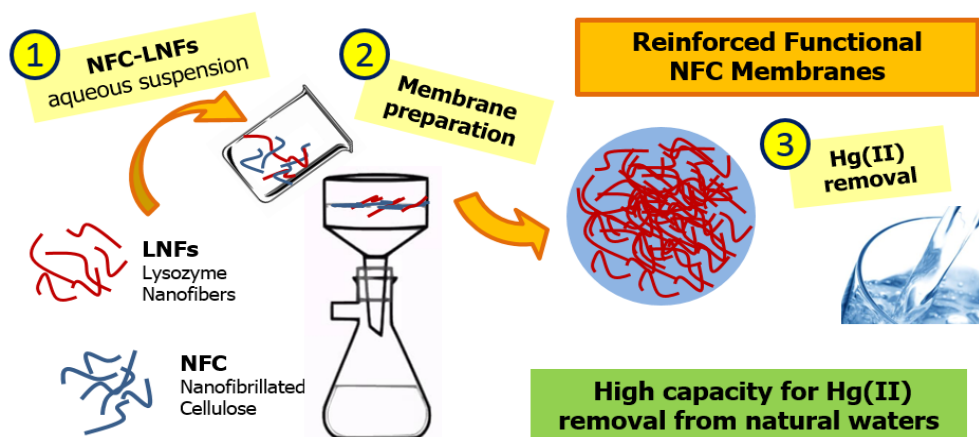
Silva, NHCS; Figueira, P; Vilela, C; Pinto, RJB; Marrucho, IM; Pereira, ME ; Freire, CSR (2018) *Innovative membranes based on nanocellulose and protein nanofibers for the removal of mercury (II) from natural waters*, In preparation.

3.1.

Pullulan-based nanocomposite films for functional food packaging: exploiting lysozyme nanofibers as antibacterial and antioxidant reinforcing additives

Nuno H. C. S. Silva,[a] Carla Vilela,[a] Adelaide Almeida,[b]

Isabel M. Marrucho,[c] Carmen S. R. Freire [a]

[a] CICECO – Aveiro Institute of Materials, Department of Chemistry, University of Aveiro, 3810-193 Aveiro, Portugal

[b] CESAM and Department of Biology, University of Aveiro, 3810-193 Aveiro, Portugal

[c] Centro de Química Estrutural, Instituto Superior Técnico, Universidade de Lisboa, Avenida Rovisco Pais, 1049-001 Lisboa, Portugal

Abstract

Homogeneous, glossy and transparent nanocomposite films composed of pullulan (PL) and lysozyme nanofibers (LNFs) were developed by simple solvent casting from aqueous suspensions. The incorporation of LNFs into the PL matrix maintained the filmogenic ability of PL and endowed the nanocomposite films with good mechanical properties (Young's modulus = 1.91–2.50 GPa) and several functionalities, confirming the potential of LNFs as bioactive reinforcing elements for nanocomposites. The set of pliable films exhibits thermal stability up to 225°C and maximum antioxidant activity around 77% (DPPH scavenging activity) for the film with the highest LNFs content (15.0 wt.%). The antibacterial activity of the ensuing nanocomposite films towards

Staphylococcus aureus, *viz.* lysozyme-resistant bacteria, was assessed, and the data show augmented antibacterial effectiveness with increasing content of nanofibers. These promising results show the potential of PL/LNFs nanocomposites as eco-friendly edible films for active packaging.

Introduction

Pullulan (PL), a non-ionic exopolysaccharide obtained from the fermentation medium of the fungus-like yeast *Aureobasidium pullulans*, is a biocompatible, biodegradable, non-toxic, non-mutagenic, non-carcinogenic, and edible water-soluble biopolymer[231] with great potential for application in a multitude of domains including tissue engineering,[241] drug and gene targeting,[242] and food packaging.[243] Driven by the impressive film-forming ability of PL that originates colorless, tasteless, odorless, transparent, heat-sealable, and oxygen impermeable films,[243] myriad publications dealing with PL-based films and coatings for protective food packaging have been published in the past decades.[233,236,239,243–251]

However, the body of literature clearly shows that the use of pure PL films in the packaging field presents some major drawbacks associated with their hydrophilic nature, brittleness and absence of active functions. The design of PL-based blends and composite films is the path of choice to overcome these intrinsic limitations and obtain multifunctional packaging tools to improve the shelf-life, safety and quality of food. PL has been combined with various functional agents (*e.g.*, sakacin-A,[244] thymol,[245] silver nanoparticles,[246] essential oils and nanoparticles,[247] lysozyme,[248] cholinium carboxylate ionic liquids,[236] graphene oxide,[239] bacterial cellulose,[233] nanofibrillated cellulose,[249] and gelatin[250]) that, as a result of the chemical and/or physical interaction between the individual components, improve the films mechanical performance,[233,249–251] and/or impart bioactivity to the films, particularly antimicrobial activity.[236,245–248]

Among the vast array of natural polymers based functional materials, protein-engineered materials display a wide range of customizable properties and are attracting considerable interest.[16,17] Proteins, such as casein, gelatin, lysozyme, soy and whey proteins, are not only used individually but also in blends and composites for the formation of edible films for food packaging.[243,248,250–252] With the advent of nanotechnology, protein nanofibers (*i.e.*, fibrillar assemblies of monomeric proteins or peptides that underwent unfolding-refolding transition into stable β-sheet structures[253]) are emerging as building nanoblocks with potential for developing innovative functional nanocomposites due to their peculiar mechanical and biological properties.[28,226,254] Although the use of protein nanofibers as nanosized reinforcing elements for nanocomposites is still in its infancy, the recent development of timesaving fibrillation

methods for the production of (i) lysozyme nanofibers (LNFs), from hen egg white lysozyme (HEWL) using a new generation of ionic solvents namely deep eutectic solvents (DESs) (see results described on chapter 2.1 and 2.2),[200] and (ii) insulin amyloid nanofibrils, using a microwave assisted synthesis,[228] will definitely contribute to their widespread use. Thus, the combination of PL and bioactive protein nanofibers is an appealing approach to design nanocomposite films with superior mechanical and biological properties. To the best of our knowledge and with special reference to the food packaging field, PL has never been used in combination with bioactive protein nanofibers for the fabrication of nanocomposite films for the simultaneous containment, protection and preservation of foods.

In this context, and following our interest in protein nanofibers,[200,228] and biopolymers-based nanocomposites,[255,256] the present work reports the preparation and characterization of nanocomposite films based on PL and lysozyme nanofibers (LNFs) obtained by casting of water-based suspensions of both biopolymers with the addition of glycerol as plasticizer. The ensuing films were characterized regarding their structure, morphology, optical properties, mechanical performance, thermal stability, antioxidant and antibacterial activities, envisaging their potential application as active food packaging films.

Experimental Details

Chemicals, materials and microorganisms

Acetic acid ($\geq$ 99.7%, Sigma-Aldrich), cholinium chloride ($\geq$ 98%, Sigma-Aldrich), glycerol ($\geq$ 99.5%, Sigma-Aldrich), glycine ($\geq$ 98.5%, Sigma-Aldrich), hen egg white lysozyme (HEWL, Sigma-Aldrich, ~70000 U mg^{-1}), pullulan powder (PL, 98%, MW 272 kDa, B&K Technology Group), Congo Red ($\geq$ 85%, BioXtra, Sigma), 2,2-diphenyl-1-picrylhydrazyl (DPPH, Aldrich), Brain-Heart Infusion (BHI, Liofilchem), phosphate buffer solution (PBS, pH 7.4, Sigma-Aldrich) and trypticase soy agar (TSA, Sigma-Aldrich) were used as received. Other chemicals and solvents were of laboratory grades.

Staphylococcus aureus ATCC 6538 was provided by DSMZ – Deutsche Sammlung von Mikroorganismen und Zellkulturen GmbH (German Collection of Microorganisms and Cell Cultures).

Production of lysozyme nanofibers (LNFs)

LNFs were produced following an established method based on the fibrillation of lysozyme using a deep eutectic solvent.[200] Briefly, HEWL was dissolved (2 mg mL^{-1}) in an aqueous solution of 10 mM HCl at pH = 2 with 20 mM glycine with 5% (v/v) of a DES composed of cholinium chloride and acetic acid (1:1). The samples were incubated at 70°C overnight under magnetic stirring. The LNFs were separated from the DES solution by centrifugation at 15000 rpm for 45 min (Thermo Scientific Megafuge 16R centrifuge). The supernatants were exchanged with Milli-Q ultrapure water and the nanofibers were freeze-dried.

Preparation of PL/LNFs nanocomposite films

PL solutions (6.0 % w/v) were prepared using a glycerol aqueous solution (10% w/v) as the solvent. Then, different amounts of LNFs were added to the polysaccharide solutions in order to obtain films with LNFs contents of 1.0, 3.0, 5.0, 10.0 and 15.0%, as summarized in Table 1. All the prepared mixtures were homogenized by mechanical stirring for 3h. The films were obtained by casting at 30°C in a ventilated oven overnight, using acrylic plates (5 × 5 cm^2) as molds. The resulting thin films were removed from the molds and kept in desiccators until their use. All films were prepared in triplicate and for comparison purposes neat PL films and PL with native lysozyme (15.0 wt.%) films were also prepared.

Table 1. Composition and thickness of the prepared PL-based films.

Sample	PL (mg)	LNFs (%)*	Glycerol (%)*	Thickness (μm)
PL	480	0.0	10.0	84.1 ± 7.7
PL/LNFs_1%	480	1.0	10.0	96.7 ± 7.8
PL/LNFs_3%	480	3.0	10.0	104.5 ± 10.8
PL/LNFs_5%	480	5.0	10.0	105.8 ± 6.4
PL/LNFs_10%	480	10.0	10.0	108.1 ± 5.4
PL/LNFs_15%	480	15.0	10.0	113.2 ± 11.6

* (w/w) relative to PL.

Characterization techniques

Films thickness was measured by a hand-held digital micrometer (Mitutoyo, Mitutoyo Corporation, Japan) with an accuracy of 0.001 mm. All measurements were randomly performed at different locations of the film sample and the average value was determined.

The FTIR-ATR spectra were collected with a Perkin-Elmer FT-IR System Spectrum BX spectrophotometer equipped with a single horizontal Golden Gate ATR cell, over the range of 600–4000 cm^{-1} at a resolution of 4 cm^{-1} averaged over 32 scans.

The X-ray diffraction (XRD) analysis was carried out on a Phillips X'pert MPD diffractometer using CuKα radiation (λ = 1.541 Å) with a scan rate of 0.05◦ s^{-1}(in 2θ scale). The patterns were collected in reflection mode with the films placed on a Si wafer with negligible background signal to provide mechanical support and to avoid bending of the samples.

SEM images of the nanocomposite films surfaces and cross-sections were obtained on a HR-FESEM SU-70 Hitachi microscope operating at 4.0 kV. The samples were previously coated with a carbon film.

The fluorescence micrographs were acquired using a Widefield fluorescence microscope Zeiss Imager M2 equipped with a 3.0 Mpix color camera (Zeiss, Germany). The images were processed in Zen 2.3 software. LNFs were previously labelled with Congo Red.

The transmittance spectra of the films were acquired with an UV-Vis Spectrophotometer (Shimadzu UV-1800) equipped with a quartz window plate with 10 mm diameter, bearing the holder in the vertical position. Spectra were recorded at room temperature in steps of 1 nm, in the range 200–700 nm.

Tensile assays were performed on an Instron 5966 Series machine in traction mode at a cross-head velocity of 5 mm min^{-1} and using a static load cell of 500 N, under ambient conditions. At least 4 rectangular specimens (50 mm × 10 mm) were tested for each film sample and the average value was recorded. Tensile strength, Young's modulus and elongation at break were calculated using the Bluehill 3 material testing software.

Thermogravimetric analysis (TGA) assays were carried out with a SETSYS Setaram TGA analyzer equipped with a platinum cell. Samples were heated at a constant rate of 10°C min^{-1} from room temperature up to 800°C under a nitrogen flow of 200 mL min^{-1}. The thermal decomposition temperature was taken as the onset of significant (~0.5 %) weight-loss, after the initial evaporation of moisture.

Antioxidant activity

The antioxidant activity of the films was determined by the DPPH radical scavenging method, following a procedure described elsewhere[257] with minor adjustments. Briefly, *ca*. 60 mg of film was added to 4 mL of methanol:water (50:50) solution, and vortex stirred during 3 cycles of 1 min. Then, 250 μL of 0.2 mM DPPH solution was added and the mixture was kept in the dark at room temperature for 2 h. The mixture was centrifuged at 12000 rpm for 30 min at room temperature. Afterwards, the absorbance of the supernatants was measured at 517 nm on a Shimadzu UV-1800 spectrophotometer (Kyoto, Japan). Lysozyme and LNFs (at different concentrations: 0.5–5.3 mg mL^{-1}) were also tested in the absence of PL for comparison purposes. The DPPH scavenging activity was calculated as:

$$DPPH\ scavenging\ activity\ (\%) = \frac{A_{control} - A_{sample}}{A_{control}} \times 100,$$ where A_{sample} is the absorbance of sample and $A_{control}$ is the absorbance of the control.

Antibacterial activity

The antibacterial activity of the nanocomposite films was tested against *S. aureus* (ATCC 6538). The bacterial pre-inoculum cultures were grown for 18–24 h in BHI at 37°C under horizontal shaking at 120 rpm until reaching a concentration of $10^8 – 10^9$ colony forming units per mL (CFU mL^{-1}). Each film sample (*ca*. 500 mg) was placed in contact with 5 mL of bacterial liquid suspension *via* a ten-fold dilution of the overnight grown culture in PBS (pH 7.4). Plasticized PL and PL/lysozyme films were tested as blank references, while a control bacteria cell suspension tested as internal reference of the method. All samples were incubated at 37 °C in static conditions. At 0, 24 and 48 h contact time, aliquots (500 μL) of each sample and controls were collected and the bacteria cell concentration (CFU mL^{-1}) was determined by plating serial dilutions on TSA medium. The plates were incubated at 25°C for 48 h. The CFU were determined on the most appropriate dilution on the agar plates. Two independent experiments were carried out and, for each, two replicates were plated. The bacteria log reduction of the samples was calculated as follows: log reduction = log CFU$_{control}$ − log CFU$_{film}$.

Statistical analysis

All samples were analyzed in triplicate (unless stated otherwise) and standard deviations were reported. Statistical significance was determined using an analysis of variance (ANOVA) and Tukey's test (OriginPro 8 SR0). Statistical significance was established at $p < 0.05$.

Results & Discussion

A set of nanocomposite films based on PL and different amounts of LNFs was prepared by solvent casting from aqueous suspensions, as listed in Table. Lysozyme, a peptidoglycan *N*-acetyl-muramoylhydrolase with a long and safe history as a natural antimicrobial agent applied as food preservative, was selected as the purveyor of protein nanofibers because it is a low-cost protein occurring in high concentration in eggs[258] and its nanofibrillation mechanism have been extensively studied.[88,117,229,230,259] The obtained LNFs have an aspect ratio of *ca.* 26.7 (length: 880.2 ± 44.0 nm, width: 33.0 ± 1.6 nm), as determined from scanning transmission electron microscopy data in accordance with previously published data.[200] The aspect ratio of protein nanofibers is one of the parameters responsible for their good mechanical performance.[226] All films were plasticized with glycerol (selected based on previous studies[233–235]) to reduce brittleness and concomitantly increase the pliability and workability of the PL-based films. The resulting nanocomposite films were characterized in terms of structure, morphology, optical properties, mechanical performance, thermal stability, antioxidant and antibacterial activities. The obtained thin nanocomposite films, prepared with the same amount of casting suspension, were in general macroscopically homogenous, highly transparent and glossy as shown in Fig. 1. Furthermore, their thickness increased from 84.1 ± 7.7 to 113.2 ± 11.6 μm by increasing the LNFs content from 0 to 15.0 wt.% (Table 1, p < 0.05). A similar trend was observed for PL edible films containing whey protein isolate, whose thickness increased with the increasing content of protein,[260] as well as for films of other polysaccharides like for example chitosan films containing ellagic acid.[257]
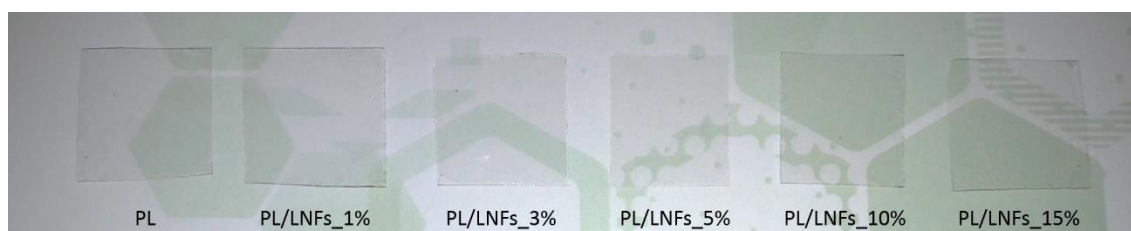
Fig. 1 - Photographs of the PL-based nanocomposite films: A) PL, B) PL/LNFs_1%, C) PL/LNFs_3%, D) PL/LNFs_5%, E) PL/LNFs_10% and F) PL/LNFs_15% (See Table for sample identification).

Structural and morphological characterization

Fig. 2 shows the infrared spectra of PL, LNFs and PL/LNFs nanocomposite films. The FTIR-ATR spectra of the films are consistent with their expected chemical structure and composition by clearly showing the distinctive absorption bands of PL backbone: 3310 cm^{-1} (O–H stretching), 2927 cm^{-1} (CH and CH$_2$ stretching), 1646 cm^{-1} (bending motion of adsorbed water (H–O–H)), 1150 to 1060 cm^{-1} (C–O–C stretching of glycosidic bridges) and 754 cm^{-1} (α-glycosidic bond stretching),[234,240,261] jointly with those of lysozyme: 3281 cm^{-1} (N–H stretching), 1625 cm^{-1} (amide I band, C=O absorption), 1528 cm^{-1} (amide II band) and 1231 cm^{-1} (amide III band).[261–263] As expected, the augment of the LNFs content from 1.0 to 15.0% increased the intensity of the bands assigned to this reinforcing element (Fig. 2).
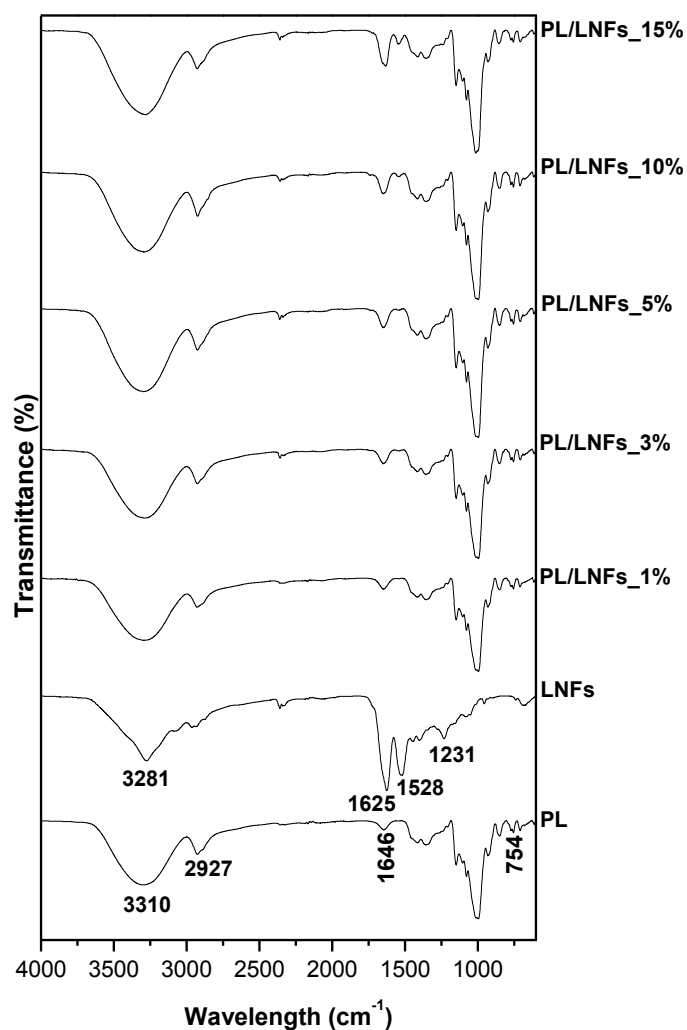
Fig. 2 - FTIR-ATR spectra of the PL/LNFs nanocomposite films and the corresponding individual components.

The XRD patterns of PL, LNFs and nanocomposite films PL/LNFs_5% and PL/LNFs_15% are given in Fig. 3. The plasticized PL film displays a diffraction pattern typical of an amorphous material with a broad diffraction peak centered at 2θ 18.4°,[233,250] whereas LNFs exhibits a diffractogram typical of lysozyme with the main diffraction peak at 2θ 18.6°.[230] In general, the PL/LNFs nanocomposite films present the amorphous diffraction pattern of PL, but as the LNFs content increases the peculiarities of LNFs become more evident, as illustrated in Fig. 3 for nanocomposite films PL/LNFs_5% and PL/LNFs_15% with 5.0 and 15.0 wt.% of LNFs, respectively.

114
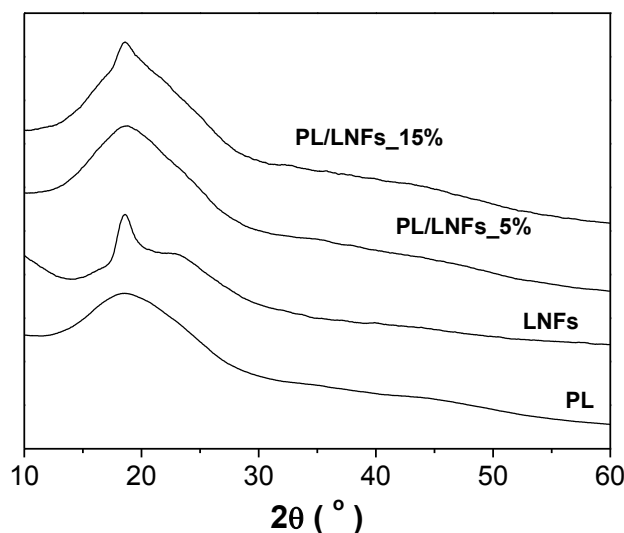
Fig. 3 - X-ray diffractograms of PL, LNFs, PL/LNFs_5% and PL/LNFs_15%.

The morphology of the PL-based films was investigated by SEM with the results illustrated in Fig. 4 (surface view) and Fig. 5 (cross-section view). The micrographs of the surface (Fig. 4) of the plasticized PL and PL/LNFs films show a homogeneous, smooth, compact and crack-free morphology even for the nanocomposite films with the higher content of nanofibers (15 wt.% of LNFs). Fig. 5 depicts the cross-section micrographs of the plasticized PL and PL/LNFs films, which are also very homogeneous and uniform, with no visible agglomeration of LNFs. In fact, these observations were expectable given the notable film-forming ability of PL and the low loadings of LNFs (1.0, 3.0, 5.0, 10.0 and 15.0 wt.%). Similar results were reported for PL films with whey protein isolate[251] and sweet basil extract,[264] that presented a smooth surface and a cross-section with no tortuosity, and also for PL films with alginate[265] which displayed a smooth surface morphology. Nevertheless, protein nanofibrils agglomeration can easily occur during film formation, as observed by Rao et al. (2012) for poly(vinyl alcohol) (PVOH) films containing amyloid fibrils; these films exhibited a rough and uneven surface morphology with the presence of sporadic voids and agglomerates, which is a clear indication of the incompatibility between PVOH and amyloid fibrils.[99]

The homogeneous distribution of the LNFs in the PL-based nanocomposite films was further corroborated by fluorescence microscopy. As exemplified in Fig. 6, the plasticized PL film is non-emissive in the presence of a fluorescent dye for protein β-sheet structures,[230] whereas the emission exhibited by the PL/LNFs_5% film with only

5 wt.% of LNFs (0.96 mg cm^{-2}) is a good indication of the presence of protein nanofibers with β-sheet structures. The LNF homogeneous distribution within the PL polymeric matrix can also be observed in Fig. 6.
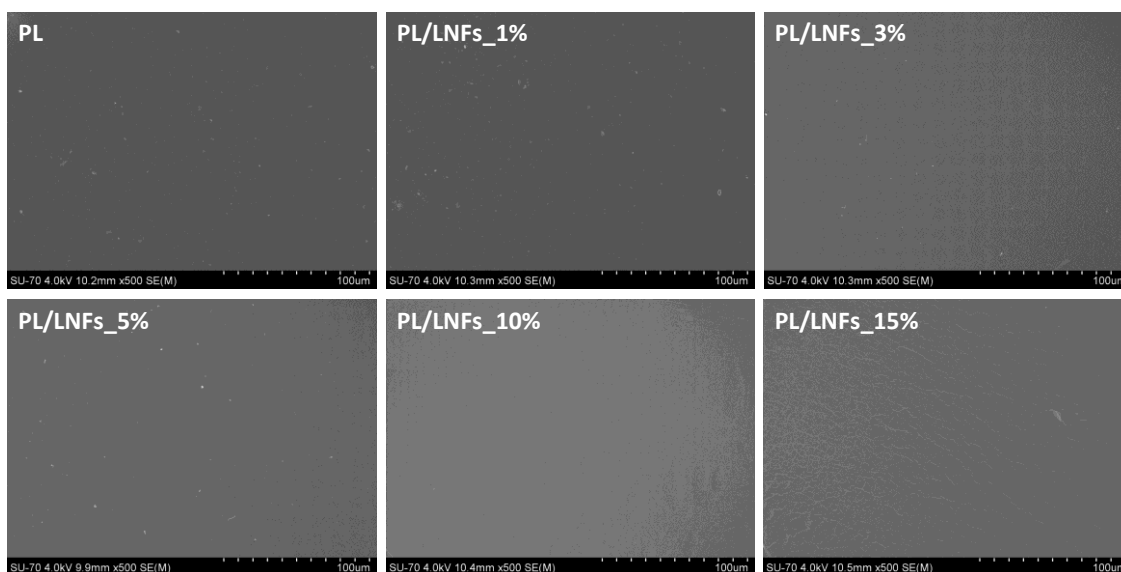
Fig. 4 - SEM micrographs of PL and PL/LNFs nanocomposite films, with different magnifications.
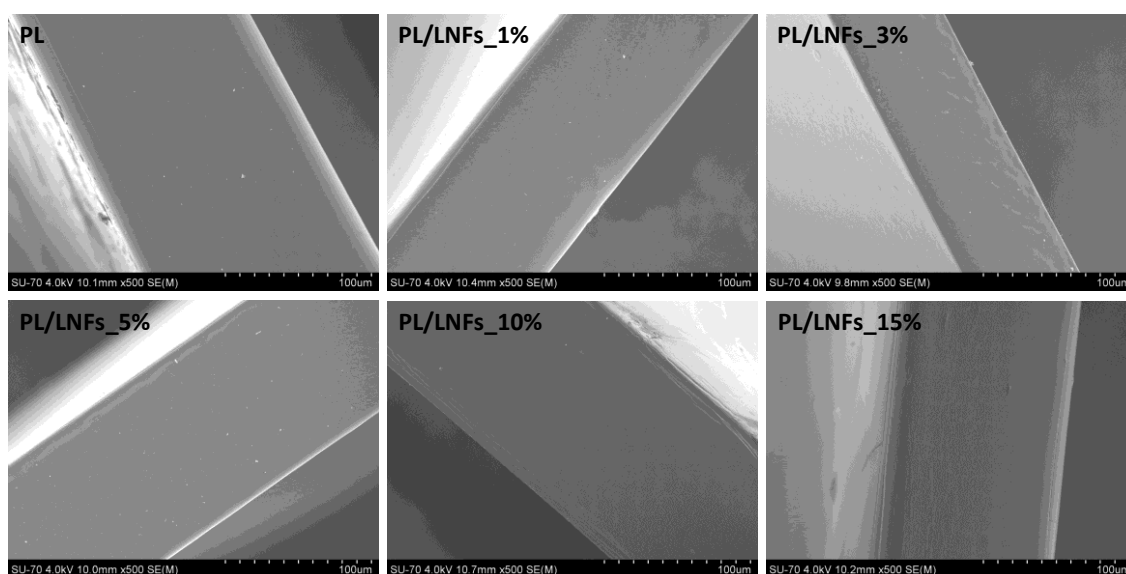
Fig. 5 - SEM micrographs of the cross-section of PL and PL/LNFs nanocomposite films, with different magnifications.
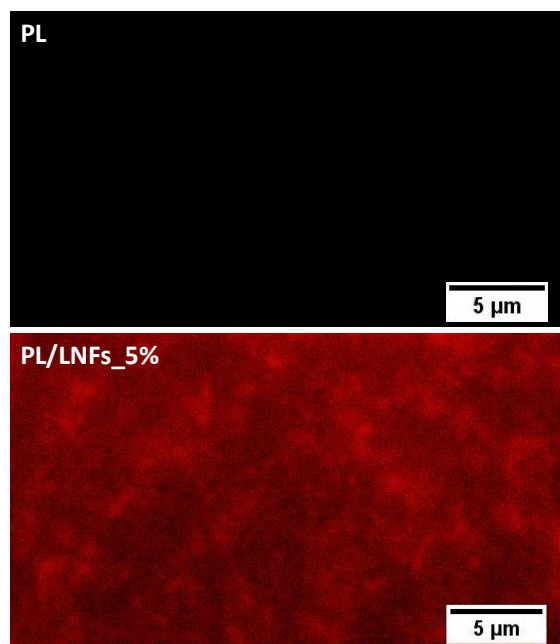
Fig. 6 - Fluorescence images of the surface of PL and PL/LNFs_5% films stained with Congo Red.

Optical properties

The optical properties of PL and PL/LNFs films were evaluated by measuring their transmittance in the range between 200 and 700 nm, as depicted in Fig. 7. The UV-visible spectra clearly show that the plasticized PL film is optically transparent, with transmittance values of 87–90% in the visible range (400−700 nm) and 7–87% in the ultraviolet range (200–400 nm), which are in agreement with previously published data.[236]

Regarding the nanocomposite films, the addition of LNFs to PL had a small impact in the transmittance values in the visible range that are still higher than 84% (Fig. 7), confirming their optical transparency (in line with the macroscopic appearance), which is an essential feature for their use as food packaging films. In contrast, the PL films reinforced with LNFs present low transmittance (and concomitant high absorbance) values in the UVC region (100–280 nm, short-wavelength radiation) that decrease with increasing LNFs content (Fig. 7). In the UVB region (280–315 nm, short-wavelength radiation), the transmittance values monotonically increase and reach a plateau in the UVA region (315–400 nm, long-wavelength radiation) (Fig. 7), before attaining the fairly constant transmittance values of the visible range. Based on these

results, it can be concluded that PL/LNFs nanocomposite films exhibit slightly higher ultraviolet light barrier properties compared to those of the plasticized PL films.
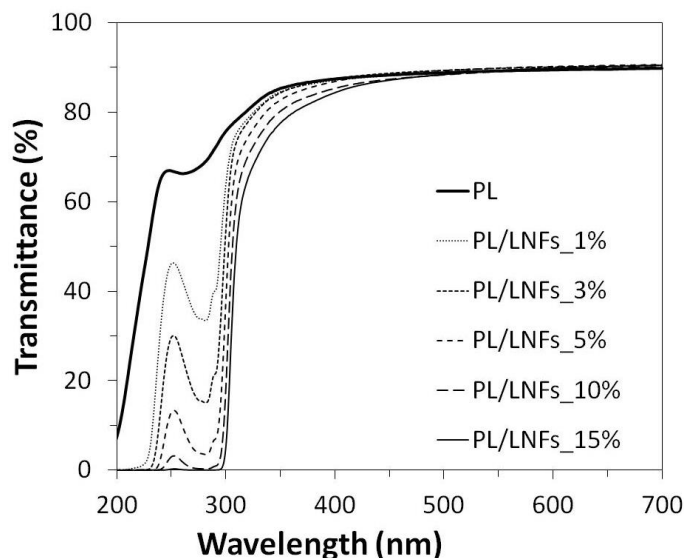
Fig. 7 - UV-vis spectra of the plasticized PL film and nanocomposite films based on PL and LNFs.

Mechanical properties

The influence of the addition of different amounts of LNFs on the stress-strain behavior of the PL/LNFs based nanocomposite films was studied by typical tensile tests, and the Young's modulus, tensile strength and elongation at break (Table 2) were determined from the stress-strain curves. For comparison purposes, a PL film containing 10% of glycerol (1.92 mg cm^{-2}) was also analyzed and the attained results showed a Young's modulus of 1.69 ± 0.04 GPa, tensile strength of 35.0 ± 4.4 MPa and elongation at break of $6.63 \pm 1.11\%$, which are in agreement with values previously reported. [239,240] The presence of LNFs noticeably affects the Young's modulus and elongation at break of the ensuing nanocomposite thin films, whereas the tensile strength is poorly influenced by the content of protein nanofibers. The incorporation of LNFs promoted an increase of the Young's modulus (Table 2, $p < 0.05$) from 1.69 ± 0.04 GPa for the plasticized PL to 1.91 ± 0.04 GPa for the nanocomposite containing 1.0 wt.% LNFs (0.19 mg cm^{-2}, PL/LNFs_1%) and 2.50 ± 0.15 GPa for the film with 15.0 wt.% LNFs (2.88 mg cm^{-2}, PL/LNFs_15%). These results evidence a higher stiffness of the nanocomposite films when compared to plasticized PL films, which was expected given the high mechanical strength of protein nanofibers.[266] Additionally, the incorporation of LNFs in the PL polymeric matrix originated a reduction of the elongation at break of

118

about 61% for 1.0 wt.% LNFs (PL/LNFs_1%) and 80% for 15.0 wt.% (PL/LNFs_15%). The drop of the elongation at break is also an indication of the rigidity of the nanocomposite films when compared with plasticized PL films. This parameter was the one experiencing the greatest impact of the addition of the protein nanofibers (Table 2, $p < 0.05$), as shown by the variance analysis. Regarding the tensile strength, the incorporation of LNFs did not have a significant effect on this parameter, *i.e.*, the means difference is not significant at the significance level ($\alpha = 0.05$), as depicted in Table 2. Worth noting is the fact that these protein nanofibers are an effective reinforcing agent for PL films even at low LNFs loadings (from 1.0 wt.% up to 15.0 wt.%), which is probably a direct result of their elevated aspect-ratio and highly ordered self-assembled nanostructure.[226]

Table 2. Young's modulus, tensile strength and elongation at break of PL and PL/LNFs films; the values are the mean of 5 replicates with the corresponding standard deviations.

Sample [a]	Young's Modulus (GPa)	Tensile Strength (MPa)	Elongation at break (%)
PL	1.69 ± 0.04	35.0 ± 4.4	6.63 ± 1.11
PL/LNFs_1%	1.91 ± 0.04	33.2 ± 3.7	2.57 ± 0.36
PL/LNFs_3%	2.09 ± 0.14	35.6 ± 2.2	2.24 ± 0.27
PL/LNFs_5%	2.26 ± 0.13	37.6 ± 2.2	1.84 ± 0.29
PL/LNFs_10%	2.35 ± 0.13	34.1 ± 1.0	1.64 ± 0.61
PL/LNFs_15%	2.50 ± 0.15	31.3 ± 2.3	1.34 ± 0.10

[a] See Table for sample identification.

Thermal stability

The thermal stability and degradation profiles of PL/LNFs nanocomposite films and the corresponding individual components were assessed by thermogravimetric analysis under nitrogen atmosphere as displayed in Fig. 8. The thermal degradation profile of the plasticized PL film follows a single weight-loss step with initial and maximum decomposition temperatures of 250 and 300°C, respectively, leaving a residue at 800°C corresponding of about 14% of the initial mass. This single-step pathway is associated with the degradation of the PL skeleton. [236,267] The thermogram of

LNFs also exhibits a single-step degradation profile with maximum degradation temperature of 308°C, where the film already lost about 35% of the initial mass, and the final residue at 800°C corresponds to *ca*. 15%. Thus, LNFs present a thermal degradation profile equivalent to lysozyme, whose single-step corresponds to the degradation of the protein backbone.[263]

As observed in Fig. 8, all nanocomposite films underwent single-step degradation mechanism, with maximum decomposition temperatures of 268–295°C, most likely associated with the simultaneous degradation of the enriched fractions of PL and LNFs. At the end of the analysis (800°C), it is evident the increase in the residue, from 17 to 25 %, with the increase of LNFs content, from 1.0 to 15.0 wt.%. Despite the slightly lower degradation temperatures compared to the plasticized PL film, the addition of LNFs to PL originated nanocomposite films with thermal stability up to 225–240°C, which allows their use under typical sterilization procedures, which take place around 150°C, required for food-based applications.
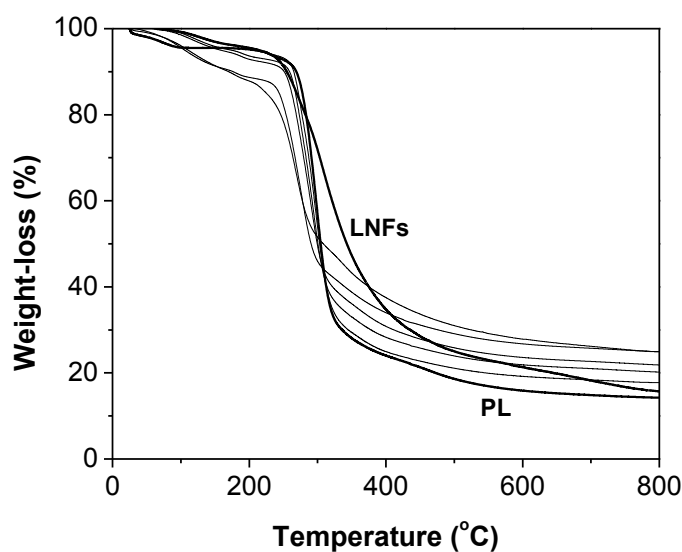
Fig. 8 - Thermogravimetric analysis of PL-based films with different amounts of LNFs.

Antioxidant activity

Natural antioxidants are known for reducing or avoiding the second main reason of food spoilage, *i.e*. oxidative degradation.[268] With this in mind, DPPH radical scavenging assays were conducted to evaluate the antioxidant potential of the PL/LNFs nanocomposite films. According to Fig. 9, the radical scavenging activity of the PL film is null, which is in agreement with data previously reported in the literature.[264] Furthermore, the addition of LNFs up to 15.0 wt.% led to an increase of the antioxidant

activity when compared to the plasticized PL film (Fig. 9, $p < 0.05$), with the DPPH scavenging activity reaching a minimum of 25.1 ± 2.2% for PL/LNFs_1% with 1.0 wt.% LNFs (0.19 mg cm^{-2}) and a maximum of 76.7 ± 2.5% for PL/LNFs_15% with 15.0 wt.% LNFs (2.88 mg cm^{-2}). An analogous effect was observed for PL films containing sweet basil extract (SBE), whose antioxidant activity increased with the increasing content of the phenolic extract (6–30 mg cm^{-2}).[264] Nevertheless, the DPPH scavenging activity of the film containing 30 mg SBE per cm^2 (<40%)[264] is almost half the value obtained in this work for the PL/LNFs_15% nanocomposite films containing 2.88 mg LNFs per cm^2 (Fig. 9).

Notably, the antioxidant activity of LNFs (without the presence of PL) is higher than that of native lysozyme, with DPPH scavenging activity values of 59.7–88.8% for the former and 4.0–26.1% for the latter, both in the same concentration range (0.5–5.3 mg mL^{-1}). The higher antioxidant activity of LNFs is probably an outcome of exposing the bioactive peptides during nanofibrillation, given that protein hydrolysates and peptides derived from lysozyme are reported to possess elevated radical scavenging activity.[269,270]
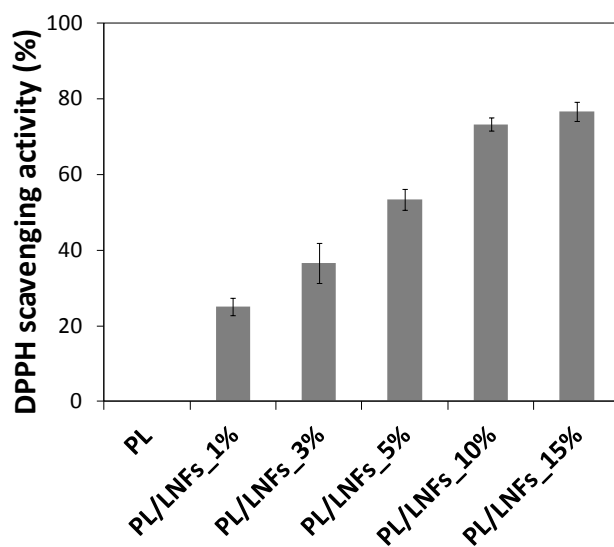
Fig. 9 - DPPH scavenging activity of the plasticized PL and PL/LNFs films; values represent the mean of three independent experiments; error bars represent the standard deviation.

Antibacterial activity

The growth of spoilage and/or pathogenic microorganisms is the major culprit of food spoilage, and causative agent of food-borne diseases. Therefore, antimicrobial

activity is the most sought active function in the food packaging field. Fig. 10 presents the antibacterial activity of PL/LNFs films, as well as of PL and PL/lysozyme films that were prepared for comparison purposes. The experimental control was produced *via* inoculation of the Gram-positive Bacterium *S. aureus* in media in the absence of sample. *S. aureus* was selected for being one of the major bacteria causing food-borne diseases in humans *via* food poisoning through the production of enterotoxins.[271] The culture containing pure plasticized PL films did not show any reduction in bacterial growth of *S. aureus* since PL is not an antibacterial agent. In fact, the PL did not inhibit the growth of the bacterium after 24 and 48 h similarly to the control, as already reported for *S. aureus*[236,240] and other bacterial strains.[236,240,246,272]

Although lysozyme (one of the most important enzymes of the human immune defense system) exhibits antimicrobial activity particularly against Gram-positive bacteria,[258] all pathogenic Staphylococcal strains which are O-acetylated, including *S. aureus*, are completely resistant to this cationic cell wall-lytic enzyme.[273–276] According to literature, the bactericidal potency of native lysozyme is simultaneously associated with its muramidase activity, and its cationic and hydrophobic nature [258]. Nevertheless, the lysozyme ability to damage the bacterial membrane by the cleavage of the *β*-1,4 glycosidic bonds between *N*-acetylmuramic acid and *N*-acetylglucosamine of bacterial peptidoglycan is blocked due to the *S. aureus* peptidoglycan modification by O-acetylation and teichoic acids modification D-alanylation.[273–276] Thus, the PL film containing 15 wt.% of native lysozyme (2.88 mg cm^{-2}) did not display, as expected, any inhibitory effect on the bacterial growth (Fig. 10).

On the contrary, the incorporation of only 5 wt.% of LNFs (0.96 mg cm^{-2}, PL/LNFs_5%) in the PL polymeric matrix was sufficient to slightly inhibit the growth of *S. aureus* with *ca.* 0.72-log reduction after 48 h. The highest growth inhibition was observed for the PL film containing the highest amount of LNFs (2.88 mg cm^{-2}, PL/LNFs_15%), registering about 3.2-log reduction after 48 h (Fig. 10). Under these conditions, the number of CFUs is more than 1000 times smaller, *i.e.*, the bacterial inactivation was higher than the 3-log of CFU reduction (killing efficiency ≥ 99.9%) established to any new approach to be termed antibacterial. Clearly, the nanofibrillation of lysozyme confers antibacterial activity to lysozyme nanofibers, most likely because of the exposed peptides. In fact, native lysozyme can acquire bactericidal capacity against *S. aureus*, for example, by heat-denaturation at 80°C and pH 6.0.[277] According to Ibrahim *et al*.[277] the heat-denatured lysozyme, with only 50% of enzymatic activity,

122

but with a higher surface hydrophobicity due to the two exposed thiol groups, shows enhanced binding capacity to peptidoglycan, *i.e.*, the major components of the outer surface of *S. aureus*, and thus, exhibited a strong bactericidal activity. This is further supported by the fact that biomaterials containing of cysteine-rich peptides, *e.g.*, cotton-based textile material functionalized with cysteine, were reported for having antibacterial activity against *S. aureus*.[278]

The antibacterial results of the PL/LNFs films prepared in this work are quite relevant in the food packaging context and constitute a stimulating encouragement to investigate the reason behind the bactericidal potency of lysozyme nanofibers against *S. aureus*. Moreover, the antibacterial behavior obtained for the nanocomposite films is superior to the results reported, *e.g.*, for PL films containing thymol,[245] which is a phenolic compound with 0.012% (w/w) of minimum inhibitory concentration (MIC) against *S. aureus*. According to that study, PL/thymol films with concentrations in the range 2.5–12.3 mg cm^{-2} of thymol in the dried film, did not display any inhibitory effect on the growth of *S. aureus*.[245] A similar behaviour was documented by Synowiec *et al.*[264] and Gniewosz *et al.*,[279] where PL films containing sweet basil extract (SBE) and meadowsweet flower extracts (EMF), respectively, only started to inhibit the growth of *S. aureus* at extracts (SBE and EMF) concentrations of 6 mg cm^{-2} in the dried film.[264,279]
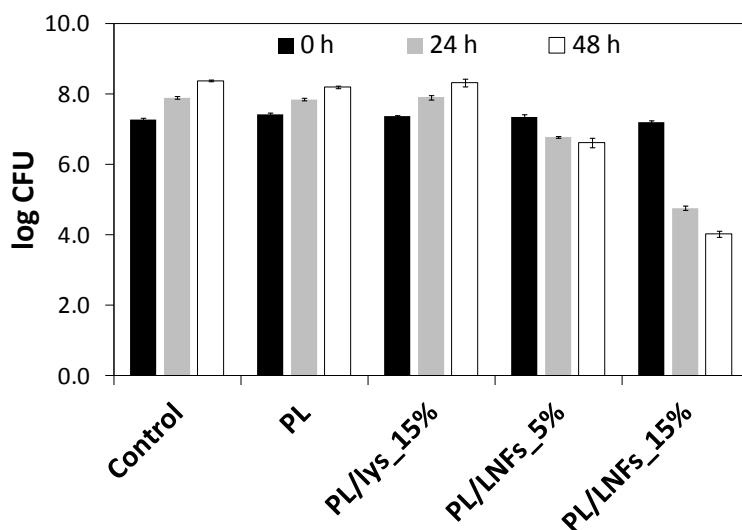
Fig. 10 - Antibacterial activity of PL, PL/LNFs_5% and PL/LNFs_15% films after 0, 24 and 48 hours. PL/lys_15% (lys: native lysozyme) film was prepared and tested under the same conditions for comparison purposes. Values represent the mean of two independent experiments; error bars represent the standard deviation.

In conclusion, the simultaneous use of filmogenic PL and lysozyme nanofibers is an interesting strategy to tailor not only the antibacterial and antioxidant activities of PL nanocomposite films, but also their optical properties, mechanical performance and thermal stability, envisaging their application as eco-friendly multifunctional bioactive systems for active packaging.

Conclusions

Coherent PL films reinforced with LNFs were fabricated by simple and cost effective solvent casting method. The resulting PL/LNFs nanocomposite films were very homogenous, transparent and glossy, and presented high mechanical performance (Young's modulus = 1.91–2.50 GPa) and thermal stability up to 225°C. The incorporation of LNFs in the PL polymeric matrix imparted, on top of the reinforcing effect, new functionalities, namely antibacterial and antioxidant activities. The set of films exhibit a maximum antioxidant activity of *ca*. 77% (DPPH scavenging activity) for the film with the highest LNFs content (15.0 wt.%), as well as antibacterial activity against the Gram-positive *S. aureus* food pathogenic bacteria that increases with the increasing content of nanofibers. These promising properties support the use of these PL films reinforced with lysozyme nanofibers as eco-friendly edible films for active packaging, where multifunctional bioactive systems are continuously necessary to protect and extend food's shelf life.

3.2.

Innovative membranes based on nanocellulose and protein nanofibers for the removal of mercury (II) from natural waters

Nuno H. C. S. Silva,[a,b] Paula Figueira,[a,c] Carla Vilela,[a] Ricardo J. B. Pinto,[a]

Isabel M. Marrucho[b,e], Maria Eduarda Pereira,[d] Carmen S. R. Freire,[a]

[a] CICECO and Chemistry Department, University of Aveiro, Campus de Santiago, 3810-193 Aveiro, Portugal

[b] Instituto de Tecnologia Química e Biológica António Xavier, Universidade Nova de Lisboa, Av. República, Ap. 127, 2780-901 Oeiras, Portugal

[c] Central Laboratory of Analysis, Univesity of Aveiro, Campus de Santiago, 3810-193 Aveiro, Portugal

[d] CESAM and Chemistry Department, Univesity of Aveiro, Campus de Santiago, 3810-193 Aveiro, Portugal

[e] Centro de Química Estrutural, Instituto Superior Técnico, Universidade de Lisboa, Avenida Rovisco Pais, 1049-001 Lisboa, Portugal

Abstract

Water pollution is currently one the main issues in what concerns the environmental public health. In particular, the increasing levels of trace metals are leading to the establishment of severe regulations that limit their concentration in waters discharged from industry. Consequently, the design of efficient and sustainable extraction systems of metal micropollutants is of great interest. In this work, an entirely bio-based sorbent film based on nanocellulose and protein nanofibers was tested for the removal of

mercury (II) from aqueous environment. A nanocellulose film was produced as a control. The films were prepared by vacuum filtration of a mixture (2:1) of nanocellulose and protein lysozyme nanofibers. The obtained films were homogenous and translucent and displayed improved mechanical performance with an increase of 78% in the Young's modulus, from 3.67 ± 0.55 GPa (nanocellulose) up to 6.56 ± 0.32 GPa (nanocellulose-protein nanofibers). The capacity of these films to remove mercury (II) from natural water was tested using the maximum concentration of mercury (II) allowed by European Union regulations (50 µg L^{-1}). It was observed that the presence of LNFs allows to increase expressively the mercury(II) removal, with efficiencies over than 80% after 24h. The maximum removal efficiency of 99% was achieved near the isoelectric point of lysozyme (pH 11.35), showing that this is a pH dependent process. Finally, a natural spring water sample was used to evaluate the matrix effect on the mercury(II) extraction and no significant changes were observed, reaching an optimal extraction efficiency of 93% at pH = 11.

Introduction

During the last century, industrial activity has led to increasing levels of environmental pollutants and micropollutants worldwide. In particular, trace levels of metals have been discharged daily into the aquatic environment without an adequate treatment, leading to a long-term negative impact on bodies of water and a foremost risk for public health.[280,281] Actually, trace metals are known for their high toxicity and persistent character in the environment and biota, which is capable to accumulate along the food chain.[282] Amongst the myriad of trace metals found in the environment, mercury (Hg) is considered one of the most harmful. The combustion of fossil fuels is one of the major anthropogenic sources of Hg emissions, with an estimated global emission of 2000t per year.[283] Thus, mercury is in the top three of the priority list of hazardous substances defined by the Agency for Toxic Substances and Disease Registry[284] and is also part of the list of priority substances of the Water Framework Directive.[285]

The removal of trace metals from water and wastewaters constitutes nowadays one of the most important environmental issues, and consequently, the development of efficient methodologies and materials for the decontamination of waters a central topic of research. A variety of methods to remove trace metals from waters and wastewaters have been described in the literature.[286–288] However, most of these methods imply high costs and are resources demanding.[282] For instance, chemical precipitation is known to be very efficient for high concentrations of metal ions but it is also quite expensive and it can originate by-products in the form of toxic fumes.[286] Electrochemical treatment is another effective technique commonly used to remove trace metals, but it is likewise costly and not suitable for decontamination of smaller amounts of trace metals due to the high cost associated to the process resources.[288] The use of ion-exchange resins,[287,289,290] including inorganic zeolites and synthetic organic resins, is also commonly used. Nevertheless, this approach is expensive because of the small volumes that can be used. Activated carbons have also been efficiently used as absorbent for the removal of various pollutants.[291,292] However, the chemical activation of the carbon based materials is a highly energy intensive process.[291]

More recently, as a result of the increasing global demand for innovative bio-based materials in different fields, the design of sustainable biopolymeric materials for water purification has also been tackled. For example, nanometric forms of cellulose, namely nanofibrillated cellulose (NFC), cellulose nanocrystals (CNC) and bacterial cellulose (BC), are gaining much attention because of the innumerable advantages associated with their abundance, biodegradability, renewability, unique morphologies, versatile surface chemistry, excellent mechanical properties and high surface area.[5] On top of that, the surface of nanocellulose fibers can be functionalized with different moieties to improve the adsorption of target water pollutants, like trace metals.[293,294] Recently, Voisin *et al.*[295] reported an extensive study on nanocellulose-based materials for water purification, with particular emphasis on materials processing (chemical functionalization), uptake capacity, selectivity and removal efficiency. Although nanocelluloses with cationic and anionic surface groups are able to remove heavy metal pollutants from aqueous solutions, with uptake capacities comparable to that of conventional adsorbents, as activated carbon and ion-exchange resins, there is still a need to address several issues, as the selectivity in the presence of more complex water streams, the material´s mechanical and structural stability.

Protein nanofibers, resulting from the self-assembly of unfolded protein or polypetides,[23,208,296] are also emerging as new potential functional nanoblocks for the development of sustainable materials for diverse applications. Several proteins, including insulin,[99,100] β-lactoglobulin[96,199] and lysozyme,[77,84] have been used to produce such protein nanofibers. Due to their exceptional properties, such as biodegradability, high strength, thermochemical stability and molecular composition, protein nanofibers have been explored for different applications,[28,297] especially as reinforcing elements in polymer nanocomposites,[107,147,161] as templates for the synthesis of nanostructures,[141–143] and as active materials for biosensores[199] and catalysis.[157] Protein nanofibers display also a high binding capacity for metal ions because of the diversity of peptide R-groups.[160,298] In this line, in a recent ground breaking work, Bolisetty and Mezzenga[160] reported the design of hybrid membranes composed of protein nanofibers obtained from β-lactoglobulin supported in activated carbon to remove trace metal ions and radioactive waste from water at pH 4. These membranes were used to remove traces of four metal ions, Au(I), Hg(II), Pb(II) and Pd(II), and adsorption efficiencies higher than 99% were obtained. Despite the fact that the concentration of Hg(II) in aqueous solutions was

reduced from 84 mg L^{-1} down to 0.4 mg L^{-1}, this value is still eight times higher than the limit established by the European Union regulations for mercury in waters discharged from industrial sectors (50 µg L^{-1}).[299] Indeed, the majority of works dealing with the removal of trace metals from waters consider concentrations (i.e., mg L^{-1} or higher) far above the realistic ones found in the environment, (µg L^{-1} or lower). This aspect is particularly important in the recent scenario of intended cessation of Hg emissions, losses and discharges, considering the new stringent environmental quality standards for surface waters,[300] emphasizing the importance of considering metal ion concentrations that are environmentally realistic and relevant.

In this vein, taking advantage of the singular properties of nanocellulose and protein nanofibers, their combination might provide an interesting strategy to design biosorbent nanomaterials with improved mechanical properties and removal efficiency for water purification and remediation. In the present work, we describe the preparation and characterization of entirely bio-based nanostructured adsorbent films based on nanofibrillated cellulose and lysozyme nanofibers for the efficient removal of Hg(II) from natural waters. The films were simply obtained by vacuum filtration of water-based suspensions of cellulose and lysozyme nanofibers and characterized in terms of structure, morphology, thermal stability and mechanical properties. Finally, their efficiency on the removal of Hg(II) was studied by atomic fluorescence spectrometry with a detection limit of 0.02 µg L^{-1}, using a natural spring water at different pHs (7, 9, 11).

Experimental Details

Chemicals

All chemicals used in this work were obtained from commercial chemical suppliers and were used without further purification: acetic acid ($\geq$ 99.7%, Sigma-Aldrich), cholinium chloride ($\geq$ 98%, Sigma-Aldrich), glycerol ($\geq$ 99.5%, Sigma-Aldrich), glycine ($\geq$ 98.5%, Sigma-Aldrich), hen egg white lysozyme (HEWL, Sigma-Aldrich, ~70000 U mg^{-1}), phosphate buffer solution (PBS, pH 7.4, Sigma-Aldrich), hydrochloric acid (37% in solution, Acros Organics), sodium hydroxide (98.3%, Fluka), standard solution of

mercury (Hg(II) solution, $Hg(NO_3)_2$, 1000 ± 2 mg L^{-1}, Merck) and nitric acid (HNO_3, 65% (m/m), Merck).

Production of Nanofibrillated Cellulose

Nanofibrillated cellulose (NFC) suspension (2.91 wt%), with fibers with an average diameter of 20–50 nm, was gently ceded by VTT Technical Research Centre (Finland) and obtained from softwood bisulfite fibers by combining mechanical and enzymatic treatments.

Production of Lysozyme Nanofibers

Lysozyme nanofibers (LNFs) were produced according to a method described in a previous study.[200] Briefly, HEWL was dissolved (2mg mL^{-1}) in an aqueous solution of 10 mM HCl at pH = 2 with 20 mM glycine with 5% (v/v) of a deep eutectic solvent (DES) based on cholinium chloride and acetic acid.[217] The samples were incubated at 70ºC, under magnetic stirring, using an oil bath. The lysozyme nanofibers were separated from the DES aqueous solution by centrifugation at 15,000 rpm, during 45 min, using a Megafuge 16R centrifuge (Thermo Scientific). The supernatants were exchanged with 0.1 M HCl solution.

Preparation of the Nanostructured Fibrous Films

The NFC and LNFs suspensions were blended in a dried mass proportion of 2:1 (70 mg NFC, 35 mg LNFs) under magnetic stirring for 1 h. Then, films (105 mg) were obtained by vacuum filtration and dried in a vacuum oven at 40ºC for 1 h. A NFC film was also prepared for comparison purposes. Pure LNFs films could not be prepared due to its high brittleness and consequent difficulty to handle them.

Fourier Transform Infrared Spectroscopy (FTIR) analysis

The FTIR-ATR spectra of the NFC-LNFs dried films, as well as of the individual components, were obtained on a Perkin Elmer spectrometer equipped with a single horizontal Golden Gate ATR cell. 32 scans were acquired in the 4,000–600 cm^{-1} range, with a resolution of 4 cm^{-1}.

Thermal Stability

Thermogravimetric analyses (TGA) were carried out with a Shimadzu TGA 50 analyzer equipped with a platinum cell. Samples were heated at a constant rate of $10°C$ min^{-1}, from room temperature up to 800°C, under a nitrogen flow of 20 mL min^{-1}. The thermal decomposition temperatures were taken as the onset of noteworthy weight loss ($\geq 0.5\%$), after the initial moisture loss.

Tensile Assays

Tensile assays were performed on an Instron 5966 Series machine, using a load cell of 500 N, operating at a deformation rate of 10 mm min^{-1}, under ambient conditions. At least 5 specimens were tested for each film. Tensile strength, Young's modulus, and elongation at break were determined using the Bluehill 3 material testing software.

Scanning electron microscopy (SEM)

SEM images of the film surfaces and cross-sections were obtained with a SU-70 Hitachi equipment operating at 4 kV, after coating with carbon.

Hg(II) Removal assays - Batch sorption studies

For the Hg(II) sorption experiments, all glassware used was previously washed with HNO_3 25% (v/v) for 24h and then rinsed abundantly with ultrapure water. Batch assays were performed in Schott Duran® glass flasks (250 mL) at room temperature (20 ± 2 °C) and under constant stirring (500 rpm). The experiments started when a known amount of NFC and NFC-LNFs was put in contact with ultrapure and natural spring water with Hg(II), at different pH (4, 7, 9, 11), with the exception of pH = 4, where only assays with ultrapure water were carried out. A sodium hydroxide solution (NaOH, 0.1 M) was used for pH adjustments. The initial Hg(II) concentration was 50 µg L^{-1} in all assays, intending to simulate low concentration scenarios as this is the guideline value for wastewater discharge[299]. Along time, aliquots were collected (*ca.* 10 mL) from the solution, centrifuged at 5000 rpm for 3 minutes and the supernatant was acidified to pH<2 and then analysed for Hg(II) by cold vapour atomic fluorescence spectrometry using a PS Analytical Model 10.025 Millennium Merlin Hg analyser. The calibration curve was obtained with 5 standards ranging from 0.0 to 0.5 µg L^{-1}, with a detection

limit of 0.02 µg L^{-1} (n = 20). Blanks and standards were always analysed with sample batches.

For quality control of the experiments, experimental controls, defined as metal spiked water in the absence of NFC sorbents, were always run in parallel under the same experimental conditions. The sorption results are expressed in terms of normalized concentration ($C_{Hg}/C_{Hg,0}$) and the percentage of Hg(II) removed was evaluated according to the expression

$$R_{Hg,e} = 100 \times (C_{Hg,0} - C_{Hg})/(C_{Hg,0})$$

The amount of Hg(II) sorbed at time t was also assessed by mass balance according to the expression

$$q_{Hg} = (C_{Hg,0} - C_{Hg}) \times (V/m)$$

where $C_{Hg,0}$ is the initial Hg(II) concentration in solution, C_{Hg} is the Hg(II) concentration at time t, V is the volume of solution and m is the mass of NFC-LNFs tested.

Results & Discussion

Nanostructured fibrous films composed of nanofibrillated cellulose (NFC) and lysozyme nanofibers (LNFs), in a mass proportion of 2:1, for application on the removal of Hg(II) from natural waters, were produced by vacuum filtration of aqueous suspensions of NFC and LNFs, followed by oven drying. Since NFC was used essentially to promote a support for the lysozyme nanofibers, a higher mass of NFC in respect to LNFs was used per film. Pure NFC films were also prepared for comparison purposes. Both NFC and NFC-LNFs films (thickness of 19 ± 0.95 µm) were very homogeneous and translucent as shown in Fig. 1.

134
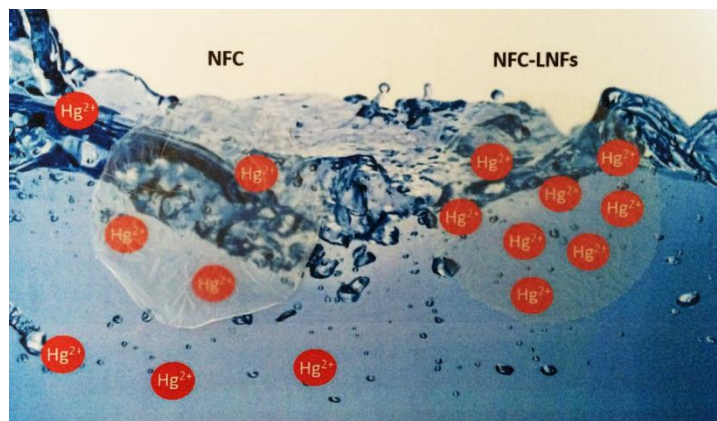
Fig. 1 - Photographs of native nanocellulose (NFC) and nanocellulose-lysozyme nanofibers (NFC-LNFs) based films.

Structural Characterization

First, NFC and NFC-LNFs films were characterized by FTIR-ATR spectroscopy. As depicted in Fig. 2, the FTIR spectrum of the NFC film shows the typical peaks of a cellulosic substrate; the broad band around 3350 cm^{-1} corresponds to the vibration of the OH groups, the peak at 2880 cm^{-1} is attributed to the C-H stretching vibrations of CH and CH$_2$ groups and those at 1115 and 1060 cm^{-1} are assigned to the stretching of the C–O–C groups.[301] On the other hand, the spectrum of lysozyme nanofibers display the characteristic peaks associated with the amide groups at 1625 cm^{-1} (amide I), 1528 cm^{-1} (amide II) and 1231 cm^{-1} (amide III), and at 3281 cm^{-1} a broad band corresponding to the N–H stretching.[261–263] As expected, the FTIR spectrum of the NFC-LNFs films is an almost perfect sum of those of the individual components, confirming the presence of both NFC and LNFs in the film as well as their contents.
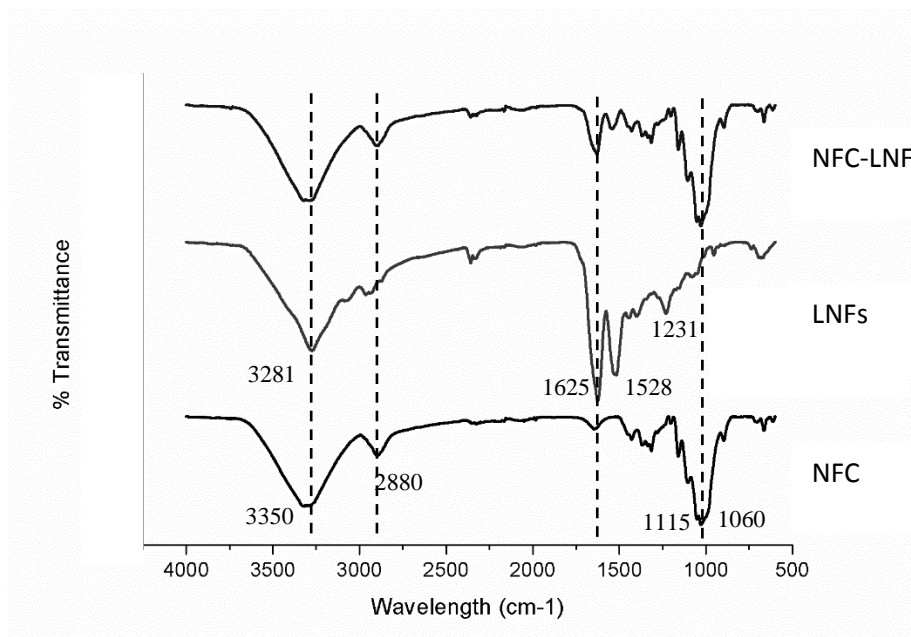
Fig. 2 - FTIR-ATR spectra of the NFC-LNFs film, as well as its individual components, NFC and LNFs.

Morphology

The morphology of the NFC-LNFs films was investigated by SEM analysis. Surface and cross-section images of both NFC and NFC-LNFs films are depicted in Fig. 3. The surface of the NFC film is quite homogeneous with cellulose nanofibers randomly distributed and entangled (Fig. 3A).[302,303] The NFC-LNFs films show a similar nanostructured fibrous morphology, confirming a good dispersion of the LNFs within the NFC film with no agglomerates. However, LNFs cannot be distinguished in the surface of the films. The cross-section images (Fig. 3B) show homogeneous morphological features for both NFC and NFC-LNFs films, not allowing to distinguish LNFs and NFC in the NFC-LNFs film.

136

Surface
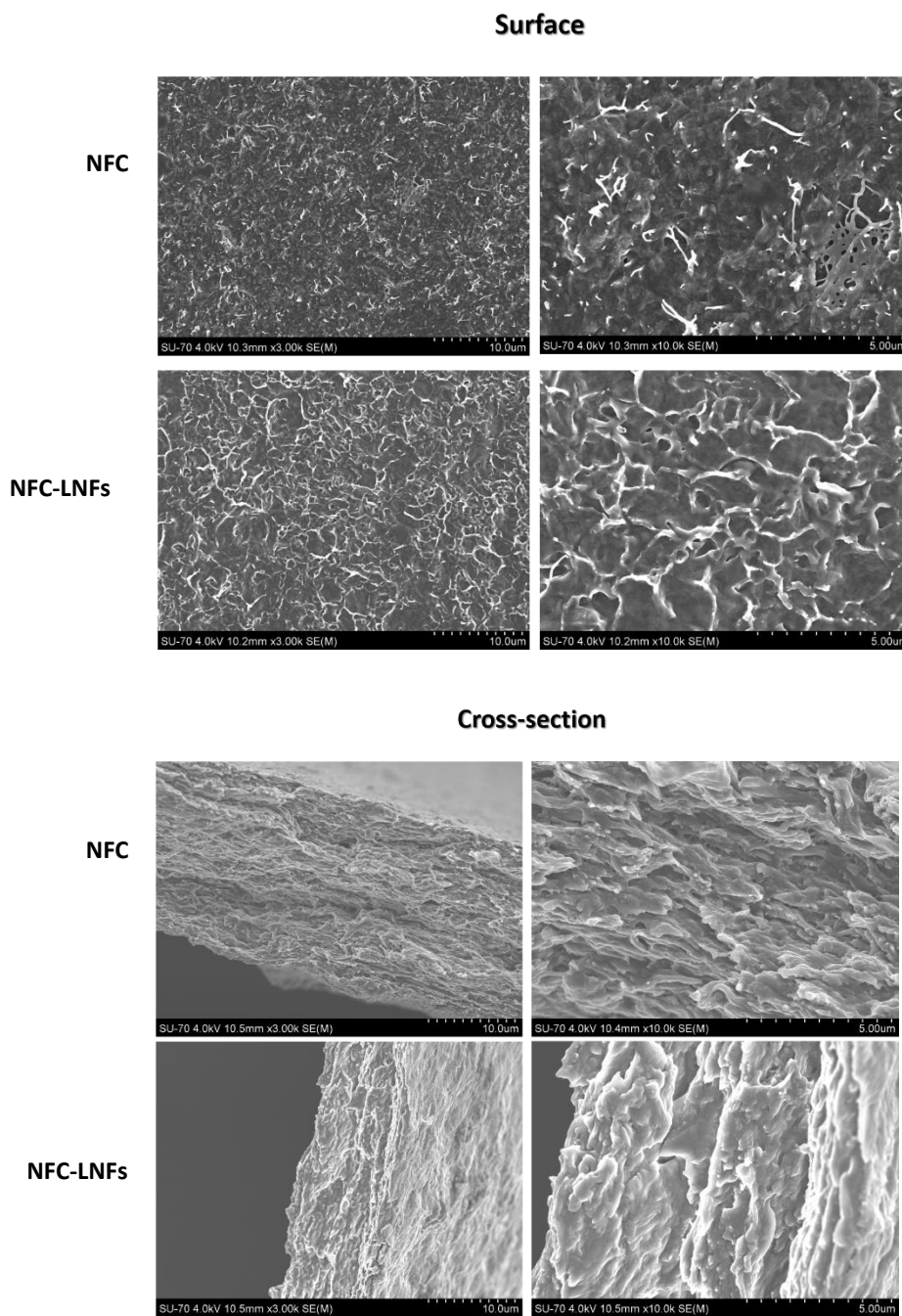
Cross-section

Fig. 3 - SEM images with different magnifications of the surface (A) and the cross section (B) of NFC and NFC-LNFs films.

Thermal Stability

The thermal stability and degradation profile of NFC-LNFs films, and of pure NFC and LNFs, were assessed by thermogravimetric analysis (TGA) under nitrogen atmosphere from room temperature up to 800ºC (Fig. 4). The degradation profile of NFC follows a typical single weight-loss step with an onset temperature of 280°C and

50% loss of the initial weight at 358ºC.[301] On the other hand, LNFs start to degrade at 240ºC and shows one main degradation step with a maximum degradation temperature at 324ºC, which is associated with the protein backbone degradation.[263] The thermogram of the NFC-LNFs film is quite similar to that of the pure LNFs, and also follows a one-step degradation profile with a maximum degradation temperature at 306ºC. These results clearly suggest that the thermal stability and degradation profile of the NFC-LNFs films is essentially governed by the presence of LNFs. Although the incorporation of the LNFs decreases their thermal stability, the films are viable for the removal of metal ions,[304,305] which takes place at room temperature.
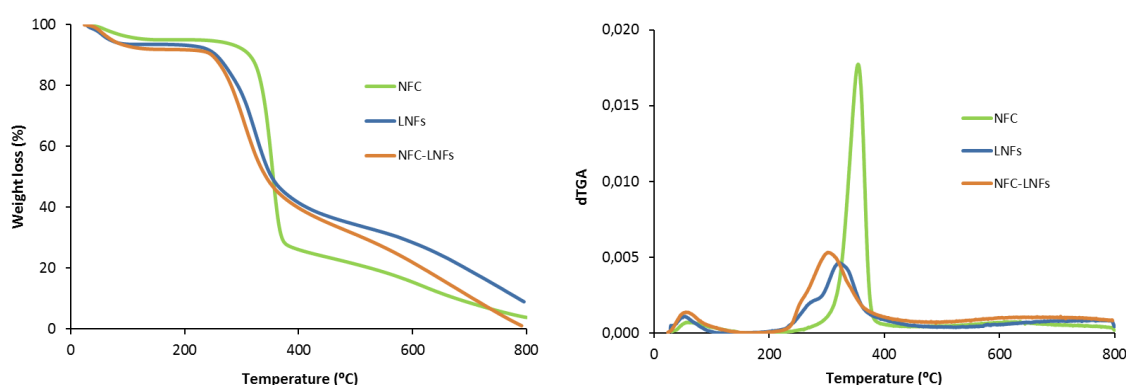
Fig. 4 - Thermogravimetric analysis (TGA) of the NFC-LNFs film, as well as its individual components.

Mechanical properties

The mechanical performance of the NFC and NFC–LNFs films was evaluated up to their failure by tensile experiments. The elongation at break, Young's modulus and tensile strength were determined from the stress–strain behaviour plots presented in Fig. 5, and are shown in Fig. 6. The incorporation of LNFs (50% in respect to the amount of NFC) had a substantial effect in the mechanical properties of the NFC film. Specifically, the incorporation of LNFs promoted an increase of 78.8% in the Young's modulus, from 3.67 ± 0.55 up to 6.56 ± 0.32 GPa, and of 25.6% in the tensile strength, where a value of 72.69 ± 2.36 MPa was registered for the NFC-LNFs film. These results clearly indicate that the NFC-LNFs films are more stiff and resistant that the native NFC films, confirming a considerable reinforcement of the NFC films with the addition of lysozyme nanofibers. This is particularly interesting considering the good mechanical properties of the NFC itself, which has been mostly used as a reinforcement in several

nanocomposite materials.[249,306,307] Concomitantly, a decrease of 62.6% on the elongation of break was observed after the incorporating LNFs, reaching a value of 2.22 ± 0.43 % for the NFC-LNFs film.

These results are comparable to those reported in literature for phosphorylated nanocellulose membranes (*ca.* 25 µm in thickness) used for copper removal that displayed Young's modulus of 6.1-8.7 GPa,[308] but considerably higher than other materials used for similar purposes, such as cellulose nanowhisker-based fibrous membranes[308] and poly(vinylidene fluoride)/graphene oxide microfiltration membranes,[309] which present less than 0.5 GPa in Young's modulus and 15 MPa in tensile strength.
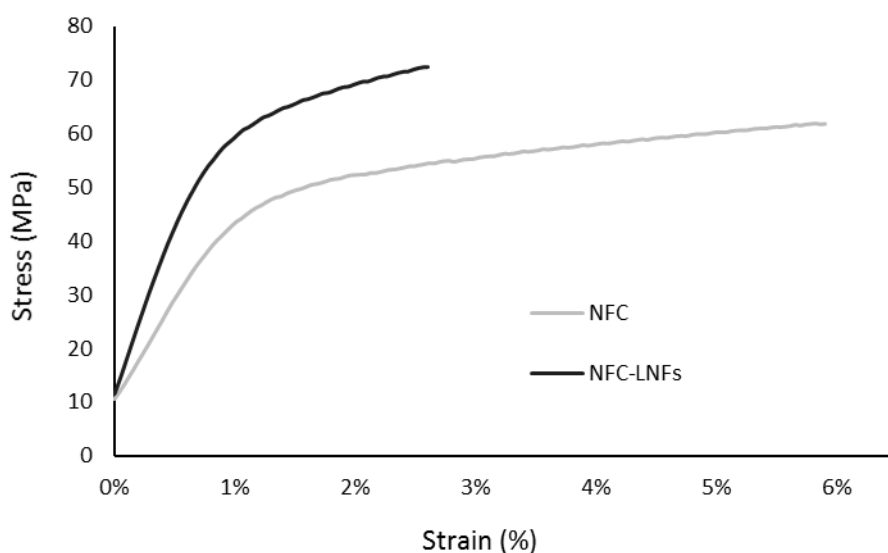
Fig. 5 - Stress-strain plots of the NFC and NFC-LNFs films.
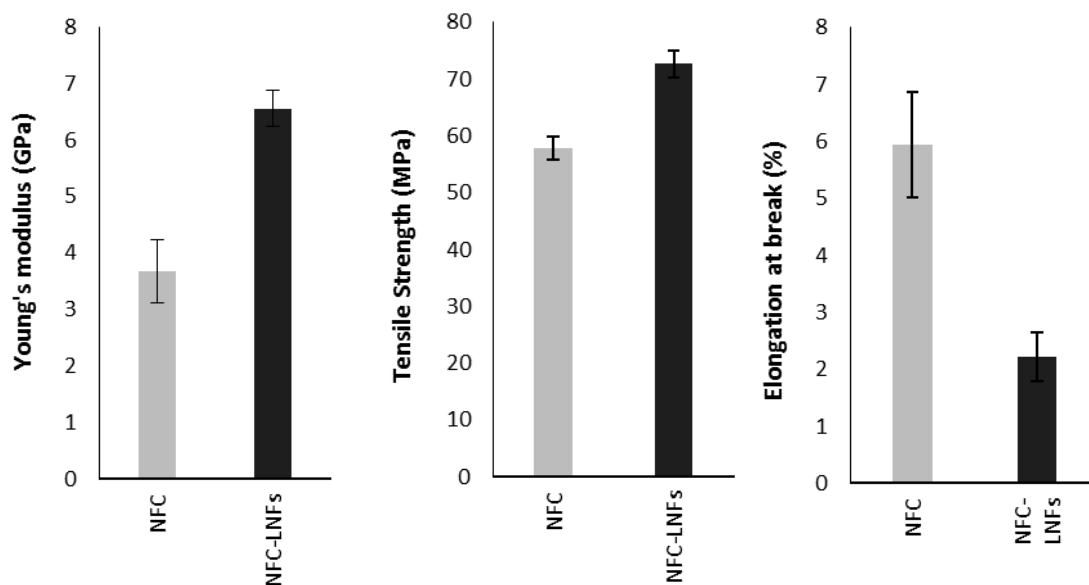
Fig. 6 - Young's modulus (GPa), tensile strength (MPa) and elongation at break (%) of the NFC and NFC-LNFs films.

Hg (II) removal by NFC-LNFs films

Finally, the capacity of the NFC-LNFs film to remove Hg(II) from natural waters was evaluated. In this work, the removal of Hg(II) was assessed by cold vapour atomic fluorescence spectrometry. Initially, an ultra-pure water (UP) spiked with Hg(II), so that the final concentration is of 50 μg was used at different pH values (4, 7, 9, 11), was used to test the prepared film and the sorption of Hg(II) was determined by the Hg(II) concentration that remained in the liquid phase after 24h. As it can be seen in Fig. 7, for the same pH, higher Hg(II) removal values were registered for the NFC-LNFs film when compared with the corresponding pure NFC film, suggesting the central role of the LNFs in the removal of Hg(II) from the solution. Remarkably, this plot also shows that the Hg(II) removal increased with the increase of the pH, with values of 35.7% (pH 4) > 73.9% (pH 7) > 79.2% (pH 9) > 99.0% (pH 11). The higher efficiencies at pH 11 are certainly related with the number of available negatively charged groups of the LNFs, since lysozyme has an isoelectric point (pI) of 11.35.[310] In fact, Bolisetty et al.[160] reported 99% removal efficiency of Hg(II) at pH 4, when using protein nanofibers obtained from β-lactoglobulin, which has a pI of 5.2, unveiling the influence of this parameter in the removal efficiency of metal ions when using protein nanofibers. The same explanation can be used to understand the removal percentages

obtained for pure NFC membranes, since the production of NFC involves a treatment of the cellulose fibers with TEMPO,[311] that may promote the oxidation of primary hydroxyl groups (C6) into carboxylate groups, generating also negatively charged groups at higher pH values.

As matter of fact, the removal efficiencies obtained with this NFC-LNFs film are comparable to those obtained for several materials reported in the literature,[160,305,312–315] where Hg(II) removal efficiencies over than 90% have been achieved. For example, graphene oxide foams have shown to remove Hg(II) up to 95% after 24h in contact with water,[314] bio-based aerogels of crosslinked carboxymethyl cellulose with cellulose nanofibril exhibited excellent adsorption capabilities for different heavy metal ions[315] and, in another vein, chitosan hydrogels and magnetite nanoparticles were functionalized with sulphur groups to increase the Hg(II) absorption.[305,313]

However, most of the studies published so far in the open literature for Hg(II) removal were carried out using highly concentrated Hg(II) solutions, much higher than the limit established in the European Union regulations[299] - 50 µg L^{-1} -, and the initial concentration used in our studies. For instance, the aerogels of crosslinked carboxymethyl cellulose with cellulose nanofibril[315] were studied using a Hg(II) solution of 50 mg L^{-1}, which is a thousand times higher than the limit established, and the use of activated carbon membranes with protein nanofibers[160] has promoted a Hg(II) removal of 99%, when the Hg(II) concentration is decreased down to 400 µg mL^{-1}, still 8 times higher than the allowed limit. Despite the high efficiencies registered in these studies, the methodology leads to unrealistic Hg(II) concentrations. In our study, the removal of Hg(II) was studied by atomic fluorescence spectrometry with a detection limit of 0.02 µg L^{-1}, which allows us to use a realistic Hg(II) concentrations, in the same order of the European Union regulations.

Another meaningful issue is that most of the studies reported in literature are carried out using very simple water matrices, such as distilled water.[304,312] It is well known that other components present in natural samples significantly affect the extraction efficiencies. Therefore, and in order to evaluate the matrix effect, we used natural spring water (NS) as a more complex water matrix. Since the NFC-LNFs film only promoted nearly 35% of Hg(II) removal using ultrapure water at pH 4, the assays with spring water were carried out only at pH 7, 9 and 11.

The same trend of increasing removal percentage of the Hg(II) with pH was observed (Fig. 7) when natural spring water was used. In fact, the Hg(II) removal values obtained with natural spring water were quite similar to those obtained with ultrapure water. This indicates that a complex water matrix containing many other ions, which could compete with Hg(II) cations for the adsorbent sites, does not have a significant affect in the removal efficiency of the NFC-LNFs membranes.
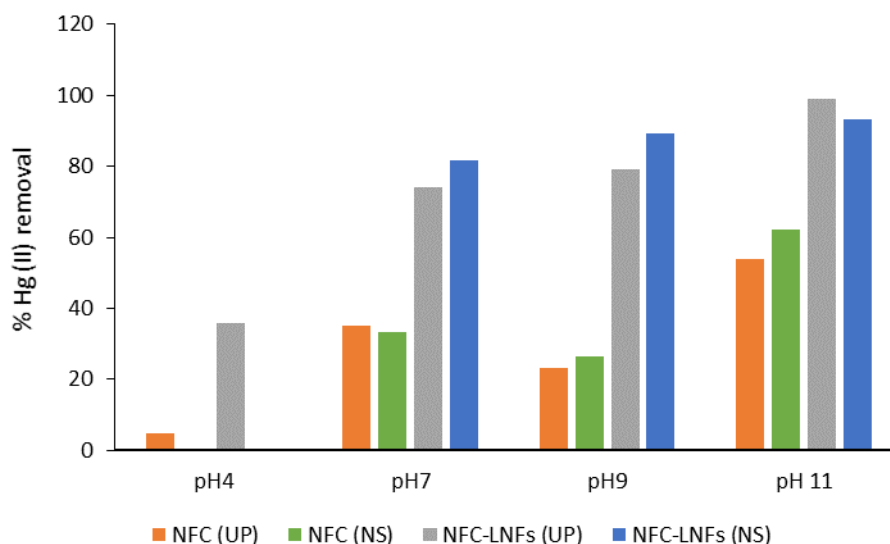
Fig. 7 - Hg(II) removal (%) by NFC and NFC-LNFs films, from ultra-pure (UP) and natural spring (NS) water, at different pHs.

In order to have a first insight into the Hg(II) kinetics removal, samples were taken after one hour of contact for the assays with natural spring water, and the Hg(II) removal (%) obtained is summarized in Table 1. It can be observed that, after 1h, the NFC film barely removes 4% Hg(II) at pH 7 and 9, while the NFC-LNFs film reach removal percentages over than 50%. At pH 11, NFC film promoted a Hg(II) removal slightly over than 20%, while the NFC-LNFs film obtained almost 75%. These results mean that, although NFC has some effect on the Hg(II) removal from water, the presence of LNFs considerably improves the affinity of Hg(II) for the films and thus the sorption kinetics. In fact, the addition of LNFs to the NFC film increased the kinetics of Hg(II) removal up to four times in the first hour when compared to the kinetics registered for NFC films.

Table 1. Hg(II) percentage removal of NFC and NFC-LNFs films after 1 h and 24 h in natural spring water spiked with 50 $\mu g\ L^{-1}$ of Hg (II), for the different pHs studied.

142

pH	t (h)	Hg(II) Removal (%)	
		NFC	NFC-LNFs
7	1	4	53
	24	33	82
9	1	4	56
	24	26	89
11	1	23	75
	24	62	93

Although NFC offers an excellent support to the LNFs, the films disintegrated in small pieces along the process as a consequence of the magnetic stirring procedure used. This is limitation that can be easily overcome by simply using a net system to hold the NFC-LNFs film, avoiding its rupture. Anyhow, further studies need to be carried out to ensure that the intact film has the same removal performance as the disintegrated film.

As a final remark, this study opens new perspectives regarding the use of protein nanofibers as natural Hg(II) sorbents. Comparing with a previous study using protein nanofibers,[160] our results confirms the ability of protein nanofibers in the removal of trace metals even for realistic concentrations of Hg(II), considering the limit established in the European Union regulations for mercury in waters discharged from industrial sectors (50 µg L^{-1}).[299] The full potential of this work is here unveiled since it is now clear that the isoelectric point of the precursor protein of the nanofibers plays a dominant role in the trace metals removal. In this work, lysozyme (pI = 11.35) was used as a model protein for nanofibers precursors. It is envisaged that other proteins with lower pIs and able to form nanofibers, like albumin (pI 4.7) β-lactoglobulin (pI 5.2), collagen (pI 6.6) and hemoglobin (pI 7.1), might provide new inputs on the removal of trace metals, approaching a wide range of waters/effluents in a wider range of pH values.

Conclusions

This study highlights the use of lysozyme nanofibers in the removal of trace metals from contaminated water, using a natural renewable material, nanocellulose, as support. The obtained films were homogenous, transparent and thermal stable up to 240ºC. The addition of 50% of lysozyme nanofibers in respect to the amount of nanocellulose promoted a mechanical reinforcement of about 78% in the Young's modulus. Regarding the Hg(II) removal assays, the presence of LNFs demonstrate to significantly increase the Hg(II) removal from natural waters, especially in the first hour. The Hg(II) removal capacity was found to be pH-dependent, and clearly linked to the pI of the protein precursor of protein used to prepare nanofibers. Consequently, higher efficiencies were obtained at higher pHs, with 82% (pH 7) < 89% (pH 9) < 93% (pH 11) after 24 h, in agreement with the lysozyme pI (11.35). This work strongly supports further investigation of protein nanofibers in the treatment of waters and effluents, where other protein precursors and materials can be studied.

4.
Conclusions and Final Remarks

Protein nanofibers, mostly known as amyloid fibrils because of their association to pathological disorders, are indeed emerging as new building nanoblocks for the development of innovative functional materials.

In this thesis, novel and fast fibrillation methodologies were reported using alternative solvents, such as ionic liquids and deep eutectic solvents. The use of ionic liquids based on imidazolium and cholinium cations combined with different anions derived from organic acids, as well as deep eutectic solvent based on cholinium chloride, have shown to fibrillate hen egg white lysozyme into worm-like nanofibers within 2-3 hours, generally achieving conversion ratios over than 70-80%. High aspect-ratio nanofibers, with typically 0.3-1 µm of length and 15-40 nm of width, were obtained. It was observed that temperature plays a key role in the kinetics of the fibrillation process. It was also observed that the acid group of hydrogen bond donor in the deep eutectic solvent plays an important role on the fibrillation efficiency and on the length of nanofibers produced. Higher aspect-ratios were obtained when using the cholinium chloride conjugated with the acid group, especially acetic and lactic acids. The aspect-ratio of the nanofibers was determinant in the mechanical properties of materials prepared with protein nanofibers. This was clearly shown when incorporating these nanofibers in pullulan films, where an increase of about 36% for the Young's modulus using only 5% of nanofibers was achieved confirming their higher reinforcing capacity.

In the pursuit for the development of new materials based on protein nanofibers, homogeneous and transparent nanocomposite films composed of pullulan and different amounts of lysozyme nanofibers were developed by simple solvent casting from aqueous suspensions. The films exhibit good thermal stability, improved mechanical properties and high antioxidant activity, and the incorporation of 15% of lysozyme nanofibers has shown antibacterial effectiveness towards *Staphylococcus aureus*, thus confirming the potential use of lysozyme nanofibers as bioactive reinforcing elements for nanocomposites. In another study, a sustainable sorbent film for the removal of mercury (II) was prepared by mixing nanocellulose fibers and

lysozyme nanofibers. The films have shown expressively mercury (II) removal efficiencies, specifically over than 50% in the first hour, and over than 80% after 24h, achieving the best results at pH 11. Notably, protein nanofibers are efficient on the removal of realistic concentrations of mercury (II), under the limit established in the European Union regulations for mercury in waters discharged from industrial sectors (50 µg L^{-1}).

In sum, this thesis demonstrates that use of ionic liquids and deep eutectic solvents can promote a faster production of protein nanofibers with tailored aspect-ratios that can be used on the development of different functional materials. Therefore, it is expected that these results will leverage the vast range of applications of protein nanofibers in the materials field from soft matter to nanotechnology. Along this doctoral thesis, many ideas have been flourishing and some future plans regarding this project can be highlighted:

- Study of the interactions established between ILs/DES and proteins so that a better understanding of the fibrillation process is achieved, as well as the mechanism of how the HBD of the DES promotes the formation of longer nanofibers (with higher aspect-ratios).

- Development of a methodology to re-use the ionic liquid, as for instance, their immobilization on magnetic nanoparticles.

- Investigate other proteins able to generate protein nanofibers, like β-lactoglobulin, albumin, hemoglobin and insulin, followed by a comparison with the nanofibers from hen egg white lysozyme regarding their structural features and properties.

- Preparation of nanocellulose based films containing other protein nanofibers (with different isoelectric point), aiming to achieve the removal of trace metals from different waters/effluents (with distinct pHs).

- Explore other polysaccharides and materials that can be combined with protein nanofibers, for the development of new materials for other applications, like scaffolds, transparent films and membranes, hydrogels and aerogels. Chitosan, alginate and gelatin are some examples.

- Study the protein fibrillation process in the presence of other polymers, as polysaccharides (*in situ* fibrillation). One example is bacterial cellulose (BC), because protein fibrillation can be promoted inside the 3-D BC network.

5.
References

1. Gandini, A. The irruption of polymers from renewable resources on the scene of macromolecular science and technology. *Green Chem.* **13,** 1061–1083 (2011).

2. Mathers, R. T. How well can renewable resources mimic commodity monomers and polymers? *J. Polym. Sci. Polym. Chem.* **50,** 1–15 (2012).

3. Wilbon, P. A., Chu, F. & Tang, C. Progress in renewable polymers from natural terpenes, terpenoids, and rosin. *Macromol. Rapid Commun.* **34,** 8–37 (2013).

4. Miller, S. A. Sustainable Polymers: Opportunities for the Next Decade. *ACS Macro Lett.* **2,** 550–554 (2013).

5. Belgacem, M. N. & Gandini, A. *Monomers , Polymers and Composites from renewable resources*. (Elsevier, 2008).

6. Yu, L., Dean, K. & Li, L. Polymer blends and composites from renewable resources. *Prog. Polym. Sci.* **31,** 576–602 (2006).

7. Jose, J. P. *et al.* in *Polymer Composites: Macro- and Microcomposites* (arg. Thomas, S., Joseph, K., Malhotra, S. K., Goda, K. & Sreekala, M. S.) **1,** 1–16 (Wiley-VCH Verlag GmbH & Co. KGaA, 2012).

8. Zhang, L. & Zeng, M. in *Monomers, polymers and composites from renewable resources* (arg. Belgacem, M. N. & Gandini, A.) 479–493 (Elsevier Ltd, 2008).

9. Kumar, A. *Protein biotechnology*. (Discovery Publishing House, 2006).

10. Kumar, R., Choudhary, V., Mishra, S., Varma, I. K. & Mattiason, B. Adhesives and plastics based on soy protein products. *Ind. Crop. Prod.* **16,** 155–172 (2002).

11. Hu, X., Cebe, P., Weiss, A. S., Omenetto, F. & Kaplan, D. L. Protein-based composite materials. *Mater. Today* **15,** 208–215 (2012).

12. de la Rica, R. & Matsui, H. Applications of peptide and protein-based materials in bionanotechnology. *Chem. Soc. Rev.* **39,** 3499–3509 (2010).

13. Gomes, S., Leonor, I. B., Mano, J. F., Reis, R. L. & Kaplan, D. L. Natural and Genetically Engineered Proteins for Tissue Engineering. *Prog. Polym. Sci.* **37,** 1–17 (2012).

14. Werkmeister, J. A. & Ramshaw, J. A. M. Recombinant protein scaffolds for tissue engineering. *Biomed. Mater.* **7,** 12002 (2012).

15. Jonker, A. M., Löwik, D. W. P. M. & Hest, J. C. M. Van. Peptide- and Protein-Based Hydrogels. *Chem. Mater.* **24,** 759–773 (2012).

16. DiMarco, R. L. & Heilshorn, S. C. Multifunctional materials through modular protein engineering. *Adv. Mater.* **24,** 3923–3940 (2012).

17. Silva, N. H. C. S. *et al.* Protein-based materials: from sources to innovative sustainable materials for biomedical applications. *J. Mater. Chem. B* **2,** 3715 (2014).

18. Sipe, J. D. & Cohen, A. S. Review: history of the amyloid fibril. *J. Struct. Biol.* **130,** 88–98 (2000).

19. Kelly, J. W. Amyloid fibril formation and protein misassembly: a structural quest for insights into amyloid and prion diseases. *Structure* **5,** 595–600 (1997).

20. Chiti, F. & Dobson, C. M. Protein misfolding, functional amyloid, and human disease. *Annu. Rev. Biochem.* **75,** 333–366 (2006).

21. Serpell, L. C. Alzheimer's amyloid fibrils: structure and assembly. **1502,** 16–30 (2000).

22. Adamcik, J. & Mezzenga, R. Proteins Fibrils from a Polymer Physics Perspective. *Macromolecules* **45,** 1137–1150 (2012).

23. Greenwald, J. & Riek, R. Biology of amyloid: structure, function, and regulation. *Structure* **18,** 1244–1260 (2010).

24. Cherny, I. & Gazit, E. Amyloids: not only pathological agents but also ordered nanomaterials. *Angew. Chem. Int. Ed. Engl.* **47,** 4062–9 (2008).

25. Makin, O. S. & Serpell, L. C. Structures for amyloid fibrils. *FEBS J.* **272,** 5950–5961 (2005).

26. Sunde, M. *et al.* Common core structure of amyloid fibrils by synchrotron X-ray diffraction. *J. Mol. Biol.* **273,** 729–39 (1997).

27. Knowles, T., Smith, J., Craig, A., Dobson, C. & Welland, M. Spatial Persistence of Angular Correlations in Amyloid Fibrils. *Phys. Rev. Lett.* **96,** 238301 (2006).

28. Knowles, T. P. *et al.* Role of intermolecular forces in defining material properties of protein nanofibrils. *Science* **318,** 1900–3 (2007).

29. Baldwin, A. J. *et al.* Metastability of native proteins and the phenomenon of amyloid formation. *J. Am. Chem. Soc.* **133,** 14160–3 (2011).

30. Hartl, F. U., Bracher, A. & Hayer-Hartl, M. Molecular chaperones in protein folding and proteostasis. *Nature* **475,** 324–32 (2011).

31. Cohen, A., Shirahama, T. & Skinner, M. in *Electron Microscopy of Protein* 165–205 (Academic Press London, 1982).

32. Morris, K. L. & Serpell, L. C. Amyloid Proteins. **849,** 121–135 (2012).

33. Eanes, E. D. & Glenner, G. G. X-Ray Diffraction Studies on Amyloid Filaments. *J. Histochem. Cytochem.* **16,** 673–677 (1968).

34. Elghetany, M. T. & Saleem, A. Methods for staining amyloid in tissues. a review.

Stain Technol. **63(4),** 201–212 (1988).

35.   Westermark, G. T., Johnson, K. H. & Westermark, P. Staining methods for identification of amyloid in tissue. *Methods Enzymol.* **309,** 3–25 (1999).

36.   Harper, J. D. & Lansbury, P. T. Models of amyloid seeding in Alzheimer's disease and scrapie: mechanistic truths and physiological consequences of the time-dependent solubility of amyloid proteins. *Annu. Rev. Biochem.* **66,** 385–407 (1997).

37.   Puchtler, H., Sweat, F. & Levine, M. On the Binding of Congo Red By Amyloid. *J. Histochem. Cytochem.* **10,** 355–364 (1962).

38.   Levine, H. Thioflavine T interaction with synthetic Alzheimer's disease B-amyloid peptides: Detection of amyloid aggregation in solution. *Protein Sci.* **2,** 404–410 (1993).

39.   Balbach, J. J. *et al.* Supramolecular Structure in Full-Length Alzheimer's beta-Amyloid Fibrils: Evidence for a Parallel beta-Sheet Organization from Solid-State Nuclear Magnetic Resonance. *Biophys. J.* **83,** 1205–1216 (2002).

40.   Antzutkin, O. N., Leapman, R. D., Balbach, J. J. & Tycko, R. Supramolecular Structural Constraints on Alzheimer's beta-Amyloid Fibrils from Electron Microscopy and Solid-State Nuclear Magnetic Resonance. *Biochemistry* **41,** 15436–15450 (2002).

41.   Antzutkin, O. N. *et al.* Multiple quantum solid-state NMR indicates a parallel, not antiparallel, organization of beta-sheets in Alzheimer's beta-amyloid fibrils. *PNAS* **97,** 13045–13050 (2000).

42.   Tycko, R. Insights into the amyloid folding problem from solid-state NMR. *Biochemistry* **42,** 3151–3159 (2003).

43.   Lazo, N. D. & Downing, D. T. New Concepts in Biochemistry Amyloid Fibrils May Be Assembled from -Helical Protofibrils †. **37,** 1–5 (1998).

44.   Chaney, M. O., Webster, S. D., Kuo, Y. & Roher, A. E. Molecular modeling of the A β 1-42 peptide from Alzheimer ' s disease. **11,** 761–767 (1998).

45.   George, A. R. & Howlett, D. R. Computationally Derived Structural Models of the beta-Amyloid Found in Alzheimer's Disease Plaques and the Interaction with Possible Aggregation Inhibitors. *Biopolymers* **50(7),** 733–741 (1999).

46.   Li, L., Darden, T. a, Bartolotti, L., Kominos, D. & Pedersen, L. G. An atomic model for the pleated beta-sheet structure of Abeta amyloid protofilaments. *Biophys. J.* **76,** 2871–8 (1999).

47.   Benzinger, T. L. *et al.* Two-dimensional structure of beta-amyloid(10-35) fibrils. *Biochemistry* **39,** 3491–9 (2000).

48.   Petkova, A. T. *et al.* Self-propagating, molecular-level polymorphism in Alzheimer's beta-amyloid fibrils. *Science* **307,** 262–5 (2005).

49.   Balbach, J. J. *et al.* Amyloid Fibril Formation by Abeta 16-2, a Seven-Residue

Fragment of the Alzheimer's beta-Amyloid Peptide, and Structural Characterization by Solid State. *Biochemistry* **39,** 13748–13759 (2000).

50. Petkova, a. T. *et al.* Solid State NMR Reveals a pH-dependent Antiparallel β-Sheet Registry in Fibrils Formed by a β-Amyloid Peptide. *J. Mol. Biol.* **335,** 247–260 (2004).

51. Gordon, D. J., Balbach, J. J., Tycko, R. & Meredith, S. C. Increasing the amphiphilicity of an amyloidogenic peptide changes the beta-sheet structure in the fibrils from antiparallel to parallel. *Biophys. J.* **86,** 428–34 (2004).

52. Fitzpatrick, A. W. P., Debelouchina, G. T., Bayro, M. J., Clare, D. K. & Caporini, M. A. Atomic structure and hierarchical assembly of a cross- β amyloid fibril. *PNAS* **14,** 5468–5473 (2013).

53. Jaroniec, C. P. *et al.* High-resolution molecular structure of a peptide in an amyloid fibril determined by magic angle spinning NMR spectroscopy. *Proc. Natl. Acad. Sci. U. S. A.* **101,** 711–6 (2004).

54. Dobson, C. M. Protein misfolding, evolution and disease. *Trends Biochem. Sci.* **24,** 329–32 (1999).

55. Fändrich, M., Meinhardt, J. & Grigorieff, N. Structural polymorphism of Alzheimer Abeta and other amyloid fibrils. *Prion* **3,** 89–93 (2009).

56. Tycko, R. in *Proteopathic Seeds and Neurodegenerative Diseases* (arg. Jucker, M. & Christen, Y.) 19–25 (Springer Berlin Heidelberg, 2013). doi:10.1007/978-3-642-35491-5

57. Pedersen, J. S. *et al.* The changing face of glucagon fibrillation: structural polymorphism and conformational imprinting. *J. Mol. Biol.* **355,** 501–23 (2006).

58. Jones, E. M. & Surewicz, W. K. Fibril conformation as the basis of species- and strain-dependent seeding specificity of mammalian prion amyloids. *Cell* **121,** 63–72 (2005).

59. Bousset, L., Thomson, N. H., Radford, S. E. & Melki, R. The yeast prion Ure2p retains its native alpha-helical conformation upon assembly into protein fibrils in vitro. *EMBO J.* **21,** 2903–2911 (2002).

60. Bousset, L., Briki, F., Doucet, J. & Melki, R. The native-like conformation of Ure2p in fibrils assembled under physiologically relevant conditions switches to an amyloid-like conformation upon heat-treatment of the fibrils. *J. Struct. Biol.* **141,** 132–142 (2003).

61. Jiménez, J. L. *et al.* Cryo-electron microscopy structure of an SH3 amyloid fibril and model of the molecular packing. *EMBO J.* **18,** 815–21 (1999).

62. Goldsbury, C. S. *et al.* Studies on the in vitro assembly of a beta 1-40: implications for the search for a beta fibril formation inhibitors. *J. Struct. Biol.* **130,** 217–31 (2000).

63. Goldsbury, C., Frey, P., Olivieri, V., Aebi, U. & Müller, S. a. Multiple assembly pathways underlie amyloid-beta fibril polymorphisms. *J. Mol. Biol.* **352,** 282–98

(2005).

64.   Meinhardt, J., Sachse, C., Hortschansky, P., Grigorieff, N. & Fändrich, M. Abeta(1-40) fibril polymorphism implies diverse interaction patterns in amyloid fibrils. *J. Mol. Biol.* **386,** 869–77 (2009).

65.   Heise, H. *et al.* Molecular-level secondary structure, polymorphism, and dynamics of full-length alpha-synuclein fibrils studied by solid-state NMR. *PNAS* **102,** 15871–15876 (2005).

66.   Madine, J. *et al.* Structural Insights into the Polymorphism of Amyloid-Like Fibrils Formed by Region 20 - 29 of Amylin Revealed by Solid-State NMR and X-ray Fiber Diffraction. 14990–15001 (2008).

67.   Morris, A. M., Watzky, M. a & Finke, R. G. Protein aggregation kinetics, mechanism, and curve-fitting: a review of the literature. *Biochim. Biophys. Acta* **1794,** 375–97 (2009).

68.   Murphy, R. M. Kinetics of amyloid formation and membrane interaction with amyloidogenic proteins. *Biochim. Biophys. Acta* **1768,** 1923–34 (2007).

69.   Frieden, C. Protein aggregation processes : In search of the mechanism. 2334–2344 (2007). doi:10.1110/ps.073164107.tems

70.   Gillam, J. E. & MacPhee, C. E. Modelling amyloid fibril formation kinetics: mechanisms of nucleation and growth. *J. Phys. Condens. Matter* **25,** 373101 (2013).

71.   Serio, T. R. *et al.* Nucleated conformational conversion and the replication of conformational information by a prion determinant. *Science* **289,** 1317–21 (2000).

72.   Uversky, V. N. *et al.* Biophysical properties of the synucleins and their propensities to fibrillate: inhibition of alpha-synuclein assembly by beta- and gamma-synucleins. *J. Biol. Chem.* **277,** 11970–8 (2002).

73.   Pedersen, J. S., Christensen, G. & Otzen, D. E. Modulation of S6 fibrillation by unfolding rates and gatekeeper residues. *J. Mol. Biol.* **341,** 575–88 (2004).

74.   Chayen, N. E. Methods for separating nucleation and growth in protein crystallisation. *Prog. Biophys. Mol. Biol.* **88,** 329–37 (2005).

75.   Fezoui, Y. & Teplow, D. B. Kinetic studies of amyloid beta-protein fibril assembly. Differential effects of alpha-helix stabilization. *J. Biol. Chem.* **277,** 36948–54 (2002).

76.   Jones, O. G. & Mezzenga, R. Inhibiting, promoting, and preserving stability of functional protein fibrils. *Soft Matter* **8,** 876–895 (2012).

77.   Swaminathan, R., Ravi, V. K., Kumar, S., Kumar, M. V. S. & Chandra, N. in *Advances in protein chemistry and structural biology* **84,** 63–111 (Elsevier, 2011).

78.   Yagi, N., Ohta, N. & Matsuo, T. Structure of amyloid fibrils of hen egg white

lysozyme studied by microbeam X-ray diffraction. *Int. J. Biol. Macromol.* **45,** 86–90 (2009).

79.   Dubey, K. & Kar, K. Type I collagen prevents amyloid aggregation of hen egg white lysozyme. *Biochem. Biophys. Res. Commun.* **448,** 480–484 (2014).

80.   Homchaudhuri, L., Kumar, S. & Swaminathan, R. Slow aggregation of lysozyme in alkaline pH monitored in real time employing the fluorescence anisotropy of covalently labelled dansyl probe. *FEBS Lett.* **580,** 2097–101 (2006).

81.   Hameed, M., Ahmad, B., Khan, R. H. & Andrabi, K. I. Tertiary Butanol Induced Amyloidogenesis of Hen Egg White Lysozyme (HEWL) Is Facilitated by Aggregation-Prone Alkali-Induced Molten Globule Like Conformational State. *Protein Pept. Lett.* **16,** 56–60 (2009).

82.   Mishra, R. *et al.* Lysozyme amyloidogenesis is accelerated by specific nicking and fragmentation but decelerated by intact protein binding and conversion. *J. Mol. Biol.* **366,** 1029–1044 (2007).

83.   Wang, Z., Xiao, H., Han, Y., Jiang, P. & Zhou, Z. The Effect of Four Imidazolium Ionic Liquids on Hen Egg White Lysozyme Solubility. *J. Chem. Eng. Data* **56,** 1700–1703 (2011).

84.   Zou, Y., Hao, W., Li, H., Gao, Y. & Sun, Y. New Insight into Amyloid Fibril Formation of Hen Egg White Lysozyme Using a Two-Step Temperature-Dependent FTIR Approach. *J. Phys. Chem. B* **118,** 9834–9843 (2014).

85.   De Felice, F. G. *et al.* Formation of amyloid aggregates from human lysozyme and its disease-associated variants using hydrostatic pressure. *FASEB J.* **15,** 1–15 (2004).

86.   Kar, K. & Kishore, N. Enhancement of Thermal Stability and Inhibition of Protein Aggregation by Osmolytic Effect of Hydroxyproline. *Biopolymers* **87,** 339–351 (2007).

87.   Wen, W.-S. *et al.* Effects of copolypeptides on amyloid fibrillation of hen egg-white lysozyme. *Biopolymers* **97,** 107–116 (2012).

88.   Kumar, E. K. & Prabhu, N. P. Differential effects of ionic and non-ionic surfactants on lysozyme fibrillation. *Phys. Chem. Chem. Phys.* **16,** 24076–24088 (2014).

89.   Wang, S. S.-S., Hung, Y.-T., Wang, P. & Wu, J. W. The formation of amyloid fibril-like hen egg-white lysozyme species induced by temperature and urea concentration-dependent denaturation. *Korean J. Chem. Eng.* **24,** 787–795 (2007).

90.   Holley, M., Eginton, C., Schaefer, D. & Brown, L. R. Characterization of amyloidogenesis of hen egg lysozyme in concentrated ethanol solution. *Biochem. Biophys. Res. Commun.* **373,** 164–168 (2008).

91.   He, J. *et al.* Myricetin Prevents Fibrillogenesis of Hen Egg White Lysozyme. *J. Agric. Food Chem.* **62,** 9442–9449 (2014).

92. Ghosh, S., Pandey, N. K. & Dasgupta, S. Crowded milieu prevents fibrillation of hen egg white lysozyme with retention of enzymatic activity. *J. Photochem. Photobiol. B Biol.* **138,** 8–16 (2014).

93. Li, C., Adamcik, J. & Mezzenga, R. Biodegradable nanocomposites of amyloid fibrils and graphene with shape-memory and enzyme-sensing properties. *Nat. Nanotechnol.* **7,** 421–427 (2012).

94. Jung, J.-M., Savin, G., Pouzot, M., Schmitt, C. & Mezzenga, R. Structure of heat-induced beta-lactoglobulin aggregates and their complexes with sodium-dodecyl sulfate. *Biomacromolecules* **9,** 2477–2486 (2008).

95. Loveday, S. M., Wang, X. L., Rao, M. a., Anema, S. G. & Singh, H. β-Lactoglobulin nanofibrils: Effect of temperature on fibril formation kinetics, fibril morphology and the rheological properties of fibril dispersions. *Food Hydrocoll.* **27,** 242–249 (2012).

96. Loveday, S. M. *et al.* Tuning the properties of β-lactoglobulin nanofibrils with pH, NaCl and CaCl2. *Int. Dairy J.* **20,** 571–579 (2010).

97. Zidar, J. & Merzel, F. Probing amyloid-beta fibril stability by increasing ionic strengths. *J. Phys. Chem. B* **115,** 2075–2081 (2011).

98. Zako, T., Sakono, M., Hashimoto, N., Ihara, M. & Maeda, M. Bovine insulin filaments induced by reducing disulfide bonds show a different morphology, secondary structure, and cell toxicity from intact insulin amyloid fibrils. *Biophys. J.* **96,** 3331–3340 (2009).

99. Rao, S. P. *et al.* Amyloid fibrils as functionalizable components of nanocomposite materials. *Biotechnol. Prog.* **28,** 248–256 (2011).

100. Carvalho, T., Pinto, R. J. B., Martins, M. A., Silvestre, A. J. D. & Freire, C. S. R. Timesaving microwave assisted synthesis of insulin amyloid fibrils with enhanced nanofiber aspect ratio. *Int. J. Biol. Macromol.* **92,** 225–231 (2016).

101. Arasteh, A., Habibi-Rezaei, M., Ebrahim-Habibi, A. & Moosavi-Movahedi, A. A. Response surface methodology for optimizing the bovine serum albumin fibrillation. *Protein J.* **31,** 457–465 (2012).

102. Vetri, V. *et al.* Bovine Serum Albumin protofibril-like aggregates formation: solo but not simple mechanism. *Arch. Biochem. Biophys.* **508,** 13–24 (2011).

103. Pan, K. & Zhong, Q. Amyloid-like fibrils formed from intrinsically disordered caseins: physicochemical and nanomechanical properties. *Soft Matter* **11,** 5898–5904 (2015).

104. Vernaglia, B. a, Huang, J. & Clark, E. D. Guanidine hydrochloride can induce amyloid fibril formation from hen egg-white lysozyme. *Biomacromolecules* **5,** 1362–1370 (2004).

105. Wicklein, B. & Salazar-Alvarez, G. Functional hybrids based on biogenic nanofibrils and inorganic nanomaterials. *J. Mater. Chem. A* **1,** 5469–5478 (2013).

106. Meier, C., Lifincev, I. & Welland, M. E. Conducting Core-Shell Nanowires by

Amyloid Nanofiber Templated Polymerization. *Biomacromolecules* **16,** 558–563 (2015).

107. Li, C. *et al.* Amyloid-hydroxyapatite bone biomimetic composites. *Adv. Mater.* **26,** 3207–3212 (2014).

108. Rogers, R. D. & Seddon, K. R. Chemistry. Ionic liquids--solvents of the future? *Science* **302,** 792–793 (2003).

109. Greaves, T. L. & Drummond, C. J. Protic Ionic Liquids : Properties and Applications. 206–237 (2008).

110. Wasserscheid, P. & Welton, T. *Ionic Liquids in Synthesis*. **7,** (Wiley-VCH, 2007).

111. Fujita, K. *et al.* Solubility and Stability of Cytochrome c in Hydrated Ionic Liquids: Effect of Oxo Acid Residues and Kosmotropicity. *Biomacromolecules* **8,** 2080–2086 (2007).

112. Fujita, K., MacFarlane, D. R. & Forsyth, M. Protein solubilising and stabilising ionic liquids. *Chem. Commun. (Camb).* **70,** 4804–4806 (2005).

113. Kalhor, H. R., Kamizi, M., Akbari, J. & Heydari, A. Inhibition of amyloid formation by ionic liquids: ionic liquids affecting intermediate oligomers. *Biomacromolecules* **10,** 2468–2475 (2009).

114. Debeljuh, N., Barrow, C. J., Henderson, L. & Byrne, N. Structure inducing ionic liquids-enhancement of alpha helicity in the Abeta(1-40) peptide from Alzheimer's disease. *Chem. Commun.* **47,** 6371–6373 (2011).

115. Debeljuh, N., Barrow, J. & Byrne, N. The impact of ionic liquids on amyloid fibrilization of Aβ16-22: tuning the rate of fibrilization using a reverse Hofmeister strategy. *Phys. Chem. Chem. Phys.* **13,** 16534–16536 (2011).

116. Goujon, N., Rajkhowa, R., Wang, X. & Byrne, N. Effect of solvent on ionic liquid dissolved regenerated antheraea assamensis silk fibroin. *J. Appl. Polym. Sci.* **128,** 4411–4416 (2013).

117. Byrne, N. & Angell, C. A. Formation and dissolution of hen egg white lysozyme amyloid fibrils in protic ionic liquids. *Chem. Commun. (Camb).* **0,** 1046–1048 (2009).

118. Hwang, H., Choi, H., Kim, H.-K., Jo, D. H. & Kim, T. D. Ionic liquids promote amyloid formation from alpha-synuclein. *Anal. Biochem.* **386,** 293–295 (2009).

119. Shang, S., Zhu, L. & Fan, J. Physical properties of silk fibroin/cellulose blend films regenerated from the hydrophilic ionic liquid. *Carbohydr. Polym.* **86,** 462–468 (2011).

120. Bae, S. Y., Kim, S., Lee, B. Y., Kim, K. K. & Kim, T. D. Amyloid formation using 1-butyl-3-methyl-imidazolium-based ionic liquids. *Anal. Biochem.* **419,** 354–356 (2011).

121. Bae, S. Y. *et al.* Amyloid formation and disaggregation of α-synuclein and its tandem repeat (α-TR). *Biochem. Biophys. Res. Commun.* **400,** 531–536 (2010).

122. Abbott, A. P., Boothby, D., Capper, G., Davies, D. L. & Rasheed, R. K. Deep Eutectic Solvents formed between choline chloride and carboxylic acids: Versatile alternatives to ionic liquids. *J. Am. Chem. Soc.* **126,** 9142–9147 (2004).

123. Welton, T. Room-Temperature Ionic Liquids. Solvents for Synthesis and Catalysis - Chemical Reviews (ACS Publications). *Chem. Rev.* **99,** 2071–2083 (1999).

124. Wasserscheid, P. & Keim, W. Ionic Liquids-New «Solutions» for Transition Metal Catalysis. *Angew. Chem. Int. Ed. Engl.* **39,** 3772–3789 (2000).

125. Abbott, A. P. *et al.* Preparation of novel, moisture-stable, Lewis-acidic ionic liquids containing quaternary ammonium salts with functional side chains. *Chem. Commun. (Camb).* **0,** 2010–2011 (2001).

126. Francisco, M., Van Den Bruinhorst, A. & Kroon, M. C. Low-transition-temperature mixtures (LTTMs): A new generation of designer solvents. *Angew. Chemie - Int. Ed.* **52,** 3074–3085 (2013).

127. Francisco, M., van den Bruinhorst, A. & Kroon, M. C. New natural and renewable low transition temperature mixtures (LTTMs): screening as solvents for lignocellulosic biomass processing. *Green Chem.* **14,** 2153–2157 (2012).

128. Zhang, Q., De Oliveira Vigier, K., Royer, S. & Jérôme, F. Deep eutectic solvents: syntheses, properties and applications. *Chem. Soc. Rev.* **41,** 7108–7146 (2012).

129. Yu, Y. *et al.* Biodegradable naphthenic acid ionic liquids: Synthesis, characterization, and quantitative structure-biodegradation relationship. *Chem. - A Eur. J.* **14,** 11174–11182 (2008).

130. Jhong, H. R., Wong, D. S. H., Wan, C. C., Wang, Y. Y. & Wei, T. C. A novel deep eutectic solvent-based ionic liquid used as electrolyte for dye-sensitized solar cells. *Electrochem. commun.* **11,** 209–211 (2009).

131. Singh, B. S., Lobo, H. R. & Shankarling, G. S. Choline chloride based eutectic solvents: Magical catalytic system for carbon-carbon bond formation in the rapid synthesis of β-hydroxy functionalized derivatives. *Catal. Commun.* **24,** 70–74 (2012).

132. Smith, E. L., Abbott, A. P. & Ryder, K. S. Deep Eutectic Solvents (DESs) and Their Applications. *Chem. Rev.* **114,** 11060–11082 (2012).

133. Oliveira, F. S., Pereiro, A. B., Rebelo, L. P. N. & Marrucho, I. M. Deep eutectic solvents as extraction media for azeotropic mixtures. *Green Chem.* **15,** 1326–1330 (2013).

134. Kareem, M. a. *et al.* Phase equilibria of toluene/heptane with deep eutectic solvents based on ethyltriphenylphosphonium iodide for the potential use in the separation of aromatics from naphtha. *J. Chem. Thermodyn.* **65,** 138–149 (2013).

135. Rodriguez, N. R., Molina, B. S. & Kroon, M. C. Aliphatic+ethanol separation via liquid–liquid extraction using low transition temperature mixtures as extracting agents. *Fluid Phase Equilib.* **394,** 71–82 (2015).

136. Ribeiro, B. D., Coelho, M. A. Z. & Marrucho, I. M. Extraction of saponins from sisal (Agave sisalana) and juá (Ziziphus joazeiro) with cholinium-based ionic liquids and deep eutectic solvents. *Eur. Food Res. Technol.* **237,** 965–975 (2013).

137. Kwan, A. H. Y. *et al.* Structural basis for rodlet assembly in fungal hydrophobins. *PNAS* **103,** 3621–3626 (2006).

138. Carrió, M., González-Montalbán, N., Vera, A., Villaverde, A. & Ventura, S. Amyloid-like properties of bacterial inclusion bodies. *J. Mol. Biol.* **347,** 1025–1037 (2005).

139. Gras, S. L., Squires, A. M., Dobson, C. M. & Ğ C. E. M. Functionalised fibrils for bio-nanotechnology. 214–216 (2006).

140. Fowler, D. M. *et al.* Functional amyloid formation within mammalian tissue. *PLoS Biol.* **4,** e6 100-107 (2006).

141. Gazit, E. Use of biomolecular templates for the fabrication of metal nanowires. *FEBS J.* **274,** 317–322 (2007).

142. Kasotakis, E. *et al.* Design of metal-binding sites onto self-assembled peptide fibrils. *Biopolymers* **92,** 164–172 (2009).

143. Zhou, X. *et al.* The fabrication and electrical characterization of protein fibril-templated one-dimensional palladium nanostructures. *Eur. Polym. J.* **49,** 1957–1963 (2013).

144. Wei, G., Reichert, J., Bossert, J. & Jandt, K. D. Novel biopolymeric template for the nucleation and growth of hydroxyapatite crystals based on self-assembled fibrinogen fibrils. *Biomacromolecules* **9,** 3258–3267 (2008).

145. Li, L., Wei, K.-M., Lin, F., Kong, X.-D. & Yao, J.-M. Effect of silicon on the formation of silk fibroin/calcium phosphate composite. *J. Mater. Sci. Mater. Med.* **19,** 577–582 (2008).

146. Colby, R., Hulleman, J., Padalkar, S., Rochet, J. & Stanciu, L. No Title. *J. Nanosci. Nanotechnol.* **8,** 973–978 (2008).

147. Sang, L., Huang, J., Luo, D., Chen, Z. & Li, X. Bone-like nanocomposites based on self-assembled protein-based matrices with Ca2+ capturing capability. *J. Mater. Sci. Mater. Med.* **21,** 2561–2568 (2010).

148. Jee, S. S., Kasinath, R. K., DiMasi, E., Kim, Y.-Y. & Gower, L. Oriented hydroxyapatite in turkey tendon mineralized via the polymer-induced liquid-precursor (PILP) process. *CrystEngComm* **13,** 2077–2083 (2011).

149. Paparcone, R., Kniep, R. & Brickmann, J. Hierarchical pattern of microfibrils in a 3D fluorapatite-gelatine nanocomposite: simulation of a bio-related structure building process. *Phys. Chem. Chem. Phys.* **11,** 2186–2194 (2009).

150. Subburaman, K. *et al.* Templated biomineralization on self-assembled protein fibers. *Proc. Natl. Acad. Sci. U. S. A.* **103,** 14672–14677 (2006).

151. Amos, F. F., Ponce, C. B. & Evans, J. S. Formation of framework nacre

polypeptide supramolecular assemblies that nucleate polymorphs. *Biomacromolecules* **12,** 1883–1890 (2011).

152. Liu, Y. *et al.* Hierarchical Intrafibrillar Nanocarbonated Apatite Assembly Improves the Nanomechanics and Cytocompatibility of Mineralized Collagen. *Adv. Funct. Mater.* **23,** 1404–1411 (2013).

153. Aimé, C., Mosser, G., Pembouong, G., Bouteiller, L. & Coradin, T. Controlling the nano-bio interface to build collagen-silica self-assembled networks. *Nanoscale* **4,** 7127–7134 (2012).

154. Fahmi, A. *et al.* Fabrication of CdSe-Nanofibers with Potential for Biomedical Applications. *Adv. Funct. Mater.* **20,** 1011–1018 (2010).

155. Scheibel, T. *et al.* Conducting nanowires built by controlled self-assembly of amyloid fibers and selective metal deposition. *Proc. Natl. Acad. Sci. U. S. A.* **100,** 4527–4532 (2003).

156. Reches, M. & Gazit, E. Casting metal nanowires within discrete self-assembled peptide nanotubes. *Science* **300,** 625–627 (2003).

157. Bolisetty, S., Arcari, M., Adamcik, J. & Mezzenga, R. Hybrid Amyloid Membranes for Continuous Flow Catalysis. *Langmuir* **31,** 13867–13873 (2015).

158. Eakins, G. L. *et al.* Functional Organic Semiconductors Assembled via Natural Aggregating Peptides. *Adv. Funct. Mater.* **25,** 5640–5649 (2015).

159. Wu, X. *et al.* Amyloid-graphene oxide as immobilization platform of Au nanocatalysts and enzymes for improved glucose-sensing activity. *J. Colloid Interface Sci.* **490,** 336–342 (2017).

160. Bolisetty, S. & Mezzenga, R. Amyloid–carbon hybrid membranes for universal water purification. *Nat Nano* **4,** 365–371 (2016).

161. Byrne, N., Hameed, N., Werzer, O. & Guo, Q. The preparation of novel nanofilled polymer composites using poly(l-lactic acid) and protein fibers. *Eur. Polym. J.* **47,** 1279–1283 (2011).

162. Oppenheim, T., Knowles, T. P. J., Lacour, S. P. & Welland, M. E. Fabrication and characterisation of protein fibril-elastomer composites. *Acta Biomater.* **6,** 1337–1341 (2010).

163. Claunch, E. C., Ridgley, D. M. & Barone, J. R. Completely self-assembled fiber composites. *Compos. Sci. Technol.* **117,** 1–8 (2015).

164. Knowles, T. P. J., Oppenheim, T. W., Buell, A. K., Chirgadze, D. Y. & Welland, M. E. Nanostructured films from hierarchical self-assembly of amyloidogenic proteins. *Nat. Nanotechnol.* **5,** 204–207 (2010).

165. Li, C. & Mezzenga, R. Functionalization of multiwalled carbon nanotubes and their pH-responsive hydrogels with amyloid fibrils. *Langmuir* **28,** 10142–10146 (2012).

166. Li, C., Alam, M. M., Bolisetty, S., Adamcik, J. & Mezzenga, R. New

biocompatible thermo-reversible hydrogels from PNiPAM-decorated amyloid fibrils. *Chem. Commun.* **47,** 2913–2915 (2011).

167. Zhang, S., Holmes, T., Lockshin, C. & Rich, a. Spontaneous assembly of a self-complementary oligopeptide to form a stable macroscopic membrane. *Proc. Natl. Acad. Sci. U. S. A.* **90,** 3334–3338 (1993).

168. Zhang, S., Lockshin, C., Cook, R. & Rich, a. Unusually stable beta-sheet formation in an ionic self-complementary oligopeptide. *Biopolymers* **34,** 663–672 (1994).

169. Caplan, M., Schwartzfarb, E., Zhang, S., Kamm, R. & Lauffenburger, D. Control of self-assembling oligopeptide matrix formation through systematic variation of amino acid sequence. *Biomaterials* **23,** 219–227 (2002).

170. Zhang, S. *et al.* Self-complementary oligopeptide matrices support mammalian cell attachment. *Biomaterials* **16,** 1385–1393 (1995).

171. Holmes, T. C. *et al.* Extensive neurite outgrowth and active synapse formation on self-assembling peptide scaffolds. *Proc. Natl. Acad. Sci. U. S. A.* **97,** 6728–6733 (2000).

172. Genové, E., Shen, C., Zhang, S. & Semino, C. E. The effect of functionalized self-assembling peptide scaffolds on human aortic endothelial cell function. *Biomaterials* **26,** 3341–3351 (2005).

173. Horii, A., Wang, X., Gelain, F. & Zhang, S. Biological designer self-assembling peptide nanofiber scaffolds significantly enhance osteoblast proliferation, differentiation and 3-D migration. *PLoS One* **2,** e190 (2007).

174. Nyström, G., Fong, W. & Mezzenga, R. Ice-Templated and Cross-Linked Amyloid Fibril Aerogel Sca ff olds for Cell Growth. *Biomacromolecules* **18,** 2858–2865 (2017).

175. Maleki, B., Tabandeh, F., Soheili, Z. & Morshedi, D. Application of proteinous nano fibrils to culture retinal pigmented epithelium cells: A versatile biomaterial. *React. Funct. Polym.* **115,** 36–42 (2017).

176. Sakono, M. *et al.* Application of two morphologically different fibrillar and filamentous insulin amyloids as a biomaterial for cell culture surfaces. *React. Funct. Polym.* **71,** 324–328 (2011).

177. Gras, S. L. *et al.* Functionalised amyloid fibrils for roles in cell adhesion. *Biomaterials* **29,** 1553–1562 (2008).

178. Sondheimer, N. & Lindquist, S. Rnq1: an epigenetic modifier of protein function in yeast. *Mol. Cell* **5,** 163–172 (2000).

179. Baldwin, A. J. *et al.* Cytochrome display on amyloid fibrils. *J. Am. Chem. Soc.* **128,** 2162–2163 (2006).

180. Kodama, H., Matsumura, S. & Mihara, H. Construction of a protein array on amyloid-like fibrils using co-assembly of designed peptides. **2,** 2876–2877 (2004).

181. Baxa, U., Speransky, V., Steven, A. C. & Wickner, R. B. Mechanism of inactivation on prion conversion of the Saccharomyces cerevisiae Ure2 protein. *Proc. Natl. Acad. Sci. U. S. A.* **99,** 5253–5260 (2002).

182. Pierschbacher, M. D. & Ruoslahti, E. Variants of the cell recognition site of fibronectin that retain attachment-promoting activity. *Proc. Natl. Acad. Sci. U. S. A.* **81,** 5985–5988 (1984).

183. Sagis, L. M. C. *et al.* Polymer microcapsules with a fiber-reinforced nanocomposite shell. *Langmuir* **24,** 1608–1612 (2008).

184. Maji, S. K. *et al.* Amyloid as a depot for the formulation of long-acting drugs. *PLoS Biol.* **6,** e17 (2008).

185. Mankar, S., Anoop, A., Sen, S. & Maji, S. K. Nanomaterials: amyloids reflect their brighter side. *Nano Rev.* **2,** 1–12 (2011).

186. Gupta, S., Chattopadhyay, T., Pal Singh, M. & Surolia, A. Supramolecular insulin assembly II for a sustained treatment of type 1 diabetes mellitus. *Proc. Natl. Acad. Sci. U. S. A.* **107,** 13246–13251 (2010).

187. Kabay, G., Ersin, A., Kaleli, G., Demirci, C. & Mutlu, M. Controlled release of a hydrophilic drug from electrospun amyloid-like protein blend nano fi bers. *Mater. Sci. Eng. C* **81,** 271–279 (2017).

188. Hendler, N. *et al.* Multiple Self-Assembly Functional Structures Based on Versatile Binding Sites of β -Lactoglobulin. *Adv. Funct. Mater.* **22,** 3765–3776 (2012).

189. Soto, C. Unfolding the role of protein misfolding in neurodegenerative diseases. *Nat. Rev. Neurosci.* **4,** 49–60 (2003).

190. Iconomidou, V. A., Vriend, G. & Y, S. J. H. Amyloids protect the silkmoth oocyte and embryo. **479,** 141–145 (2000).

191. Fowler, D. M. & Kelly, J. W. Functional Amyloidogenesis and Cytotoxicity — Insights into Biology and Pathology. **10,** 10–13 (2012).

192. Iconomidou, V. A. & Hamodrakas, S. J. Natural Protective Amyloids. *Curr Protein Pept Sci.* **9,** 291–309 (2008).

193. Watt, B., Niel, G. van, Raposo, G. & Marks, M. S. PMEL: A pigment cell-specific model for functional amyloid formation. *Pigment Cell Melanoma Res.* **26,** 300–315 (2014).

194. Mostaert, A. S., Higgins, M. J., Fukuma, T., Rindi, F. & Jarvis, S. P. Nanoscale mechanical characterisation of amyloid fibrils discovered in a natural adhesive. *J. Biol. Phys.* **32,** 393–401 (2006).

195. Garcia-Sherman, M., Lundberg, T., Sobonya, R., Lipke, P. & Klotz, S. A unique biofilm in human deep mycoses: fungal amyloid is bound by host serum amyloid P component. *NPJ Biofilms Microbiomes* **1,** 15009 (2015).

196. Fowler, D. M., Koulov, A. V, Balch, W. E. & Kelly, J. W. Functional amyloid--

from bacteria to humans. *Trends Biochem Sci.* **32 (5),** 217–224 (2007).

197. Romero, D. & Kolter, R. Functional amyloids in bacteria. *Int Microbiol.* **17 (2),** 65–73 (2014).

198. Tomczynska-Mleko, M., Terpilowski, K. & Mleko, S. New product development: Cellulose/egg white protein blend fibers. *Carbohydr. Polym.* **126,** 168–174 (2015).

199. Li, C., Adamcik, J. & Mezzenga, R. Biodegradable nanocomposites of amyloid fibrils and graphene with shape-memory and enzyme-sensing properties. *Nat. Nanotechnol.* **7,** 421–427 (2012).

200. Silva, N. H. C. S., Pinto, R. J. B., Freire, C. S. R. & Marrucho, I. M. Production of lysozyme nanofibers using deep eutectic solvent aqueous solutions. *Colloids Surf B Biointerfaces* **147,** 36–44 (2016).

201. Laemmli, U. Cleavage of structural proteins during the assembly of the head of bacteriophage T4. *Nature* **227,** 680–685 (1970).

202. Knorr, A., Fumino, K., Bonsa, A.-M. & Ludwig, R. Spectroscopic evidence of 'jumping and pecking' of cholinium and H-bond enhanced cation–cation interaction in ionic liquids. *Phys. Chem. Chem. Phys.* **17,** 30978–30982 (2015).

203. Micsonai, A. *et al.* Accurate secondary structure prediction and fold recognition for circular dichroism spectroscopy. *Proc. Natl. Acad. Sci. U. S. A.* **112,** E3095-103 (2015).

204. Greenfield, N. J. Using circular dichroism spectra to estimate protein secondary structure. *Nat Protoc.* **1,** 2876–2890 (2006).

205. Krebs, M. R. *et al.* Formation and seeding of amyloid fibrils from wild-type hen lysozyme and a peptide fragment from the beta-domain. *J. Mol. Biol.* **300,** 541–549 (2000).

206. Frare, E., Polverino De Laureto, P., Zurdo, J., Dobson, C. M. & Fontana, A. A highly amyloidogenic region of hen lysozyme. *J. Mol. Biol.* **340,** 1153–1165 (2004).

207. World Health Organization. Dementia: a Public Health Priority. 112 (2012).

208. Khurana, R. *et al.* Mechanism of thioflavin T binding to amyloid fibrils. *J. Struct. Biol.* **151,** 229–238 (2005).

209. Yonezawa, Y. *et al.* An insight into the pathway of the amyloid fibril formation of hen egg white lysozyme obtained from a small-angle X-ray and neutron scattering study. *J. Mol. Biol.* **323,** 237–251 (2002).

210. Xu, M. *et al.* The first step of hen egg white lysozyme fibrillation, irreversible partial unfolding, is a two-state transition. *Protein Sci.* **16,** 815–832 (2007).

211. Xu, M., Ermolenkov, V. V., Uversky, V. N. & Lednev, I. K. Hen egg white lysozyme fibrillation: A deep-UV resonance Raman spectroscopic study. *J. Biophotonics* **1,** 215–229 (2008).

212. Tysseling-mattiace, V. M. *et al.* Self-Assembling Nanofibers Inhibit Glial Scar Formation and Promote Axon Elongation after Spinal Cord Injury. *J. Neurosci.* **28,** 3814–3823 (2009).

213. Wang, X., Li, Y. & Zhong, C. Amyloid-directed assembly of nanostructures and functional devices for bionanoelectronics. *J. Mater. Chem. B* **3,** 4953–4958 (2015).

214. Zhong, C. *et al.* Strong underwater adhesives made by self-assembling multi-protein nanofibres. *Nat. Nanotechnol.* **9,** 858–866 (2014).

215. Chen, A. Y. *et al.* Synthesis and patterning of tunable multiscale materials with engineered cells. *Nat. Mater.* **13,** 515–23 (2014).

216. Esquembre, R. *et al.* Thermal unfolding and refolding of lysozyme in deep eutectic solvents and their aqueous dilutions. *Phys. Chem. Chem. Phys.* **15,** 11248–11256 (2013).

217. Florindo, C., Oliveira, F. S., Rebelo, L. P. N., Fernandes, A. M. & Marrucho, I. M. Insights into the Synthesis and Properties of Deep Eutectic Solvents Based on Cholinium Chloride and Carboxylic Acids. *ACS Sustain. Chem. Eng.* **2,** 2416–2425 (2014).

218. Arnaudov, L. N. & de Vries, R. Thermally induced fibrillar aggregation of hen egg white lysozyme. *Biophys. J.* **88,** 515–526 (2005).

219. Dai, Y., Witkamp, G. J., Verpoorte, R. & Choi, Y. H. Tailoring properties of natural deep eutectic solvents with water to facilitate their applications. *Food Chem.* **187,** 14–19 (2015).

220. Gutiérrez, M. C., Ferrer, M. L., Mateo, C. R. & Monte, F. Del. Freeze-drying of aqueous solutions of deep eutectic solvents: A suitable approach to deep eutectic suspensions of self-assembled structures. *Langmuir* **25,** 5509–5515 (2009).

221. Fujiwara, S., Matsumoto, F. & Yonezawa, Y. Effects of Salt Concentration on Association of the Amyloid Protofilaments of Hen Egg White Lysozyme Studied by Time-resolved Neutron Scattering. **2836,** 21–28 (2003).

222. Juárez, J., Taboada, P. & Mosquera, V. Existence of different structural intermediates on the fibrillation pathway of human serum albumin. *Biophys. J.* **96,** 2353–2370 (2009).

223. Juárez, J., López, S. G., Cambón, A., Taboada, P. & Mosquera, V. Influence of electrostatic interactions on the fibrillation process of human serum albumin. *J. Phys. Chem. B* **113,** 10521–10529 (2009).

224. Juárez, J. *et al.* Hydration effects on the fibrillation process of a globular protein: the case of human serum albumin. *Soft Matter* **8,** 3608 (2012).

225. Usov, I., Adamcik, J. & Mezzenga, R. Polymorphism in bovine serum albumin fibrils: morphology and statistical analysis. *Faraday Discuss.* **166,** 151–162 (2013).

226. Knowles, T. P. J. & Mezzenga, R. Amyloid Fibrils as Building Blocks for

Natural and Artificial Functional Materials. *Adv. Mater.* **28,** 6546–6561 (2016).

227. Oppenheim, T., Knowles, T. P. J., Lacour, S. P. & Welland, M. E. Fabrication and characterisation of protein fibril-elastomer composites. *Acta Biomater.* **6,** 1337–1341 (2010).

228. Carvalho, T., Pinto, R. J. B., Martins, M. A., Silvestre, A. J. D. & Freire, C. S. R. Timesaving microwave assisted synthesis of insulin amyloid fibrils with enhanced nanofiber aspect ratio. *Int. J. Biol. Macromol.* **92,** 225–231 (2016).

229. Holley, M., Eginton, C., Schaefer, D. & Brown, L. R. Characterization of amyloidogenesis of hen egg lysozyme in concentrated ethanol solution. *Biochem. Biophys. Res. Commun.* **373,** 164–168 (2008).

230. Vernaglia, B. A., Huang, J. & Clark, E. D. Guanidine hydrochloride can induce amyloid fibril formation from hen egg-white lysozyme. *Biomacromolecules* **5,** 1362–1370 (2004).

231. Singh, R. S., Kaur, N., Rana, V. & Kennedy, J. F. Pullulan : A novel molecule for biomedical applications. *Carbohydr. Polym.* **171,** 102–121 (2017).

232. Cheng, K. C., Demirci, A. & Catchmark, J. M. Pullulan: Biosynthesis, production, and applications. *Appl. Microbiol. Biotechnol.* **92,** 29–44 (2011).

233. Trovatti, E. *et al.* Sustainable nanocomposite films based on bacterial cellulose and pullulan. *Cellulose* **19,** 729–737 (2012).

234. Chen, C. T., Chen, K.-I., Chiang, H.-H., Chen, Y.-K. & Cheng, K.-C. Improvement on Physical Properties of Pullulan Films by Novel Cross-Linking Strategy. *J. Food Sci.* **82,** 108–117 (2017).

235. Vuddanda, P. R., Montenegro-Nicolini, M., Morales, J. O. & Velaga, S. Effect of plasticizers on the physico-mechanical properties of pullulan based pharmaceutical oral films. *Eur. J. Pharm. Sci.* **96,** 290–298 (2017).

236. Tomé, L. C. *et al.* Bioactive transparent films based on polysaccharides and cholinium carboxylate ionic liquids. *Green Chem.* **17,** 4291–4299 (2015).

237. Teale, F. W. . & Weber, G. Ultraviolet Fluorescence of the Aromatic Amino Acids. *Biochem J.* **65,** 476–482 (1957).

238. Goldfarb, A., Saidel, L. & Mosovick, E. The Ultraviolet Absorption Spectra of Proteins. *J. Biol. Chem.* **193(1),** 397–404 (1951).

239. Unalan, I. U. *et al.* Exceptional oxygen barrier performance of pullulan nanocomposites with ultra-low loading of graphene oxide. *Nanotechnology* **26,** 275703 (2015).

240. Fernandes, S. C. M. *et al.* Antimicrobial pullulan derivative prepared by grafting with 3-aminopropyltrimethoxysilane: Characterization and ability to form transparent films. *Food Hydrocoll.* **35,** 247–252 (2014).

241. Singh, R. S., Kaur, N., Rana, V. & Kennedy, J. F. Recent insights on applications of pullulan in tissue engineering. *Carbohydr. Polym.* **153,** 455–462 (2016).

162

242. Singh, R. S., Kaur, N. & Kennedy, J. F. Pullulan and pullulan derivatives as promising biomolecules for drug and gene targeting. *Carbohydr. Polym.* **123,** 190–207 (2015).

243. Farris, S., Unalan, I. U., Introzzi, L., Fuentes-Alventosa, J. M. & Cozzolino, C. A. Pullulan-Based Films and Coatings for Food Packaging: Present Applications, Emerging Opportunities, and Future Challenges. *J. Appl. Polym. Sci.* **131,** 40539 (2014).

244. Trinetta, V., Floros, J. D. & Cutter, C. N. Sakacin A-containing pullulan film: An active packaging system to control epidemic clones of Listeria Monocytogenes in ready-to-eat foods. *J. Food Saf.* **30,** 366–381 (2010).

245. Gniewosz, M. & Synowiec, A. Antibacterial activity of pullulan films containing thymol. *Flavour Fragr. J.* **26,** 389–395 (2011).

246. Pinto, R. J. B. *et al.* Antifungal activity of transparent nanocomposite thin films of pullulan and silver against Aspergillus niger. *Colloids Surfaces B Biointerfaces* **103,** 143–148 (2013).

247. Morsy, M. K., Khalaf, H. H., Sharoba, A. M., El-Tanahi, H. H. & Cutter, C. N. Incorporation of Essential Oils and Nanoparticles in Pullulan Films to Control Foodborne Pathogens on Meat and Poultry Products. *J. Food Sci.* **79,** M675–M684 (2014).

248. Kandemir, N. *et al.* Production of Antimicrobial Films by Incorporation of Partially Purified Lysozyme into Biodegradable Films of Crude Exopolysaccharides Obtained from Aureobasidium pullulans Fermentation. *Food Technol. Biotechnol.* **43,** 343–350 (2005).

249. Trovatti, E. *et al.* Pullulan − nanofibrillated cellulose composite films with improved thermal and mechanical properties. *Compos. Sci. Technol.* **72,** 1556–1561 (2012).

250. Zhang, C., Gao, D., Ma, Y. & Zhao, X. Effect of Gelatin Addition on Properties of Pullulan Films. *J. Food Sci.* **78,** C805–C810 (2013).

251. Hassannia-Kolaee, M., Khodaiyan, F. & Shahabi-Ghahfarrokhi, I. Modification of functional properties of pullulan-whey protein bionanocomposite films with nanoclay. *J. Food Sci. Technol.* **53,** 1294–1302 (2016).

252. Tomasula, P. M. *et al.* Short communication : Electrospinning of casein / pullulan blends for food-grade applications. *J. Dairy Sci.* **99,** 1837–1845 (2016).

253. Li, C. & Mezzenga, R. The interplay between carbon nanomaterials and amyloid fibrils in bio-nanotechnology. *Nanoscale* **5,** 6207–6218 (2013).

254. Babitha, S. *et al.* Electrospun protein nanofibers in healthcare: A review. *Int. J. Pharm.* **523,** 52–90 (2017).

255. Gadim, T. D. O. *et al.* Nanostructured Bacterial Cellulose-Poly(4-styrene sulfonic acid) Composite Membranes with High Storage Modulus and Protonic Conductivity. *ACS Appl. Mater. Interfaces* **6,** 7864–7875 (2014).

256. Vilela, C. *et al.* Exploiting poly(ionic liquids) and nanocellulose for the development of bio-based anion-exchange membranes. *Biomass and Bioenergy* **100,** 116–125 (2017).

257. Vilela, C. *et al.* Bioactive chitosan/ellagic acid films with UV-light protection for active food packaging. *Food Hydrocoll.* **73,** 120–128 (2017).

258. Masschalck, B. & Michiels, C. W. Antimicrobial properties of lysozyme in relation to foodborne vegetative bacteria. *Crit. Rev. Microbiol.* **29,** 191–214 (2003).

259. Zou, Y., Li, Y., Hao, W., Hu, X. & Ma, G. Parallel beta-sheet fibril and antiparallel beta-sheet oligomer: new insights into amyloid formation of hen egg white lysozyme under heat and acidic condition from FTIR spectroscopy. *J. Phys. Chem. B* **117,** 4003–4013 (2013).

260. Gounga, M. E., Xu, S.-Y. & Wang, Z. Whey protein isolate-based edible films as affected by protein concentration, glycerol ratio and pullulan addition in film formation. *J. Food Eng.* **83,** 521–530 (2007).

261. Bellamy, L. J. *The Infrared Spectra of Complex Molecules.* (Chapman and Hall, Ltd., 1975).

262. Liang, M. *et al.* Cross-linked lysozyme crystal templated synthesis of Au nanoparticles as high-performance recyclable catalysts. *Nanotechnology* **24,** 245601 (2013).

263. Top, A. & Çetinkaya, H. Zinc oxide and zinc hydroxide formation via aqueous precipitation: Effect of the preparation route and lysozyme addition. *Mater. Chem. Phys.* **167,** 77–87 (2015).

264. Synowiec, A. *et al.* Antimicrobial and antioxidant properties of pullulan film containing sweet basil extract and an evaluation of coating effectiveness in the prolongation of the shelf life of apples stored in refrigeration conditions. *Innov. Food Sci. Emerg. Technol.* **23,** 171–181 (2014).

265. Prasad, P., Guru, G. S., Shivakumar, H. R. & Sheshappa Rai, K. Investigation on Miscibility of Sodium Alginate/Pullulan Blends. *J. Polym. Environ.* **20,** 887–893 (2012).

266. Fukuma, T., Mostaert, A. S. & Jarvis, S. P. Explanation for the mechanical strength of amyloid fibrils. *Tribol. Lett.* **22,** 233–237 (2006).

267. Katsikas, L., Jeremic, K., Jovanovic, S., Velickovic, J. S. & Popovic, I. G. The thermal degradation kinetics of dextran and pullulan. *J. Therm. Anal.* **40,** 511–517 (1993).

268. Sanches-Silva, A. *et al.* Trends in the use of natural antioxidants in active food packaging: a review. *Food Addit. Contam. Part A* **31,** 374–395 (2014).

269. Memarpoor-Yazdi, M., Asoodeh, A. & Chamani, J. A novel antioxidant and antimicrobial peptide from hen egg white lysozyme hydrolysates. *J. Funct. Foods* **4,** 278–286 (2012).

270. You, S. J., Udenigwe, C. C., Aluko, R. E. & Wu, J. Multifunctional peptides from egg white lysozyme. *Food Res. Int.* **43,** 848–855 (2010).

271. Hennekinne, J. A., De Buyser, M. L. & Dragacci, S. Staphylococcus aureus and its food poisoning toxins: characterization and outbreak investigation. *FEMS Microbiol. Rev.* **36,** 815–836 (2012).

272. Pattanayaiying, R., H-Kittikun, A. & Cutter, C. N. Incorporation of nisin Z and lauric arginate into pullulan films to inhibit foodborne pathogens associated with fresh and ready-to-eat muscle foods. *Int. J. Food Microbiol.* **207,** 77–82 (2015).

273. Bera, A., Herbert, S., Jakob, A., Vollmer, W. & Götz, F. Why are pathogenic staphylococci so lysozyme resistant? The peptidoglycan O-acetyltransferase OatA is the major determinant for lysozyme resistance of Staphylococcus aureus. *Mol. Microbiol.* **55,** 778–787 (2005).

274. Bera, A., Biswas, R., Herbert, S. & Götz, F. The presence of peptidoglycan O-acetyltransferase in various staphylococcal species correlates with lysozyme resistance and pathogenicity. *Infect. Immun.* **74,** 4598–4604 (2006).

275. Bera, A. *et al.* Influence of wall teichoic acid on lysozyme resistance in Staphylococcus aureus. *J. Bacteriol.* **189,** 280–283 (2007).

276. Pushkaran, A. C. *et al.* Understanding the structure-function relationship of lysozyme resistance in Staphylococcus aureus by peptidoglycan o-acetylation using molecular docking, dynamics, and lysis assay. *J. Chem. Inf. Model.* **55,** 760–770 (2015).

277. Ibrahim, H. R. *et al.* Partially Unfolded Lysozyme at Neutral pH Agglutinates and Kills Gram-Negative and Gram-Positive Bacteria through Membrane Damage Mechanism. *J. Agric. Food Chem.* **44,** 3799–3806 (1996).

278. Caldeira, E., Piskin, E., Granadeiro, L., Silva, F. & Gouveia, I. C. Biofunctionalization of cellulosic fibres with l-cysteine: Assessment of antibacterial properties and mechanism of action against Staphylococcus aureus and Klebsiella pneumoniae. *J. Biotechnol.* **168,** 426–435 (2013).

279. Gniewosz, M. *et al.* The antimicrobial activity of pullulan film incorporated with meadowsweet flower extracts (Filipendulae ulmariae flos) on postharvest quality of apples. *Food Control* **37,** 351–361 (2014).

280. Shannon, M. A. *et al.* Science and technology for water purification in the coming decades. *Nature* **452,** 301–310 (2008).

281. Montgomery, M. A. & Elimelech, M. W. Water and sanitation in developing countries: including health in the equation. *Environ. Sci. Technol.* **41,** 17–24 (2007).

282. Fu, F. & Wang, Q. Removal of heavy metal ions from wastewaters : A review. *J. Environ. Manage.* **92,** 407–418 (2011).

283. Pacyna, J. M. *et al.* Current and future levels of mercury atmospheric pollution on a global scale. *Atmos. Chem. Phys.* **16,** 12495–12511 (2016).

284. Agency for Toxic Substances and Disease Registry. Priority List of Hazardous Substances. (2015).

285. EU. Directive 2008/105/EC of the European Parliament and of the Council on environmental quality standards in the field of water policy, amending and subsequently repealing Council Directives 82/176/EEC, 83/513/EEC, 84/156/EEC, 84/491/EEC, 86/280/EEC and amen. *Off. J. Eur. Union* 348/84 (2008).

286. Fu, F. *et al.* Effective removal of coordinated copper from wastewater using a new dithiocarbamate-type supramolecular heavy metal precipitant. *Chemosphere* **69,** 1783–1789 (2007).

287. Argun, M. E. Use of clinoptilolite for the removal of nickel ions from water : Kinetics and thermodynamics. *J. Hazard. Mater.* **150,** 587–595 (2008).

288. Shafaei, A., Rezayee, M., Arami, M., Nikazar, M. & Al, A. Removal of Mn 2 + ions from synthetic wastewater by electrocoagulation process. *DES* **260,** 23–28 (2010).

289. EPA, U. S. E. P. A. Control and Treatment Technology for the Metal Finishing Industry - Ion Exchange. 1–46 (1981).

290. Misaelides, P. Microporous and Mesoporous Materials Application of natural zeolites in environmental remediation : A short review q. *Microporous Mesoporous Mater.* **144,** 15–18 (2011).

291. Hadi, P. *et al.* Aqueous mercury adsorption by activated carbons. *Water Res.* **3,** (2015).

292. Hadi, P. *et al.* A critical review on preparation , characterization and utilization of sludge-derived activated carbons for wastewater treatment. *Chem. Eng. J.* **260,** 895–906 (2015).

293. Sehaqui, H. & Perez, U. Enhancing adsorption of heavy metal ions onto biobased nanofibers from waste pulp residues for application in wastewater treatment. *Cellulose* **21,** 2831–2844 (2014).

294. Srivastava, S., Kardam, A. & Raj, K. R. Nanotech Reinforcement onto Cellulosic Fibers : Green Remediation of Toxic Metals. *Int. J. Green Nanotechnol.* **4,** 37–41 (2012).

295. Voisin, H., Bergström, L., Liu, P. & Mathew, A. P. Nanocellulose-Based Materials for Water Purification. *Nanomaterials* **7,** 1–19 (2017).

296. Portillo, A. *et al.* Biochimica et Biophysica Acta Role of monomer arrangement in the amyloid self-assembly. *BBA - Proteins Proteomics* **1854,** 218–228 (2015).

297. Knowles, T. P. J. & Mezzenga, R. Amyloid Fibrils as Building Blocks for Natural and Artifi cial Functional Materials. *Adv. Mater.* **28,** 6546–6561 (2016).

298. Rufo, C. M. *et al.* Short peptides self-assemble to produce catalytic amyloids. *Nat Chem* **6,** 303–309 (2014).

299. EU. Directive 2008/105/EC of the European Parliament and of the Council of the European Union, on environmental quality standards in the field of water policy, amending and subsequently repealing Council Directives 83/513/ EEC and 84/156/EEC and amending Dire. *Off. J. Eur. Communities* 348/84 (2008).

300. EU. Directive 2013/39/EU of the European Parliament and of the Council of 12 August 2013 amending Directives 2000/60/EC and 2008/105/ EC as regards priority substances in the field of water policy. *Off. J. Eur. Union* **L226,** 1–17 (2013).

301. Hassanpour, A. & Asghari, S. Synthesis, characterization and antibacterial evaluation of nanofibrillated cellulose grafted by a novel quinolinium silane salt. *RSC Adv.* **7,** 23907–23916 (2017).

302. Sehaqui, H., Liu, A., Zhou, Q. & Berglund, L. A. Fast Preparation Procedure for Large , Flat Cellulose and Cellulose / Inorganic Nanopaper Structures. *Biomacromolecules* **11,** 2195–2198 (2010).

303. Sehaqui, H., Morimune, S., Nishino, T. & Berglund, L. A. Stretchable and Strong Cellulose Nanopaper Structures Based on Polymer-Coated Nano fi ber Networks: An Alternative to Nonwoven Porous Membranes from Electrospinning. *Biomacromolecules* **13,** 3661–3667 (2012).

304. Singh, V., Singh, A., Joshi, S. & Malviya, T. Synthesis, characterization and mercury (II) removal using poly (vinylacetate) grafted guar gum. *Adv. Mater. Lett.* **7,** 573–578 (2016).

305. Zhu, X., Yang, R., Gao, W. & Li, M. Sulfur-modified Chitosan Hydrogel as an Adsorbent for Removal of Hg (II) from Effluents. *Fibers Polym.* **18,** 1229–1234 (2017).

306. Fernandes, S. C. M. *et al.* Transparent chitosan films reinforced with a high content of nanofibrillated cellulose. *Carbohydr. Polym.* **81,** 394–401 (2010).

307. Lee, K., Aitomäki, Y., Berglund, L. A., Oksman, K. & Bismarck, A. On the use of nanocellulose as reinforcement in polymer matrix composites. *Compos. Sci. Technol.* **105,** 15–27 (2014).

308. Mautner, A., Kobkeatthawin, H. A. M. T., Karim, V. K. Z. & Phosphorylation, I. Á. Phosphorylated nanocellulose papers for copper adsorption from aqueous solutions. *Int. J. Environ. Sci. Technol.* **13,** 1861–1872 (2016).

309. Zhao, C., Xu, X., Chen, J. & Yang, F. Optimization of preparation conditions of poly (vinylidene fl uoride)/ graphene oxide micro fi ltration membranes by the Taguchi experimental design. *Desalination* **334,** 17–22 (2014).

310. Wetter, L. & Deutsch, H. Immunological Studies in Egg White Proteins. *J. Biol. Chem.* **192,** 237–242 (1951).

311. Saito, T., Kimura, S., Nishiyama, Y. & Isogai, A. Cellulose Nanofibers Prepared by TEMPO-Mediated Oxidation of Native Cellulose. *Biomacromolecules* **8,** 2485–2491 (2007).

312. Tawabini, B., Atieh, M. & Khaled, M. Removal of mercury from water by multi-

walled carbon nanotubes. *Water Sci Technol.* **61,** 591–598 (2010).

313. Figueira, P. *et al.* Removal of mercury (II) by dithiocarbamate surface functionalized magnetite particles : Application to synthetic and natural spiked waters. *Water Res.* **45,** 5773–5784 (2011).

314. Henriques, B. & Gonc, G. Optimized graphene oxide foam with enhanced performance and high selectivity for mercury removal from water Mercedes Vila. *J. Hazard. Mater.* **301,** 453–461 (2016).

315. Chen, B. *et al.* Mechanically strong fully biobased anisotropic cellulose aerogels. *RSC Adv.* **6,** 96518–96526 (2016).